NASA CONTRACTOR REPORT

NASA CR-1980

NASA CR-1980

DEMONSTRATION OF THE RANGE OVER WHICH THE LANGLEY RESEARCH CENTER DIGITAL COMPUTER CHARRING ABLATION PROGRAM (CHAP) CAN BE USED WITH CONFIDENCE

Comparisons of CHAP Predictions and Test Data for Three Ablation Materials

by Carl B. Moyer and Kenneth A. Green

Prepared by
AEROTHERM CORPORATION
Mountain View, Calif. 94040
for Langley Research Center

NATIONAL AERONAUTICS AND SPACE ADMINISTRATION • WASHINGTON, D. C. • FEBRUARY 1972

1. Report No.	2. Government Accession No.	3. Recipient's Catalog No.
NASA CR-1980		

4. Title and Subtitle	5. Report Date
DEMONSTRATION OF THE RANGE OVER WHICH THE LANGLEY RESEARCH CENTER DIGITAL COMPUTER CHARRING ABLATION PROGRAM (CHAP) CAN BE USED WITH CONFIDENCE – COMPARISONS OF CHAP PREDICTIONS AND TEST DATA FOR THREE ABLATION MATERIALS	February 1972
	6. Performing Organization Code
7. Author(s) Carl B. Moyer and Kenneth A. Green	8. Performing Organization Report No. 71-35
	10. Work Unit No.
9. Performing Organization Name and Address Aerotherm Corporation Mountain View, California 94040	11. Contract or Grant No. NAS1-10136
	13. Type of Report and Period Covered Contractor Report
12. Sponsoring Agency Name and Address National Aeronautics and Space Administration Washington, DC 20546	14. Sponsoring Agency Code

15. Supplementary Notes

16. Abstract

The report presents comparisons of ablation calculations with the Langley Research Center charring ablation computer code (CHAP) and ablation test data over a wide range of envrionmental conditions in air for three materials: low-density nylon phenolic, Avcoat 5026-39HC/G, and a filled silicon elastomer. Heat fluxes considered range from over 500 BTU/ft^2-sec to less than 50 BTU/ft^2-sec. Pressures ranged from 0.5 atm to .004 atm. Enthalpies ranged from about 2000 BTU/lb to 18000 BTU/lb. Predictions of recession, pyrolysis penetration, and thermocouple responses are considered. Recession predictions for nylon phenolic are good as steady state is approached, but strongly transient cases are underpredicted. Pyrolysis penetrations and thermocouple responses are very well predicted. Recession amounts for Avcoat and silicone elastomer are less well predicted, although high heat flux cases near steady state are fairly satisfactory. Pyrolysis penetrations and thermocouple responses are very well predicted.

17. Key Words (Suggested by Author(s))	18. Distribution Statement
Ablation performance predictions Ablation analysis Thermal protection	Unclassified – Unlimited

19. Security Classif. (of this report)	20. Security Classif. (of this page)	21. No. of Pages	22. Price*
Unclassified	Unclassified	115	$3.00

*For sale by the National Technical Information Service, Springfield, Virginia 22151

TABLE OF CONTENTS

LIST OF TABLES

SYMBOLS

A	pre-exponential factor in pyrolysis relation, Equation (1), p. 4	lb/ft^2sec
A_c	pre-exponential factor in oxidation equation, Equation (3), p. 4	$lb/ft^2sec\ atm^n$
A_s	pre-exponential factor in sublimation law, Equation (1), p. 5	lb/ft^2sec
B	activiation energy in pyrolysis relation, Equation (1), p. 4	°R
B'	dimensionless ablation rate $\dot{m}/\rho_e u_e C_M$	---
B_c	activation energy in oxidation equation, Equation (3), p. 4	°R
B_s	activation energy in sublimation law, Equation (1), p. 5	°R
B'_o	value of B' before reduction in $\rho_e u_e C_M$ due to blowing	---
b	blowing reduction quantity given by Equation (11), p. 6	---
C_e	mass fraction of available oxygen at outer edge of boundary layer	lb/lb
C_H	see $\rho_e u_e C_H$	
C_M	see $\rho_e u_e C_M$	
$\bar{C}_p$	specific heat of pyrolysis gases	BTU/lb°R
C_w	mass fraction of available oxygen adjacent to heated surface	lb/lb
h_c	see Δh_c	

h_e	recovery enthalpy, driving potential for energy transfer	BTU/lb
h_s	see Δh_s	
h_w	enthalpy of gases adjacent to heated surface	BTU/lb
K	quantity defined by Equation (8), p. 5	$lb/ft^2 sec\ atm^n$
K	empirical constant in Equation (24), p. 29	$lb/ft^{3/2} sec\ atm^{1/2}$
k	thermal conductivity	BTU/ft sec°F
L	quantity defined by Equation (7), p. 5; see also ΔL	---
Le	Lewis number	---
$\dot{m}_c$	char oxidation erosion rate	$lb/ft^2 sec$
$\dot{m}_{ox}$	flux of available oxygen to surface	$lb/ft^2 sec$
$\dot{m}_p$	rate of pyrolysis gas generated at pyrolysis plane	$lb/ft^2 sec$
$\dot{m}_s$	char sublimation erosion rate	$lb/ft^2 sec$
n	oxidation reaction order, Equation (3), p. 4	---
P	see ΔP	
p	pressure	atm
$\dot{q}$	convective heat flux	$BTU/ft^2 sec$
q_c	cold wall convective heat flux	$BTU/ft^2 sec$
q_R	radiative heat flux to wall	$BTU/ft^2 sec$
r	radius of curvature	ft
$\dot{s}$	recession rate	ft/sec

SS	denotes "steady state"	---
T_m	melt temperature	°R
T_w	surface temperature	°R
u_e	see $\rho_e u_e C_H$, etc.	
y	distance from heated surface	ft
GREEK		
α	surface absorptance	---
α_c	blowing correction coefficient for char flux, Equation (12), p. 6	---
α_p	blowing correction coefficient for pyrolysis gas flux, Equation (12), p. 6	---
γ	lb of carbon removed per lb of oxygen, Equation (13), p. 10	---
Δh_c	heat of combustion of char	BTU/lb
Δh_s	heat of sublimation of char	BTU/lb
ΔL	recession during observation	ft
ΔP_1	$\Delta S + \delta_c$	ft
ΔP_2	$\Delta S + \delta_c + \delta_p$	ft
ΔS	total test recession	ft
ΔT	temperature increment	°R
Δt	time of observation	sec
δ	thickness of char or of pyrolysis zone	ft

δ_c	char thickness	ft
δ_p	pyrolysis zone thickness (Ref. 5)	ft
ε	surface emittance	---
λ	lb of char removed per lb of available oxygen reaching surface	---
ρ	density	
$\rho_e u_e C_H$	convective heat transfer coefficient	$lb/ft^2 sec$
$\rho_e u_e C_{H_o}$	convective heat transfer coefficient with no blowing reduction or blockage effect	$lb/ft^2 sec$
$\rho_e u_e C_M$	convective mass transfer coefficient	$lb/ft^2 sec$
$\rho_e u_e C_{M_o}$	Convective mass transfer coefficient with no blowing reduction or blockage effect	$lb/ft^2 sec$
σ	Stefan-Boltzmann constant	$BTU/ft^2 sec°R^4$
τ	total test time	sec

SUBSCRIPTS

C*	denotes carbon
c	denotes char, oxidation of char, or combustion of char
carbon	denotes carbon
e	denotes outer edge of boundary layer; also see h_e, $\rho_e u_e C_H$, $\rho_e u_e C_{H_o}$, $\rho_e u_e C_M$, $\rho_e u_e C_{M_o}$
H	see $\rho_e u_e C_H$, $\rho_e u_e C_{H_o}$
M	see $\rho_e u_e C_M$, $\rho_e u_e C_{M_o}$
m	denotes melt

o	denotes no blowing or no blockage value
obs	denotes observed experimental value
ox	denotes available oxygen
p	denotes pyrolysis or pyrolysis gas
pred	denotes computer code prediction
R	denotes radiation flux to heated surface
s	denotes sublimation
v	denotes virgin material
w	denotes heated surface
1,2	denote successive estimates; also see ΔP_1, ΔP_2

SUPERSCRIPTS

' (prime)	see B', B'_o
*	see C*
—	see $\overline{C}_p$
·	see $\dot{s}$

SECTION 1

INTRODUCTION

The work reported here aimed to define the range of applicability of a simple charring ablation computer code as applied to three materials. The basic computer code employed is denoted CHAP I; it was developed at the NASA Langley Research Center and is described in References 1 and 2. Some supplemental calculations were done with a later, more elaborate version of CHAP I, denoted CHAP II, which has not yet been described in the literature. The three materials considered included a low density nylon phenolic, the Apollo heat shield material, and a filled silicone elastomer. These materials will be described in more detail subsequently.

The overall program had two major tasks, each with a number of subtasks, as indicated in Table 1.

TABLE 1

OUTLINE OF STUDY PROGRAM

Task	Sub-Task	Activity
I		Material Properties Data and Ablation Test Data Collection; Qualifying Calculations
	I.1	Material Properties Data Collection
	I.2	Ablation Test Data Collection
	I.3	Establishment of Agreement Criteria; Qualifying Calculations
	I.4	Reporting and Review
II		Determination of the Applicable Range of the CHAP Program
	II.1	Iterative Computations to Define Properties
	II.2	Review of Properties
	II.3	Computation of Remaining Cases (Final Calculations)
	II.4	Reporting

The two major tasks of the program are reported separately. The properties and ablation test data collected under Task I are reported in the previously issued Reference 3. The data of Reference 3 are not republished here due to the large volume of data, except in the case of particular ablation test cases chosen.

As indicated in Table 1, Task II had two computational phases, denoted Subtask II.1, Iterative Calculations, and Subtask II.3, Final Calculations. The Iterative Calculations studied a limited number (four or five) test cases, with each test case being examined with a number of CHAP I runs to identify those input material properties that allowed the best match of predictions and data. The Final Calculations then used these properties in single computations of interesting test cases.

The three materials considered in this study were defined as follows:

- Low density nylon phenolic; composition by mass of about 23 to 37 percent phenolic (phenol-formaldehyde) resin, 22 to 27 percent hollow phenolic microspheres, 40 to 60 percent nylon (cloth or powder); nominal virgin density about 36 lb/ft^3
- Low density filled silicone elastomer; composition by mass of about 72 to 78 percent silicone elastomer (polydimethyl siloxane or polymethylphenyl/dimethyl siloxane), 12 to 16 percent hollow silica microspheres, 8 to 12 percent hollow phenolic microspheres; nominal virgin density about 34 to 40 lb/ft^3
- Apollo heat shield material, commercially designated Avcoat 5026-39-HC/G; principally epoxy novolac with hollow phenolic microspheres, with silica fibers added, gunned into phenolic/fiberglass honeycomb; nominal density 32 lb/ft^3

These materials were selected because numerous property and ablation test data were available for them, and because they are roughly similar to candidate charring ablators being proposed for thermal protection systems on reusable spacecraft (for example, the space shuttle).

Test conditions of interest were defined as:

- stagnation pressure $\leq$ 1.0 atm.
- stagnation point heating rate = 10 to 600 Btu/ft^2sec.
- test stream total enthalpy = 2,000 to 20,000 Btu/lbm.
- stream oxygen mass fraction = 0. to 0.23

with interest centering on a nominal space shuttle environment, namely, heating rates of 50 BTU/ft^2 sec and less at an enthalpy of 10,000 to 15,000 BTU/lb with a total pressure of 0.1 atmosphere.

Mr. Stephen S. Tompkins of the Materials Division, Langley Research Center, Hampton, Virginia, was the technical representative for this project.

SECTION 2

BRIEF DESCRIPTION OF THE CHAP I AND CHAP II CODES

The CHAP codes are described elsewhere (References 1 and 2), but some brief orientation in the present report may be useful. The CHAP I code is basically an implicit transient heat conduction code with elaborations to account for in-depth pyrolysis and for energy pick-up by the pyrolysis gas as it passes from the pyrolysis zone out through the char into the boundary layer. Pyrolysis is assumed to occur at a plane of zero width (the "pyrolysis plane") according to the relation

$$\dot{m}_p = Ae^{-B/T} \tag{1}$$

where A and B are input constants. The location and temperature of the plane is determined at each instant by in-depth energy events. A fixed heat of pyrolysis is assumed.

The surface energy balance may take a number of forms, but only two were used in this study. In Option 1, a full surface energy balance is computed to determine surface temperature and recession rate. The surface energy balance is

$$q_c \left(1 - \frac{h_w}{h_e}\right)(1 - b) + \alpha q_R + \dot{m}_c \Delta h_c = \sigma \varepsilon T_w^4 - k \frac{\partial T}{\partial y} + \dot{m}_s \Delta h_s \tag{2}$$

In this equation, the quantity 1 - b is the "blockage effect" or "blowing reduction", Δh_c a heat of combustion (input as a function of T_w and p), $\dot{m}_c$ an oxidation rate of char, and $\dot{m}_s$ a sublimation rate of char removal. This equation is used in conjunction with two mass loss equations for determining $\dot{m}_c$ and $\dot{m}_s$, and a blockage equation to compute b.

The oxidation rate $\dot{m}_c$ is computed with a conventional kinetic control - plus - diffusion limit relation, as discussed in Reference 2. The basic kinetic relation is

$$\dot{m}_c = A_c e^{-B_c/T_w} (C_w p)^n \tag{3}$$

The diffusion restriction is

$$\dot{m}_{ox} = \frac{\dot{m}_c}{\lambda} = \rho_e u_e C_M (C_e - C_w) \tag{4}$$

where the mass transfer coefficient $\rho_e u_e C_M$ is given by

$$\rho_e u_e C_M = Le^{0.6} \frac{q_c}{h_e} \quad (1 - b) \tag{5}$$

For a half order reaction (n = 1/2), equations (3) and (4) may be combined to yield the mass loss law

$$\dot{m}_c = \frac{1}{2}\left\{-L + \left(L^2 + 4K^2 p C_e\right)^{\frac{1}{2}}\right\} \tag{6}$$

where

$$L = \frac{K^2 p}{\lambda \rho_e u_e C_M} \tag{7}$$

and

$$K = A_c e^{-B_c/T_w} \tag{8}$$

For first order (n = 1) kinetics, we obtain

$$\dot{m}_c = \frac{K p C_e}{1 + \frac{Kp}{\lambda \rho_e u_e C_M}} \tag{9}$$

The sublimation law is

$$\dot{m}_s = A_s e^{-B_s/T} - \dot{m}_c \tag{10}$$

but this is set equal to zero unless it exceeds zero.

It should be observed from the above that the CHAP I code is basically a frozen pyrolysis gas code in that the pyrolysis gases do not appear in the surface energy balance (no pyrolysis gas combustion term) and do not reduce the amount of oxygen available to the char surface.

The blockage factor b was computed from a built-in second order correlation:

$$b = 0.724B_0' - 0.13B_0'^2 \tag{11}$$

where

$$B_0' = \frac{\alpha_c \dot{m}_c + \alpha_p \dot{m}_p}{\rho_e u_e C_{M_0}} \tag{12}$$

The input constants α_c and α_p allow the code user to discriminate between the effectiveness of the char and pyrolysis gas in blowing reduction.

In the Option 2 boundary condition of CHAP, the surface recession and either the surface temperature or the cold wall heat flux may be input.

The CHAP II is basically the CHAP I code with a revised pyrolysis law and with a subroutine to compute the chemical history of the pyrolysis gas as it passes through the char. A chemical kinetic calculation determines the molecular make-up of the pyrolysis gas throughout the char layer, and accounts as necessary for "coking" or carbon deposition from the gas as it travels through the char.

SECTION 3

ITERATIVE CALCULATIONS

3.1 PRELIMINARIES

The iterative study required three preliminary activities:

- a selection of initial property values for the first calculation
- a statement of the criteria which will define satisfactory agreement between iterative case predictions and test data
- a selection of the iterative cases

The following subsections will treat these preliminary activities.

3.1.1 Initial or "Nominal" Property Values

The initial property values were chosen to be the property values cited in the tables presented in Appendix A. These properties were developed at the NASA Langley Research Center during earlier ablation prediction studies and thus constitute logical first choices. Furthermore, these properties proved to be consistent with the experimental properties data reported in Reference 3.

3.1.2 Agreement Criteria

Agreement criteria were established during Task I effort and are reported in Reference 3. In summary, the criteria are

- Surface temperature

  The agreement criterion was set at $\pm$ 200°R with an important cautionary note about frequent substantial systematic errors due to uncorrected window and mirror losses, gas cap radiation interference, non-normal viewing angle effects, and emittance assumptions.

- Surface recession

  The recession prediction is considered satisfactory if the predicted recession matches the observed recession to within 20 percent of the observed recession, except that agreement is not required to be closer than 0.010 inches due to random measurement errors due primarily to surface roughness effects. Furthermore one must frequently allow for systematic effects of char swell and char shrinkage.

- Pyrolysis Penetration Depth

  Pyrolysis penetration depth is defined as the total penetration of the pyrolysis zone as measured from the initial location of the heated surface. Since CHAP I uses a simple pyrolysis plane model, the code provides an unambiguous statement of the location of this line. Test data, on the other hand, show a pyrolysis zone of non-zero width, so that some caution is needed in interpreting reported data.

  The agreement criterion was set at 10 per cent of the observed depth, but not closer than 0.010 inches.

- Thermocouple Criteria

  Agreement between calculated and observed thermocouples responses will be judged satisfactory if

$$(T_{calc} - T_m) \leq 4 \text{ sec } \frac{dT_m}{d\theta} + 0.1\ T_m$$

This criterion in effect specifies a permissible 4 to 5 second time lead for a thermocouple response prediction during rapid temperature rise periods. The criterion is therefore biased in favor of over-prediction since thermocouples generally lag the material reponse due to thermocouple capacitance and thermal contact effects.

3.1.3 Selection of Iterative Test Cases

3.1.3.1 General Criteria

For the purpose of defining material properties by iterative calculations, it was desired to have at least three test cases covering a range of environment conditions for each of the three materials studied. The three cases should if possible be close to the nominal shuttle conditions. Since none of the test cases matches the nominal shuttle condition closely, the choice of the three cases presents an interesting problem.

The following criteria were established to guide the selection:

1. The tests should have apparently reliable data, preferably with several thermocouples.
2. The surface temperature should reach 3000°R to 4000°R; the range corresponding to the nominal shuttle condition (50 Btu/ft^{2}sec, 0.1 atm, 10000-15000 Btu/lb) implies a surface temperature of about 3300°R to 3500°R.

3. One case should be at about 4000°R to be certain to be on the diffusion controlled plateau for carbon surfaces.

4. For nylon phenolic, one case should be clearly in the kinetically controlled oxidation regime; this point will be discussed below.

5. At least one case should show a recession large compared with the char thickness (to avoid char swell or shrinkage influences on the recession); as a minimum objective, this case should have a recession > 50 mils.

6. The q_c should match the nominal shuttle condition as close as is convenient; this will follow almost automatically from condition (2) since q_c is the most important variable influencing surface temperature for the materials and conditions of interest here.

7. If possible, the three cases should bracket the nominal shuttle condition in pressure, heat flux, and recovery enthalpy.

8. At least one of the cases should have (a) a reliable surface temperature measurement or (b) a reliable cold wall heat flux measurement to allow runs to be made with (a) specified surface temperature and recession or (b) specified cold wall heat flux and recession; such runs will allow the verification of in-depth properties without interference from failures to predict surface events properly.

3.1.3.2 Consideration of Kinetically Controlled Carbon Oxidation

The one non-obvious point in this list is Condition (4), concerning the kinetically controlled regime. This condition is included because many shuttle conditions (although possibly not the nominal condition above) will imply kinetic control of the carbon oxidation mechanism of surface recession. Therefore, since the kinetic recession rate data available are uncertain at best, it would be desirable to use this calculation activity to obtain improved or more reliable data. It is not entirely obvious, however, how to be certain that any given test case represents kinetically controlled data. Two procedures can give information on this point:

1. Compare the observed recession to that which would be expected from the oxidation limited rate. This cannot be done easily due to transient effects, uncertainty about the chemical role played by the pyrolysis gases in the low temperature regimes of interest, and difficulties in computing the blowing reduction.

2. Compute, from the built-in CHAP kinetic models and the best available kinetic parameters, curves of recession rate versus surface temperature and note the temperature range where kinetic effects dominate; compare this temperature range with that of the data.

The first procedure was deemed to involve more effort than justified by the scope of the iterative calculations. The second method is illustrated by Figure 1, which is a plot of Equation (9):

$$\dot{m}_c = \frac{KpC_e}{1 + \frac{Kp}{\lambda \rho_e u_e C_M}}$$

Define

$$\gamma = \left\{ \begin{matrix} \text{lb of carbon removed from the} \\ \text{char per lb of oxygen} \end{matrix} \right\} = 0.75 \qquad (13)$$

then

$$B'_{carbon} = \frac{\dot{m}_{carbon}}{\rho_e u_e C_M} = \frac{\dot{m}_c}{\rho_e u_e C_M} \frac{\gamma}{\lambda} = \frac{(\gamma C_e) \left[\frac{K}{\gamma} \frac{p}{\rho_e u_e C_M} \right]}{1 + \left[\frac{K}{\gamma} \frac{p}{\rho_e u_e C_M} \right]} \qquad (14)$$

In this relation K = K(T) implies that temperature is an independent variable. Figure 1 is constructed from Equation (14) with the A and B values given in the contract for first order oxidation and a λ of 0.75, and shows the dimensionless carbon removal parameter B'_{carbon} plotted versus surface temperature T, with the dimensional quantity $p/\rho_e u_e C_M$ as a parameter. For the nominal shuttle condition, this parameter will be about 20 atm/(lb/ft^{2}sec). Most test data are nearer to a value of unity.

The plot shows the kinetically controlled transition from no recession to the diffusion limited "plateau" to occur at (very roughly) 3000°R; this is in harmony with the rough rule-of-thumb that for "normal" pressure and transfer coefficients the transition takes place at

$$T = B/\ell nA \qquad (15)$$

which in this case gives 3310°R. Few of the available test data for nylon phenolic will fall in the kinetically controlled regime according to Figure 1. Furthermore, the kinetic constants used to construct Figure 1 are relatively slow ones. The much faster kinetics quoted in Appendix A for the silicone elastomer, also known as "Scala's fast kinetics" (Ref. 4) will yield a transition at approximately 1970°R. Confirming this observation, Figure 2 shows carbon B'-T curves analogous to those of Figure 1 for both "Scala's fast kinetics" ($A = 6.73 \times 10^6$ lb/ft^{2}sec atm$^{\frac{1}{2}}$, $B = 39875$°R (44 kcal/mole°K), $n = 1/2$) and "Scala's slow kinetics" ($A = 4.473 \times 10^4$ lb/ft^{2}sec atm$^{\frac{1}{2}}$, same B and $n = 1/2$). The slow kinetics are generally thought to apply to pyrolytic graphites; "Scala's fast kinetics" presumably represent carbon ablation chars at least roughly.

The only nylon phenolic test data which appear fairly sure to be kinetically controlled are

Tab. No.*	Model	q_c Btu/ft^{2}sec	T_w °R	$\frac{p(h_e - h_w)}{q_c}$ $\frac{\text{atm}}{\text{lb/ft}^2\text{sec}}$	$\frac{p^{\frac{1}{2}}(h_e - h_w)}{q_c}$ $\frac{\text{atm}^{\frac{1}{2}}}{\text{lb/ft}^2\text{sec}}$
21	PLL91	43	3300	0.8	10
22	PLH91	44	3300	0.8	10

It is not likely that carbon kinetics data have much relevance to the low temperature ablation rates of Avcoat 5026-39 and the silicone elastomer. The silica content of the former, although fairly small, causes the surface of low temperature models to be covered to a greater or lesser degree with silica. Similarly, the silicon content of the elastomer and the silica microspheres of the filler material lead to partial coverage of low temperature surfaces with silica.

3.1.3.3 Selection of Iterative Cases

Table 2 lists the cases for each material which were selected on the basis of the discussion points of Sections 3.1.3.1 and 3.1.3.2 for iterative calculation.

*Tabulation number in Reference 3.

TABLE 2

ITERATION CASE SELECTIONS

Material	Tab No.	Model No.	q_c $\left(\frac{BTU}{ft^2 sec}\right)$	T_w Final (°R)	p (atm)	Run Time (sec)	$\frac{ph_e}{q_c}$ $\left(\frac{atm\ ft^2 sec}{LB}\right)$	$\frac{p^{\frac{1}{2}} h_e}{q_c}$ $\left(\frac{atm^{\frac{1}{2}} ft^2 sec}{LB}\right)$	$\frac{\text{Recession}}{\text{Char Thickness}}$ $\left(\frac{in}{in}\right)$	Choice Objective
Nylon Phenolic	19	PLL90	145	4300	.0199	34.7	1	7	.073/.159	"average" conditions
	21	PLL91	43	3300	.007	120.0	1	12	.078/.171	possible kinetic control
	22	PLH91	44	3300	.007	120.0	1	12	.054/.124	
	16	PLL93	256	4600*	.284	30.0	5	9	.137/.099	high heat flux, high recession/ char thickness
	17	PLH93	250	4600*	.284	30.0	5	9	.119/.115	
Avcoat 5026-39	66	119/BH/4	119	4100	.0279	30.8	3	18	.096/.100	"average" conditions, intermediate surface temperature
	52	82/BH/2	215	4400	.0290	60.3	1.4	8.3	.215/.160	
	92	111/BH/1	577	4800	.0817	39.6	1.5	5.2	.388/.08	high heat flux, high recession/char thickness
	62	120/BH/4	91	3200	.0081	90.2	1	11	.137/.130	"average" conditions, low surface temperature
Silicone Elastomer	12	SP91	45	3040	.007	120.0	1	9	+.048/.200	low heat flux, low surface temperature
	4	SP89	200	3550	.00847	25.0	5	8	.004/.121	moderate conditions
	5	SP93	273	3660	.284	30.0	5	8	.070/.117	high heat flux
	1	SP96	63	2800	.0109	75.5	2	18	+.052/.205	low heat flux, low surface temperature

*Temperature history not available

3.2 ITERATIVE CALCULATION RESULTS

The iterative calculations were divided into two phases. In the first phase, the surface conditions such as recession rate were specified as known inputs, and only the in-depth results (char thickness and thermocouple response histories) were computed. This Option 2 phase aimed to determine in-depth properties as accurately as possible by isolating the char depth and thermocouple predictions from the consequences of possible failure to predict surface recession and temperature properly. In the second phase, the CHAP I code was run in its Option 1 mode, with the environment specified and the surface recession predicted.

3.2.1 Specified Recession (Option 2) Calculations

The CHAP I code can perform Option 2 studies with surface recession rate and either surface temperature or cold wall heat flux specified. The runs reported here specified the cold wall heat flux, since reported surface temperatures are frequently far less reliable than reported heat flux values for the types of tests considered here.

3.2.1.1 Nylon-Phenolic

Figures 3, 4, and 5 show the predicted results for the three nylon phenolic cases chosen. The thermocouple predictions of Figure 3 (Tab. 21, q_c = 43.2 Btu/ft^{2}sec) are generally satisfactory, although the first thermocouple data history appears faulty. The char thickness prediction is excellent; the surface temperature prediction is quite low, but this may provisionally be ascribed to poor data. Figure 4 (Tab. 19, q_c = 145 Btu/ft^{2}sec) shows acceptable thermocouple predictions. The predicted char thickness is somewhat low, and the total pyrolysis pentration is 14% low, a somewhat larger error than desired. Figure 5 (Tab. 16, q_c = 256 Btu/ft^{2}sec) shows good thermocouple agreement for a high heat flux case. The char thickness is 30% high and the char penetration is 14% high. The reported surface temperature is grossly underpredicted.

An overview of the results shown in Figures 3, 4, and 5 yields the following conclusions:

1. The best surface temperature predictions are 800°R low, whereas the worst thermocouple predictions are 400°R low, and most are substantially better. Therefore, either the material properties are greatly in error or the reported surface temperatures are not to be trusted. The second possibility seems much more likely.

2. The prediction discrepancies for thermocouple response and char thickness of Figures 4 and 5 are very similar but opposite. Therefore it seems likely that the properties are good but that the reported heat fluxes are somewhat in error, being too high for Figure 5 and too low for Figure 4.

3. Thermocouple predictions for temperatures less than about 1000°R are consistently low. The virgin material conductivity values could perhaps be raised. Figure 4 shows the results of two additional runs with higher virgin conductivities. To examine the improvement attainable, Run 19-3 employed the conductivity of Reference 2-8b of the Reference 3, which has higher virgin conductivity values above 900°R. Run 19-4 (not shown) used approximately the highest conductivity justifiable from the data of Figure 2-1 of Reference 3. The predictions were not appreciably improved.

On balance, the nylon-phenolic cases seemed acceptable, provided that the discrepancies of Case 19 (Figure 4) and Case 16 (Figure 5) could be rationalized. The first of these cases showed underpredicted thermocouple temperatures and char thickness; the second showed overpredictions. Clearly no change in the in-depth properties could improve both predictions; therefore, it seemed attractive to consider possible errors in reported heat fluxes. To explore this possibility, it was estimated that the expected error in heat flux measurements is about 10%, and that the maximum error experienced under normal circumstances might be about 20%. To see if the maximum error could change the predicted results of Cases 19 and 16 by appreciable amounts, Case 19 was run with a 20% higher heat flux value than reported. Figure 4 shows the results. This new prediction is quite accurate.

Therefore the observed discrepancies in the nylon-phenolic cases were ascribed to surface heat flux errors, and the nominal in-depth properties cited in Appendix A were deemed adequate.

3.2.1.2 Avcoat 5026-39 HC/G

Figures 6, 7, and 8 show the first run results for three Avcoat test cases. In the low heat flux case 66 (Figure 6) the thermocouple predictions are somewhat low but char thickness is overpredicted. Case 62 (Fig. 7) appears to show a similar results, although the results are somewhat confused by what appears to be a faulty second thermocouple. This thermocouple is at the final char depth, but shows a final temperature of 2400°R, far above the 1100°R to 1400°R temperatures expected near the pyrolysis zone. Furthermore, a reference to the CHAP I output listings for all these runs shows that the predicted pyrolysis plane temperature is at about 1100°R, which is at the lower bound of the pyrolysis data reported in Reference 3. Apparently the assumed pyrolysis kinetics were too

fast, and it was desired to change these to place the CHAP I pyrolysis plane at about 1400°R. Revised pyrolysis kinetics were estimated by fixing the activation energy B and adjusting the pre-exponential factor A to yield a higher pyrolysis temperature. For estimation purposes, it was assumed that

$$T_{pyrolysis} \sim B/\ell nA$$

so that

$$\frac{T_{pyrolysis\ 2}}{T_{pyrolysis\ 1}} = \frac{\ell nA_1}{\ell nA_2}$$

Solving $T_{pyrolysis\ 1}$ equal to the observed prediction value of 1100°R for A_1 = 1.28×10^5 lb/ft^{2}sec and $T_{pyrolysis\ 2}$ equal to a more desirable value of 1400°R yields $A_2 = 1.03 \times 10^4$ lb/ft^{2}sec. These revised pyrolysis kinetics will yield thinner predicted char layers and higher thermocouple predictions. Preliminary calculations indicated that thermocouple predictions would in fact be unacceptably higher. These could be revised downward by changes in the char and virgin material thermal conductivity functions, and by changes in the pyrolysis gas specific heat $\bar{C}_p$. Additional preliminary calculations showed that changes in $\bar{C}_p$ values had a very strong effect on predicted thermocouples. Furthermore, the value of $\bar{C}_p$ = 1 Btu/lb°R used in the first calculation seemed substantially lower than computed equilibrium values for $\bar{C}_p$ as reported for Avcoat in Reference 5. Figure 9 shows the enthalpy data given in Reference 5, which were computed with condensed phase carbon excluded as a possible equilibrium product, and the specific heat data derived from it.

Figures 10, 11, and 12 show the results of new predictive runs with the new $\bar{C}_p$ function of Figure 9 and the reduced pyrolysis kinetics (Runs 62-4, 66-3 and 92-3). Cases 62 and 66 are improved over the results shown in Figures 6 and 7 but they still show substantial underpredictions of the responses of the thermocouples nearest to the heated surface. In the high heat flux Case 92 (Fig.12) all thermocouple responses were still substantially overpredicted. The revised pyrolysis kinetics shifted the CHAP pyrolysis line to a temperature of about 1400°R $\pm$ 50°R in all cases. These slower kinetics served to offset the increase in thermocouple temperatures so that the predicted char thicknesses remain about the same. Figure 13 shows a new case run with the same properties (Run 52-1). Case 52 (Figure 13) shows an excellent prediction.

It was desired to obtain a further improvement in Cases 62 and 66 before dealing with the apparently pathological Case 92. Both cases 62 and

66 have low surface temperatures ($\sim$3000°R). It was hypothesized that the equilibrium $\bar{C}_p$ used in the calculations was invalid at low temperatures, due to chemical kinetic effects, and that a frozen model would be more appropriate. A temperature of 3500°R was selected as the "freezing temperature". A frozen $\bar{C}_p$ of 0.9 Btu/lb was selected as (1) appearing likely (based on hand calculations) to produce a satisfactory prediction, and (2) consistent, as well as could be estimated, with a frozen specific heat of the actual mixture of molecules believed to be produced by the pyrolysis of phenolic (which is chemically similar to the epoxy-novolak in the Avcoat material). Figure 9 shows the frozen/equilibrium $\bar{C}_p$ model and the associated enthalpy functions.

All cases were re-run with the new $\bar{C}_p$ function. For Cases 62 and 66, the results are shown as Runs 62-4A and 66-4 on Figures 11 and 10. The improvement is substantial. However, Case 52 (Fig. 13) showed some damage to the deeper thermocouple predictions, although the overall prediction is still within the criteria. In Case 92 (Fig. 12) the thermocouple predictions were moved substantially in the wrong direction. The first thermocouple prediction is still quite acceptable, however. The deeper thermocouples are marginally acceptable.

It is not apparent from these runs that the frozen/equilibrium $\bar{C}_p$ model can be preferred over the equilibrium model. A case could be made that in the calculations with the frozen/equilibrium model there is too much energy transfer through the material in the 2500°R to 3500°R band. The relative overprediction of the second thermocouple in Figs. 11, 12, and 13 should be noted. Therefore it may be worth changing the transition temperature from frozen to equilibrium pyrolysis gas to 3000°R or to 2500°R, or, for simplicity, selecting the equilibrium $\bar{C}_p$.*

*Valuable insight into the choice of the pyrolysis gas enthalpy function can be obtained from the CHAP II code, which computes the detailed history of the pyrolysis gases as they pass through the char layer. To illustrate this point, Case 64 was run with CHAP II with the following assumed initial pyrolysis gas composition, which is elementally consistent with an assumed elemental composition C_6H_6O for the epoxy-novolak and with the assumed virgin and char densities:

Species	Mole Fraction
H_2	.355
CH_4	.071
C_6H_6	.146
H_2O	.177
CO	.251

For this assumption, the results indicated that the pyrolysis gas species CH_4 and C_6H_6 cracked even at low temperatures to yield carbon deposition and a pyrolysis gas of some 90 mole percent H_2 with a specific heat of about 2 BTU/lb°R in the 3000°R to 4000°R range. Further studies with CHAP II could obviously be quite useful in defining the correct pyrolysis gas specific heat, but such studies were beyond the scope of the effort reported here.

One must also consider the possibility that errors in reported heat flux are clouding the picture. To illustrate this possibility, Case 66 was rerun with a heat flux value assumed at 20% higher than the reported value, which, as discussed in Section 3.2.1.1 above, is about the maximum error which could be expected. Figure 10 shows that the effect is substantial.

In general, char thicknesses are somewhat overpredicted. These slightly high values of predicted char thicknesses prompted a brief study to determine whether still slower pyrolysis kinetics could be used. The pyrolysis constants reported in Reference 3 were converted to CHAP input constants by the method of Appendix A of that report. The pyrolysis constants computed indicated that the revised pyrolysis constants noted above are about the slowest kinetics that can be justified by the reported data.

As a further exploration of char depth predictions, the reported data of Reference 5 from which all of the Avcoat test cases are taken were restudied. The "char depths" reported in Ref. 5 were located by visual identification of a qualitatively defined blackness. The "pyrolysis zone depth" was located by a perceptible change in hardness. Cross correlating the reported char and pyrolysis depths with the predicted temperature profiles of Figure 9-51 of Ref. 5 reveals that the reported char depths correspond to a maximum temperature attained of about 2000°R$\pm$ 200°R. The pyrolysis line did not correlate well, being observed at 1100°R (which seems accurate) in one case and at 1700°R in the second case. It would seem indicated to compare CHAP predicted char depths to either the "pyrolysis depths" of Ref. 5 or to the average of the char and pyrolysis depths for the tests of Ref. 5. It is unfortunately impossible to resolve this matter more closely without extensive correlation studies between reported in-depth temperature profiles and reported char and pyrolysis depths for the cases of Ref. 5.

Therefore the overpredictions of char thickness in Cases 52, 62, and 66 are ascribed to the inherent difference between the meaning of the CHAP pyrolysis line on the one hand and the definitions of test char and pyrolysis thicknesses on the other, as described above. To aid in the assessment of this affect, the "pyrolysis thickness" noted by Schaefer, et al., in Ref. 5 has been added to the tables of Figures 10 through 12. The char thickness predictions of Cases 52, 62, and 66 are quite close to the "total pyrolysis layer" observations of Ref. 5.

Case 92 (Figure 12) remains to be discussed. All in all, the prediction is objectionably high, although the criteria of Section 3.1.2 above are marginally met. To explore whether certain changes might improve the predictions, two additional runs were made. The first, 92-4, delayed the amount of recession

by 3 secs, duplicating an induction time often observed in tests and harmonious with the initial surface temperature transient. The second (92-5) used a heat flux reduced by 20%. Figure 12 shows that both of these effects are large, but neither in itself explains the discrepancy between prediction and data. The implications of the frozen/equilibrium pyrolysis gas model were discussed above.

All in all, the Case 92 predictions are marginally acceptable. It is believed that all the following factors are playing some role in causing the mismatch of data and predictions:

- A delay of several seconds in initiating recession; this effect is relatively large in this high heat flux, high recession rate case
- A possible overstatement of the heat flux
- Possible response lag of the thermocouples

It was concluded that the final Option 2 predictions for runs 62-4, 66-3/5, and 52-1 are adequate for Avcoat and confirm the revised in-depth properties. The recommended properties may be summarized as follows:

Virgin and char densities, specific heats, conductivities	Nominal (see Appendix A)
Pyrolysis kinetics	Activation energy as in Appendix A, pre-exponential factor reduced from 1.28×10^5 to 1.03×10^4 lb/ft^2sec (moving pyrolysis plane temperature from about 1100°R to about 1400°R)
Pyrolysis gas specific heat	Changed from nominal value of 1 Btu/lb°F to the equilibrium model of Figure 9

3.2.1.3 Silicone Elastomer

Figure 14 shows the results for the low heat flux in Case 12. The data showed approximately 50 mils (net) of char swell. Although CHAP I will accept the input of "positive recession", it is not possible to compute meaningful thermocouple responses in this manner since

- inappropriate energy terms will appear in the surface energy balance
- the thermocouples will not be assumed to be displaced with the local surrounding material, but will remain fixed relative to the back wall

Therefore, the computer run was made with zero recession. The first thermocouple prediction does not agree well with the data, which evidently are faulty in this case. The deeper thermocouples look more believable. In particular, the second thermocouple response, extrapolated to the final test time, agrees well with the expected pyrolysis temperatures reported in Reference 3, as it should since it is located very near the final pyrolysis depth.

Figure 15 shows the results for the somewhat similar Case 1. Here again the results are confused somewhat by char swell, which caused the surface to "grow" 52 mils rather than to recede. This case, like Case 12, was run with zero recession. The results are satisfactory even without attempts to correct for char swell. Since the thermocouple data for this case look quite good, an attempt was made to correct for the effects of char swell. Temperature profiles were plotted and "translated" by hand-plotting to allow approximately for char swell effects with the assumption that thermocouples in the char are displaced with the surrounding material. The results of this approximate correction are also shown in Figure 15; they suggest that the prediction is a very good one.

Figure 16 shows the results for Case 4, a much higher heat flux case. The first thermocouple is obviously faulty after entering the pyrolysis zone at about 1000°R. The reported depth of this thermocouple places it in the pyrolysis zone at the final time; this is inconsistent with a reported final temperature of 2200°R. The prediction appears excellent except for the surface temperature, which again probably represents bad data.

Figure 17 shows the results of Case 5, representing a still higher heat flux case. The prediction is quite good in all respects.

It was concluded on the basis of these runs that the nominal in-depth properties seemed adequate for the silicone elastomer material.

3.2.2 Specified Environment (Option 1) Calculations

The second phase of the iterative calculations employed the in-depth properties determined in the first phase, as described in Section 3.2.1 above. Runs were made at specified pressure and heat flux, for the same cases used in the previous section. For this set of calculations, emphasis was placed on predicting surface recession.

3.2.2.1 Nylon-Phenolic

3.2.2.1.1 General Discussion

The first Option 1 runs for the nylon-phenolic employed the nominal in-depth properties selected in Section 3.2.1 above. The heat of combustion was the nominal table function presented in Appendix A. The surface oxidation kinetics were the (nominal) first order kinetics presented in Figure 1. The virgin density was set at 36 lb/ft^3. The char density was set at 15 lb/ft^3, which differs slightly from the (nominal) value of 12 lb/ft^3 cited in Appendix A but which closely matches the reported data of the test cases in Reference 3.

Figures 18, 19, and 20 show these first results as Cases 21-3, 19-6, and 16-4. In two cases surface recession is markedly underpredicted: no recession is predicted for Case 21 (compared with data of 107 mils) and for Case 19, the recession is low by a factor of three. Although these underpredictions could stem from various causes, the most likely candidate is an inappropriate choice of oxidation kinetics. Cases 21 and 19 were re-run with "Scala fast" kinetic values (A_c = 6.73 x 10^8, B_c = 39875°R, n = 1/2); the results are shown as Figures 18 and 19 as runs 21-4 and 19-8. Run 21-4 is in every respect a good prediction. To explore the question of whether heat flux variations of the magnitudes discussed in the Option 2 discussion of Section 3.2.1.1 could be affecting the conclusions here, Case 21 was re-run with the first order nominal kinetics but with a 20% higher heat flux. The results are indicated in Figure 18 as Run 21-5 and show that a heat flux variation of this magnitude is far from sufficient to cause the observed recession to be predicted.

Case 19-8 (Fig. 19), even with the fast kinetics values, still substantially underpredicts the recession; this is conjectured to be due to too low a value of heat flux. The importance of this effect was explored in the earlier run 19-7 (with nominal kinetics) which increased the erosion by 60% from 22 mils to 35 mils. The same increase applied to the "Scala fast" prediction would yield 64 mils recession, an acceptable prediction. (A computer run was not made for economy reasons.)

Case 16 was also restudied with "Scala fast" kinetics, but since the recession was already overpredicted in this case, the heat flux was simultaneously reduced by 20%, a change believed of interest from the Option 2 study. The resulting prediction, shown as Figure 20, is excellent. The char thickness is slightly overpredicted, but another test run at the same conditions (Case 17) showed 115 mils char thickness, so that the prediction seems within range of measurement errors in this case.

3.2.2.1.2 Comparison With Limiting Values

Since the nylon-phenolic char surface is simply carbon, it is possible to estimate rather simply the diffusion limited steady state recession rates for these cases. Applying this recession rate for the entire test time yields an interesting upper bound limit for the expected surface recession. Observed recession should be below this value by varying amounts in each case due to initial transient effects. Such calculations are shown in Table 3.

TABLE 3

NYLON-PHENOLIC RECESSION RESULTS

Case	ΔS (mils)			Conjectured q_c Error
	Observed	Scala Fast Prediction	Steady State Limit	
21	107	92	118	negligible
19	73	40	58	low by about 10%
16	137	127*	183	high by about 10%

*at $.8q_c$

Table 3 indicates that the steady state results harmonize with the conjectured heat flux errors, although an extensive study of the predicted results to break out the initial transient effects would be required to explore this matter fully.

3.2.2.1.3 Conclusions

For nylon-phenolic, the nominal oxidation kinetics are too slow and should be replaced by "Scala fast" kinetics. All three iterative cases are satisfactorily predicted provided that it is assumed that the reported heat flux for Case 19 is about 10% too low and that the reported heat flux for Case 16 is about 10% too high. Since this is within the range of experimental heat flux measurement accuracy, it is felt that the predictions are accurate.

3.2.2.2 Avcoat 5026-39 HC/G

3.2.2.2.1 General Discussion of Initial Runs

The first Option 1 runs for Avcoat 5026-39 HC/G used the in-depth properties selected after the iterative Option 2 runs discussed in Section 3.2.1.2 above, except that for the first iterative calculations the pyrolysis gas specific heat was taken from the frozen/equilibrium model presented in Figure 9 rather than the straight equilibrium model.

The heat of combustion was taken as the carbon heat of combustion table presented in Appendix A. Thus the basic thermochemical ablation model for Avcoat is the oxidation of carbon. The silica in effect, runs off, with no energy term associated with the melting. The blowing parameter of the char, α_c in Equation (12), is 0.5. The virgin density was set at 31 lb/ft^3 as reported for the test data in Reference 3. The char density was set at 18 lb/ft^3, which closely approximates the average reported for the test specimens in Reference 3.

Table 4 summarizes these first Option 1 recession prediction results. The most significant feature of these results is the extreme recession underprediction of Cases 62 and 66 and 52. Some underprediction had been anticipated for Cases 62 and 66, since it was one of the many Schaefer (Ref. 5) cases known to be well above steady state carbon ablation theory. Nevertheless, the underpredictions of Cases 62 and 66 are much larger than had been expected from a study of the Schaefer data. Case 83, on the other hand, is substantially overpredicted, while Case 92 shows an excellent prediction.

The pyrolysis penetration results are quite good, especially when the predictions are compared with the deeper of the two penetration data points, ΔP_2 of Ref. 5, obtained by adding the recession, the char thickness, and the pyrolysis zone thickness.

The following subsections discuss each of these results in detail.

3.2.2.2.2 Detailed Discussion of Subsequent Runs

Case 66

Figure 21 shows the Case 66 results. Run 66-06 was made with the frozen/equilibrium $\bar{C}_p$ model. In explaining the discrepancy between data and prediction for Run 66-06, it is of interest to compare the prediction to a steady state carbon oxidation plateau result, which may readily be computed by hand. We have

TABLE 4

INITIAL AVCOAT OPTION 1 PREDICTION RESULTS

Case	q_c $\left(\frac{BTU}{ft^2 sec}\right)$	h_e $\left(\frac{BTU}{lb}\right)$	p (atm)	τ (sec)	$T_{obs.}$ (°R)	$T_{pred.}$ (°R)	$\Delta S_{obs.}$ (mils)	$\Delta S_{pred.}$ (mils)	$\delta c_{obs.}$ (mils)	$\delta c_{pred.}$ (mils)	$\Delta P1_{obs}$ (mils)	$\Delta P2_{obs}$ (mils)	ΔP_{pred} (mils)
62	91	10,500	.008	90.2	3280	3402	137	35	130	347	267	327	382
83	115	3,692	.029	90.0	3500	3540	241	329	125	208	366	416	537
66	117	10,976	.028	30.8	4100	3450	96	25	100	196	196	236	221
52	215	10,445	.029	60.3	4370	4410	215	64	160	348	375	415	412
92	560	10,588	.080	39.6	4820	5260	388	345	80	166	468	488	511

$$\dot{S} = \frac{\dot{m}}{\rho} = \frac{B'(\rho_e u_e C_H)}{\rho} = \frac{B'_{C*}\rho_e u_e C_H}{\rho_{C*}} \tag{16}$$

where

$$\rho_e u_e C_H = \rho_e u_e C_{H_o} \frac{\ell n(1 + B')}{B'} \tag{17}$$

and

$$B' = B'_{C*} \frac{\rho_v}{\rho_{C*}} \tag{18}$$

Selecting B'_{C*} equal to the plateau value 0.174, and ρ_v = 31 lb/ft^3*, ρ_{C*} = 1/2(18) = 9 lb/ft^3, we obtain

$$\dot{S} = 206 \frac{\text{mils}}{\text{sec(lb/ft}^2\text{sec)}} \rho_e u_e C_{H_o} \tag{19}$$

This yields a recession prediction of 68 mils, compared with the CHAP prediction of 41 mils. This shortfall from the plateau value is due to three effects. First, at the final time, the predicted surface temperature is 3450°R, which puts the ablation rate in the kinetically controlled regime.** In fact, B'_{C*} is about 0.14 or about 80 percent of the plateau value of B'_{C*}. Secondly, this B'_{C*} does not translate into anything approaching the steady state recession rate because the convective transfer coefficient is greatly reduced due to "excessive" pyrolysis gas blowing. At the final time, CHAP predicts

$$\dot{m}_c = 0.00203 \text{ lb/ft}^3 \tag{20}$$

$$\dot{m}_p = 0.00502 \text{ lb/ft}^3 \tag{21}$$

*Here we have let the silica component be effective in blocking, which is not consistent with the CHAP ablation model for Avcoat, but the discrepancy is not large.

**Case 66 was selected with this possibility in mind.

The ratio $\dot{m}_p/\dot{m}_c$ is 2.48, far above the steady state value of (31-18)/18 = 0.722. The mass flux at the final time causes the blowing reduction ratio to be about 0.70, whereas in the steady state it will be about 0.78. At earlier times the difference is of course even greater, leading to a greater suppression of surface recession rate. A detailed study of the output indicates that about a 50 percent to 60 percent increase in average transfer coefficient would be obtained if the pyrolysis gas were not effective in blockage. Predicted recession would rise even more due to increased surface temperatures when recession is in the kinetically controlled regime.

Therefore a substantial improvement in the prediction could be achieved by bringing it closer to the steady state value. This could be accomplished to some extent with faster oxidation kinetics. A second change of interest would be to remove the pyrolysis gas as an effective blocking agent. This would obviously have a powerful effect on the prediction, as noted above, not only bringing it closer to steady state but substantially increasing the steady state recession rate. Less obvious is the justification for this lack of blockage effectiveness, although if the test model chars cracked and the pyrolysis gases passed preferentially up the cracks, then it is evident that the convection blockage due to the "slot injection" of pyrolysis gases would be quite small. In fact, most of the Schaefer models were cracked (although these cracks may have developed during post-test cooling). Bartlett and Anderson carried out an extensive study of the Schaefer data using very general thermochemical ablation models and showed that this "non-blockage" or fissure model for the pyrolysis gas allowed a good correlation of the Schaefer data (Refs. 6, 7).

To explore these possibilities, Run 66-8 was made with the pyrolysis gas blocking effectiveness entirely suppressed ($\alpha_p = 0$),* while Run 66-9 used the normal pyrolysis blockage model but employed Scala fast kinetics. Figure 21 shows all the results, which are about as hypothesized. The fissure model led to a substantial increase in surface temperature which damaged the thermocouple predictions. If this model were to be adopted, the Option 2 study would need review.

The combination of both models would undoubtedly allow the predicted recession to reach the observed value. A further discussion of this possibility must be deferred pending a discussion of other results.

---

*A truly consistent fissure model would also employ an adjusted $\bar{C}_p$ function to minimize energy pick-up by the pyrolysis gases as they pass through the char.

Case 62

The first Tab 62 prediction (Run 62-5) shown in Figure 22 displayed features quite similar to the first Tab 66 prediction. At the final time the normalized char ablation rate B'_c has reached only 68 percent of the plateau value and recession is suppressed still further by pyrolysis gas blowing far in excess of the steady state value. As with Tab 66, an additional run was made with Scala fast kinetics and one further run was made with the pyrolysis gas blockage effect suppressed. The results were comparable to those obtained for Tab 66 (see Figure 21).

Case 52

Case 52, not illustrated, has a test stream oxygen content of 7 percent and represents a considerably higher heat flux condition than Cases 66 and 62 discussed above. A detailed study of the output reveals that the predicted normalized recession rate B'_c of the first run (52-2) reaches the plateau quickly. Furthermore, the blowing reduction (blockage) is smaller in this case than in the others due to the relatively high transfer coefficient. A detailed study of the output indicates that the same computational experiments tried for Cases 62 and 66 would yield only about 10 percent recession increases.

Interesting insight into Case 52 is obtained from Reference 5, which discusses the effect of test stream oxygen mass fraction. It is seen that the data from the series from which Case 52 is taken do not extrapolate to zero recession at zero oxygen content, and that Case 52 lies far above a line passing through the air data with a slope proportional to C_e.

Therefore it is hardly surprising that the CHAP code, based on oxidation theory, underpredicts Case 52 by a considerable amount. The role of nitrogen in the chemical ablation of Avcoat in reduced oxygen environments has never been adequately explained. Therefore Case 52 was a poor choice for an iterative case for the CHAP study, and the results should be ignored.

Case 83

In contrast to the three cases discussed above, the recession in Case 83 is overpredicted (Figure 23). This is a high transfer coefficient, low enthalpy case. Detailed study of the CHAP output shows that at the final problem time the ablation has reached quite steady conditions and the normalized recession B'_c is at 84 percent of the carbon plateau value, well down into the kinetically controlled regime. Clearly, increasing the oxidation kinetics and/or introducing the fissure model for the pyrolysis gas blockage would increase the amount of overprediction.

Case 92

Case 92 is a high heat flux case. The recession is fairly well predicted. The thermocouple predictions of Figure 24 show a time shift similar to that observed in the Option 2 runs. A detailed study of the output shows that the prediction quickly approaches steady state conditions.

3.2.2.2.3 Summary Discussion

The ablation model used in the CHAP Option 1 runs treats the ablation of Avcoat as char carbon oxidation by the oxygen in the environment gases. The silica component of the char in effect "runs off" as the carbon is oxidized.

The data of Cases 66 and 62 are not consistent with this model, the surface recession being excessive in both cases. In Case 66, the recession is even greater than could be accounted for by a steady state ablation rate applied during the entire problem time.

It would be possible to force the CHAP predictions to match the data by selecting the input parameter λ of Equations (4), (6), and (9) appropriately for each case. However, the cases considered are not numerous enough to allow a believable $\lambda(T,p)$ function to be defined. Furthermore, Cases 66 and 83 conflict in this regard, having substantially the same p and (predicted) T but requiring very different λ values.*

An alternative device which would allow better predictions of Avcoat recession would suppress the blockage effectiveness of the pyrolysis gas. This is the "fissure model" of Bartlett and Anderson (Refs. 6, 7), which was effective in correlating all of the Schaefer air data. However, this is only one possibility of many thermochemical models which could be suggested, and the evidence is hardly strong enough to recommend this model over other possibilities. Furthermore, this model would apparently require some changes in the Avcoat property values determined during the Option 2 studies reported earlier.

The low temperature ablation of Avcoat is evidently more complex than envisioned when the basic plan of attack of this study was formulated. A limited number of iterative cases are not adequate to define CHAP input constants with sufficient clarity. It was concluded, therefore, that the Scala fast carbon oxidation kinetics should be selected as a nominal set and that the final calculations should be undertaken without the benefit of the kind of resolution that was obtained for nylon-phenolic and the silicone elastomer (discussed below).

*The situation is not so bad for p and observed T, but it is not clear that the observed T can indeed be predicted in these particular cases.

3.2.2.3 Filled-Silicone Elastomer

3.2.2.3.1 General Discussion

The first Option 1 runs for the silicone elastomer employed the nominal in-depth properties (determined to be adequate by the Option 2 studies reported in Section 3.2.1.3 above and the nominal surface oxidation kinetics ("Scala fast"). The heat of combustion is taken as the carbon heat of combustion function given in Appendix A. The value λ in Equations (4), (6), and (9) was taken as the nominal value 0.1, which reflects the observed fact in earlier unreported NASA Langley Research Center Studies that at low heat fluxes the silicone elastomer material appeared to show a "depressed" carbon-oxidation behavior. This was rationalized as due to partial coverage of the surface by silica.

The virgin material density was set at 33.5 lb/ft^3 as reported in Reference 3. The char densities reported in Reference 3 varied over a considerable range from about 12 lb/ft^3 to 19 lb/ft^3. Most of the cases considered here showed char densities close to 16 lb/ft^3, however, and this value was selected for all runs. Since the melt temperature option was not included in the version of CHAP used in this study, melting was simulated with a "steep" sublimation curve, with sublimation rate to rise from a very low value at $T_m-\Delta T$ to a very high value at $T_m+\Delta T$. The initial runs used T_m = 3800°R and ΔT = 200°R.

Figures 25 and 26 show the results for Case 1 (Run 1-2) and Case 4 (Run 4-2). Run 1-2 is a satisfactory prediction considering that char swell obscures the recession prediction. Although no quantitative data are available on char swell, the observed surface growth of 52 mils is about 25% of the observed char thickness, which is a believable amount of swelling. Run 4-2 predicted some melting, with a predicted recession of 60 mils, compared with an observed negligible recession. The observed char thickness of 121 mils is perhaps a little low to allow the difference between predicted and observed recession to be attributed to char swell, calling for a swell equal to 50% of the char thickness. Tentatively, however, this prediction could be accepted. An additional run was made with melting suppressed ($T_m = \infty$) to check the adequacy of the prediction with no melting. Figure 26 shows the result as Run 4-3. It is an excellent prediction.

Case 5, which showed a high rate of melt in the prediction, ran so slowly that the prediction was not allowed to continue until the final time, particularly since the recession prediction was going to be excessively high (340 mils, compared with test data of 70 mils). Subsequent runs were made with various higher melt temperatures to improve this prediction. Table 5 summarizes the results.

TABLE 5

SUMMARY OF MELT TEMPERATURE RUNS, SILICONE ELASTOMER, CASE 5

Test	5-2C	5-3	5-5	5-6
T melt (°R)	3800	∞	4100	4300
Melt Range (°R)	±200	---	±400	±400
A_s (lb/ft²sec)	1.5×10^{35}	0	3.162×10^{18}	3.162×10^{19}
B_s (°R)	331,632		191,720	211,046
Recession (in.)	.070	.340*	.026	.237	.172
Char δ (in.)	.117	.030	?	.034	.048
Final T_w (°R)	4300	3890	4850	4070	4250

*extrapolated

It is apparent from this study that the melt temperature apparatus will not yield an acceptable prediction for Case 5 unless the melt temperature is chosen somewhere above 4500°R. This does not seem to be an acceptable ablation model for the silicone elastomer material. Ref. 8, which was published after the data survey of the Task I Final Report (Ref. 3), reports an empirical mass loss model for this material which differs from the melting model:

$$\dot{m}_c = \rho_c \frac{\Delta L}{\Delta t} = 20.79 \left(\frac{p}{r}\right)^{0.28} e^{-16117/T} \quad \begin{cases} T \text{ in } °K \\ p \text{ in atm} \\ r \text{ in m} \\ \Delta L \text{ in m} \\ \Delta t \text{ in sec} \\ \rho_c \text{ in kg/m}^3 \end{cases} \tag{22}$$

If we assume from Reference 8 that

$$q \sqrt{\frac{r}{p}} = K(h_e - h_w) \tag{23}$$

and hence that

$$q_c \sqrt{\frac{r}{p}} \simeq K h_e \tag{24}$$

then with (24) we can eliminate p/r in (22) and obtain

$$\dot{m}_c = \frac{20.79}{K^{.56}} \left(\frac{q_c}{h_e}\right)^{.56} e^{-16117/T} \tag{25}$$

If we substitute K = .0461 $lb/ft^{3/2}$ sec $atm^{1/2}$ from Ref. 9 into Equation (25) and change the units to the English system, we have

$$\dot{m}_c = 33.3 \frac{lb}{sec\ ft^{1.72}} \left(\frac{q_c}{h_e}\right)^{.56} e^{-\frac{29011°R}{T}} \tag{26}$$

This form may be used directly in the CHAP program by suppressing oxidation entirely and setting the sublimation constants as

$$A_s = 33.3 \left(\frac{q_c}{h_e}\right)^{.56} \quad lb/ft^2 sec \tag{27}$$

$$B_s = 29011°R \tag{28}$$

Cases 1, 4, and 5 were re-run with this input model; the results are indicated on Figures 25, 26, and 27 as Runs 1-3, 4-4, and 5-7. Cases 1 and 4 show considerably more recession with the new model, but still not so much that char swell could not make up the difference between prediction and observation. It should be noted, however, that both the predicted and measured temperatures for these two cases are below the lower limit of the data (4250°R) used by McLain in Ref. 8 to obtain the empirical recession correlation employed in these predictions. In Case 5 the new model overpredicts the recession by a factor of two. This discrepancy is barely within reach of a char swell explanation. The assumed (input) char density corresponded to the reported char density of 16 lb/ft^3. If the "actual" (unswelled) char density were 20 lb/ft^3, the recession would be (very roughly) 25% less, and then char swell to 16 lb/ft^3 would reduce the observed recession another 25%. The net effect would apparently be a fairly accurate prediction.

Evidence that char swell actually occurs has previously been noted in the discussion of Cases 1 and 4. Additional evidence may be derived from Run 5 together with runs at the same test condition but for different run times. Models SP30 and SP32 from the Langley AMPD test series of Ref. 10 (not included in the tabulation of Ref. 3) show an interesting relationship to Case 5, as shown in Table 6.

TABLE 6

COMPARISON OF THREE SILICONE ELASTOMER TESTS AT SAME TEST CONDITIONS

Tab	Run	Run Time (sec)	Recession (in)	Char δ (in)
---	SP30	14	+.004	.097
5	SP93	30	.070	.117
---	SP32	60	.214	.097

These results are plotted in Figure 28, which shows that the observed recession appears to be affected by char swell in this series of tests, perhaps by as much as 70 mils.* Additional evidence suggesting char swell is provided by the wide range of observed char densities in the tabulations of Ref. 3, which range from 11.6 lb/ft^3 to 19.1 lb/ft^3, with no correlation of char density with test conditions.

It appears that the three iterative cases 1, 4, and 5 are influenced by char swell. Although it is not possible quantitatively to allow for swell in CHAP predictions (since (a) the program cannot account for it, and (b) no quantification of swell is available), approximate allowances for swell suggest that the predictions are acceptable. For an additional check, predictions were made for two additional cases showing a large amount of recession compared with char thickness. Table 7 summarizes the prediction results for recession and char thickness (no temperature data are available for these runs).

TABLE 7

DATA AND PREDICTIONS FOR TWO HIGH HEAT FLUX SILICONE ELASTOMER CASES

		Test			Prediction		
Tab	Run	Recession (in)	Char δ (in)	ρ (lb/ft^3)	Recession (in)	Char δ (in)	ρ_c (input) (lb/ft^3)
6	6-1	.082	.049	14.2	.125	.028	16.0
7	7-1	.412	.022	18.1	.356	.029	16.0

*Initial effects make a straight extrapolation to zero time invalid, so it is impossible to separate the effect of char swell alone.

As hoped, the predictions for three cases are much closer to the data. However, discrepancies between observed and predicted recession are still significant and Case 6 is not within criteria for surface recession. Here again, however, char swell may be influencing the data to some extent; the reported char density for this case is low and the two observed recession amounts do not extrapolate to zero but to a net char swell at zero test time.

3.2.2.3.2 Conclusions

- For surface temperatures above 4200°R, the nominal low temperature recession correlation cannot be combined with any reasonable melt temperature to predict high heat flux recession amounts. The empirical correlation of McLain seems adequate for this range. The correlation studies of McLain indicate that his correlation should be good for cold wall heat fluxes above about 250 Btu/ft^2sec.

- Both the McLain model and the nominal model predicted satisfactorily for the cases examined below 250 Btu/ft^2sec provided that some allowance was made for the effect of char swell, which apparently confuses the data considerably. The nominal model appears superior in this range; however, it does not blend smoothly with the McLain model at temperatures corresponding to 250 Btu/ft^2sec and the available cases are not numerous enough to clarify this matter.

- Char swell cannot be quantified or correlated from existing data; therefore, it is extremely difficult to predict recession amounts in low heat flux cases unless the recession greatly exceeds the char thickness.

- In view of the difficulty of making accurate predictions at low heat fluxes, the McLain ablation model was chosen for all Final Calculations.

SECTION 4

FINAL CALCULATIONS

The Final Calculations represent one calculation of a number of test cases representing a wide range of environmental conditions. The chief points bearing on the selection of the additional (non-iterated) cases are

1. Coverage of a wide range of conditions
2. Straddling the nominal shuttle condition

Tables 8, 9, and 10 list the cases selected. The iterative cases are marked with an asterisk. The remaining runs are marked with a priority ranking. Priority 1 indicates that the case definitely was to be run in the Final Calculation. Priority 2 indicates either that the case is similar to other cases or was expected to run very long; these cases could be run if time and funds permitted. Priority 3 indicates that it was preferred to study this case with the slower running CHAP II Code if time and funds permitted.

4.1 NYLON PHENOLIC

4.1.1 Results

The nylon phenolic cases were run with the properties of Appendix A, except that the oxidation kinetics were revised to "Scala fast" values as a result of the Iterative Calculations described in Section 3.2 above. The virgin and char material density values were the same as for the Iterative Calculations: 35 lb/ft^3 and 15 lb/ft^3 respectively.

Table 11 summarizes the Final Calculation recession and char thickness results, and compares the recession results to a simple steady state prediction of the total recession based on the assumption that recession occurs in the steady state on the carbon plateau for the entire problem time. Figures 29-34 show the results for those cases not already a part of the iterative calculation. Figure 35 shows a $p\text{-}q_c$ map of all the nylon-phenolic cases and indicates the percent errors in recession and total pyrolysis penetration predictions by classifying the ratios of the calculated quantities to the measured quantities for each test as low (L), good (G), and high (H). Low means measured quantity underpredicted, good means prediction within the specified criteria, and high means measured quantity overpredicted. For example, in figure 35, perfect agreement would be indicated by 100% or G.

The most striking feature of the nylon phenolic results is that with only one exception the new (non-iterated) cases all show substantial underpredictions of recession. Furthermore, in most of these cases, the observed recession is in excess of the steady state prediction, whereas the CHAP prediction is somewhat below this limit, as it should be. Figure 35 shows that the shortfalls in recession prediction do not follow a clear pattern.

TABLE 8

CASE SELECTIONS - NYLON PHENOLIC

Priority	Tab. No.	Model Number	h_e (BTU/lb)	q_c $\left(\frac{BTU}{ft^2 sec}\right)$	p (atm)	Run Time (sec)	T_w (°R)	Recession / Char Thick. (in/in)	$\frac{ph_e}{q_c}$ $\left(\frac{atm\ ft^2 sec}{lb}\right)$	$\frac{p^{1/2}h_e}{q_c}$ $\left(\frac{atm^{1/2} ft^2 sec}{lb}\right)$	Remarks
2	3	PLL96	10,670	85	.0109	75.4	3500.	.107/.122	1.4	13.1	
1	7	PLH98	10,322	85	.0111	75.3	3500.	.115/.132	1.4	12.8	
1	12	PLL87	12,664	117.1	.00572	50.6	620.	.064/.117	0.6	8.2	Good Temperature Data
*	16	PLL93	4,900	256.	.284	30.0	4400.	.137/.099	5.4	10.2	High Heat Flux, High Temperature
*	17	PLH93	4,900	250.	.284	30.0	4400.	.119/.115	5.6	10.4	
1	18	PLL97	5,583	80.	.0204	60.5	3600.	.096 .126	1.4	10.0	
*	19	PLL90	10,200	145	.0199	34.7	4100.	.073/.159	1.4	10.0	Close to Nominal Shuttle Condition
1	20	PLH90	10,200	144.	.0199	34.9	3800.	.025/.135	1.4	10.0	
*	21	PLL91	5,140	43.	.0070	120.0	3200.	.107/.178	0.84	10.0	Low Heat Flux, Low Temperature
*	22	PLH91	5,180	44.	.0070	120.0	3100.	.078/.171	0.82	9.9	
1	23	PLL94	14,855	103.	.00511	50.0	3500.	.054/.124	0.74	10.3	
1	24	PLH94	15,035	98.	.00511	50.0	3400.	.049/.122	0.78	11.0	
2	33	---	3,000	113.	1.0	257.0	--	.721/.204	26.6	26.6	Good Temperature Data, High Pressure
2	36	---	3,000	93.	1.0	125.0	--	.283/.167	32.2	32.2	
2	37	---	3,000	114.	1.0	210.0	--	.610 .148	26.3	26.3	
2	42	13	3,550	198.	~1.0	292.0	--	.25/.70	17.9	17.9	

Priority: * Iteration Case
1 Final Case
2 Optional Final Case

TABLE 9

CASE SELECTIONS - AVCOAT 5026-39

Priority	Tab. No.	Model No.	h_e $\left(\frac{BTU}{lb}\right)$	q_c $\left(\frac{BTU}{ft^2 sec}\right)$	p (atm)	Run Time (sec)	T_w (°R)	Recession / Char Thick. (in/in)	$\frac{ph_e}{q_c}$ $\left(\frac{atm\ ft^2 sec}{lb}\right)$	$\frac{p^{\frac{1}{2}}h_e}{q_c}$ $\left(\frac{atm^{\frac{1}{2}} ft^2 sec}{lb}\right)$	Remarks
3	11	4	3,400	17.0	0.036	320.0	2500.	.06/.21	7.2	38.0	Low Heat Flux, Low Temperature
3	13	7	2,300	22.8	0.062	570.0	2400.	.25/.53	6.2	25.2	
3	20	46/FF/1.25	3,100	157.0	0.112	20.1	3800.	.07/.09	2.2	6.6	Higher Pressure at ∿ Same Flux as Tabs, 27, 41, 46, 100
3	27	39/FF/1.25	5,100	102.0	0.071	26.0	4100.	.081/.09	3.6	13.4	Lower Pressure Than Tab 20
3	35	95/BH/2	3,500	33.9	0.0082	120.3	2700	.076/.16	0.85	9.4	Low Heat Flux, Low Pressure
3	41	108/BH/2	16,300	155.0	0.0080	60.4	3600.	.147/.10	0.84	9.4	Moderate Heat Flux, Low Pressure
3	46	23/BH/2	5,800	151.0	0.0278	60.8	3800	.050/.21	1.1	6.4	Moderate Heat Flux ∿ Nominal Pressure, Nitrogen
*	52	82/BH/2	10,450	215.0	0.0290	60.3	4400.	.215/.16	1.4	8.3	Higher Heat Flux, ∿ Nominal Pressure
1	55	101/BH/2	17,400	313.0	0.0287	45.2	4600.	.215/.08	1.6	9.4	Still Higher Heat Flux, ∿ Nominal Pressure
*	62	128/BH/4	13,500	91.0	0.0081	90.2	3300.	.137/.13	1.2	13.4	Flux Between Tabs 35 & 41, Same Low Pressure
3	64	117/BH/4	4,600	56.0	0.0279	30.3	3300.	.026/.08	2.3	13.7	Low Flux, Same ∿ Nominal Pressure as Tabs 46, 52, 55
*	66	119/BH/4	10,976	119.0	0.0279	30.8	4100.	.096/.10	2.6	15.3	
3	69	25/BH/2	5,450	121.0	0.0270	45.6	3500.	.112/.12	1.2	7.4	Part of Same Pressure Sequence as Tabs 64, 46, 52
*	83	34/H/2	3,692	115.0	0.0289	90.0	3500	.241/.125	0.93	5.5	
*	92	111/BH/1	10,600	577.0	0.0817	39.6	4800.	.388/.08	1.5	5.2	High Heat Flux
1	94	31/H/2	10,400	505.0	0.0842	40.5	4800.	.338/.045	1.7	6.0	
1	95	129/BH/1	3,515	510.0	0.373	20.1	4800	.325/.04	2.6	4.2	
2	96	138/BH/1	3,515	510.0	0.373	15.4	4700	.247/.055	2.6	4.2	
3	100	364	3,515	145.0	0.0028	40.0	--	.074/.077	0.06	1.2	Low Pressure, ∿ Same Flux As Tabs 20, 27, 41, 46
1	109	501	5,420	250.0	0.50	9.9	3600	.059/.067	10.8	15.3	High Pressure
1	112	522	13,400	575.0	0.50	9.1	4300	.028/.022	11.3	15.9	High Heat Flux, High Pressure
2	113	523	13,400	595.0	0.50	4.0	4300	.035/.024	11.3	15.9	

Priority: * Iteration Case
1 Final Case
2 Optional Final Case
3 Low Flux Case, CHAP II Candidate

TABLE 10

CASE SELECTIONS - SILICONE ELASTOMER

Priority	Tab No.	Model No.	h_e $\left(\frac{BTU}{lb}\right)$	q_c $\left(\frac{BTU}{ft^2 sec}\right)$	p_w (atm)	Run Time (sec)	T_w (°R)	Rec. Char Thick. $\left(\frac{in}{in}\right)$	$\frac{ph_e}{q_c}$ $\left(\frac{atm\,ft^2\,sec}{lb}\right)$	$\frac{p^{1/2}h_e}{q_c}$ $\left(\frac{atm^{1/2}\,ft^2\,sec}{lb}\right)$	Remarks
*	1	SP96	10,700	62.9	.0109	75.5	2800.	+.052/.205	1.8	17.8	
*	4	SP89	19,700	221.0	.00847	25.0	3350.	.004/.121	0.76	8.2	
*	5	SP93	4,900	273.0	.284	30.0	4100.	.070/.117	5.1	9.6	High Heat Flux, High Temperature
1	6	SP29	9,700	481.0	.293	11.0	--	.082/.049	6.0	10.9	|
1	7	SP31	9,700	539.0	.293	30.0	--	.412/.022	5.3	9.8	
1	8	SP97	5,500	77.7	.020	100.7	2700.	+.025/.217	1.4	10.0	
1	9	SP90	10,200	145.0	.0199.	35.0	3500.	.004/.127	1.4	9.9	
1	10	SP3	10,100	66.0	.0041	32.7	--	+.036/.109	0.63	9.9	
*	12	SP91	5,200	44.2	.0070	120.0	2800.	+.048/.200	0.82	9.9	Low Heat Flux, Low Temperature
1	14	SP8	10,600	417.0	.139	17.0	--	.190/.032	3.5	9.5	

Priority:

* Iteration Case
1 Final Case
2 Optional Final Case

TABLE 11

FINAL CALCULATION RESULTS - NYLON PHENOLIC

Tab. No.	h_e $\left(\frac{BTU}{lb}\right)$	q_c $\left(\frac{BTU}{ft^2 sec}\right)$	p (atm)		T_w (°R)	Recession (inches)	Char Thickness (inches)	Pyrolysis Penetration (inches)
7	10,322	85	.0111	Test	3500	.115	.132	.247
				CHAP	3060	.049	.206	.255
				SS†	--	.063	--	--
12	12,664	117	.00572	Test	--	.064	.117	.211
				CHAP	3250	.035	.183	.218
				SS	--	.052	--	--
16	4,900	256	.284	Test	4650	.137	.099	.236
				CHAP	3800	.127*	.128	.255
				SS	--	.185	--	--
18	5,583	80	.0204	Test	3600	.189	.156	.345
				CHAP	3130	.140	.208	.348
				SS		.170	--	--
19	10,200	145	.0199	Test	4350	.073	.159	.232
				CHAP	3420	.040**	.156	.196
				SS	--	.058	--	--
20	10,200	144	.0199	Test	3800	.025	.135	.160
				CHAP	3540	.040	.156	.196
				SS	--	.082	--	--
21	5,140	43	.007	Test	3350	.107	.178	.285
				CHAP	2660	.092	.199	.291
				SS	--	.118	--	--
23	14,855	103	.00511	Test	3500	.054	.124	.178
				CHAP	3040	.022	.171	.193
				SS	--	.041	--	--
24	15,035	98	.00511	Test	3400	.049	.122	.171
				CHAP	2980	.021	.167	.188
				SS	--	.038	--	--

*q_c - 20%

**q_c believed low

†SS - steady state

It is noteworthy that predicted surface temperatures are considerably lower than observed temperatures. However, this has only a secondary effect on recession predictions since all cases studied are on the diffusion controlled carbon oxidation plateau during most of the problem time.

Failures to predict recession properly are to a large extent compensated in-depth by an overpredicted char layer thickness. The net effect is a generally excellent pattern of prediction success for total pyrolysis penetration, and quite good thermocouple predictions.

4.1.2 Discussion

The p-q_c map shown by Figure 35 does not indicate a consistent recession error pattern. Similarly, there is no obvious correlation of recession error with q_c and h_e, except that all the good predictions are at low enthalpies ($\sim$ 5000 BTU/lb) and all the low predictions are at enthalpies above 10,000 BTU/lb. There is, however, an interesting correlation of discrepancies between recession predictions and data with the degree of approach to steady state. The parameter $\dot{m}_p/\dot{m}_c$ provides a useful index of this approach. Detailed study of the CHAP output indicates that this ratio at the final time exceeds 4.0 for Cases 7, 12, 23, and 24. In all these cases the predicted recession is well below the observed recession. Furthermore, the steady state recession is noticeably below the observed recession in these cases. In contrast, Cases 16, 18, and 21 (we discount Cases 19 and 20 as being anomalous) have $\dot{m}_p/\dot{m}_c$ less than 2.75 at the final time and show good agreement between predicted and observed recession. Furthermore, for these Cases the observed recession is below the steady state recession except in Case 18, where it exceeds the steady state value slightly. This evidence suggests that the blowing correction (blockage) is too great for the pyrolysis gas, an effect which would be noticeable when most of the mass transfer represents pyrolysis gas. Thus this evidence tends to support a fissure model or some related model.

Finally, of course, it must be recognized that all the comparisons between data and experiment hinge upon the adequacy with which the test environment has been characterized. A careful attempt has been made in this work to select believable data. Nevertheless, the possibilities for errors remain large, particularly when test stream non-uniformities typical of arc tunnels are present. Case 12 presents an example of the possibilities. Reference 3 reports two enthalpies for this test differing by a factor of two. The higher one, based on a heat flux measurement, was chosen for the prediction because it was felt to represent the test location more accurately. However, had the lower value (presumably the bulk value) been chosen, the prediction would have been quite close.

Cases 19 and 20 present another interesting example, representing the same test condition and the same run time, but with observed recessions differing by a factor of three.

The CHAP code, as applied here to nylon phenolic, represents simple carbon oxidation. To the extent that observed recession data fall above a steady state plateau limit, the CHAP code will not predict observed recession without program changes. Possible new ablation models which might be explored are

- The fissure model, in which the pyrolysis gas is not effective in reducing convective heating and mass transfer (blockage). This model would raise CHAP surface tempeatures and recessions considerably.
- Mechanical erosion of char.
- Char shrinkage. Even a 10% shrinkage would be significant in some of the cases studied due to the relatively large char thickness compared with recession amounts.
- Test stream ingestion through a poorly sealed or cracked test model.

4.2 AVCOAT 5026-39HC/G

4.2.1 Results

The Avcoat runs were made with the in-depth properties of Appendix A revised according to the results of Section 3.2: slower pyrolysis kinetics and an equilibrium pyrolysis gas specific heat model shown in Figure 9. The surface oxidation kinetics were revised to the "Scala fast" values cited in Figure 2. The virgin material density was taken as 31 lb/ft^3. The char density was assumed to be 18 lb/ft^3.

Table 12 summarizes the Final Calculation recession and char thickness results. For most of the Avcoat runs a pyrolysis zone thickness was reported in addition to the char layer thickness; where available, this quantity is shown also. Figures 36-43 show the thermocouple results for those cases not already discussed and illustrated in Section 3.2. Figure 44 shows a $p\text{-}q_c$ map of the conditions studied and indicates the percent errors in recession and total pyrolysis penetration predictions.

4.2.2 Discussion

The Avcoat recession results are rather similar in pattern to the nylon-phenolic results, except there are several rather high predictions. The low heat flux cases show a particularly mixed pattern of success. As was the case for

TABLE 12

FINAL CALCULATION RESULTS - AVCOAT 5026-39HC/G

Tab. No.	h_e (BTU/lb)	q_c (BTU/ft^{2}sec)	p_w (atm)		T_w (°R)	Recession (inches)	Char Thickness (inches)	Pyrolysis Zone Thickness (inches)	Pyrolysis Penetration (inches)
27	5,100	102	.071	Test CHAP SS	4100 3870 --	.081 .075 .107	.090 .160 --	.020 -- --	.191 .235 --
41	16,300	155	.008	Test CHAP SS	3600 3840 --	.147 .075 .118	.100 .260 --	.070 -- --	.317 .335 --
46	5,800	151	.0278	Test CHAP SS	3800 4040 --	.050 .000 .033	.210 .330 --	.060 -- --	.320 .330 --
55	17,400	313	.0287	Test CHAP SS	4600 4780 --	.215 .127 .177	.080 .230 --	.040 -- --	.335 .357 --
62	13,500	91	.0081	Test CHAP SS	3280 3340 --	.137 .079 .125	.130 .281	.060 --	.190 .360
66	10,976	119	.0279	Test CHAP SS	4100 3460 --	.096 .041 .068	.100 .167	.040 --	.236 .208
83	3,692	115	.0289	Test CHAP* SS	3500 3540 --	.241 .329 .579	.125 .208 --	.050 -- --	.416 .537 --
92	10,600	577	.0817	Test CHAP* SS	4800 5260 --	.388 .345 .441	.080 .166 --	.020 -- --	.488 .511 --
94	10,400	505	.0842	Test CHAP SS	4700 5260 --	.338 .350 .406	.045 .132 --	.030 -- --	.413 .482 --
95	3,515	510	.373	Test CHAP SS	4800 4480 --	.325 .538 .602	.040 .034 --	.010 -- --	.375 .572 --
109	5,420	250	.500	Test CHAP SS	3600 4130 --	.059 .077 .094	.067 .082 --	-- -- --	.126 .159 --
112	13,400	575	.500	Test CHAP SS	4300 5310 --	.028 .064 .081	.022 .104 --	-- -- --	.050 .168 --

nylon phenolic, however, the low prediction Cases 41, 55, 62, and 66 are all strongly transient cases for which the pyrolysis gas evolution rate is excessive compared with the steady state value corresponding to char loss rate. Otherwise there is no appreciable pattern to the observed errors.

It is not really clear that the ablation for Avcoat is well described by a carbon oxidation model. Case 52, a 7% oxygen case, was predicted very poorly, as discussed in Section 3.2. Case 46 represents a pure nitrogen case. for which the CHAP prediction with an oxidation model is of course zero, whereas the observed recession is substantial.

Also as was the case for nylon phenolic, the total pyrolysis penetration predictions are better than the surface recession predictions, although for Avcoat the discrepancies are larger than desired.

4.3 SILICONE ELASTOMER

4.3.1 Results

The silicone elastomer runs were made with the in-depth properties of Appendix A, but with a revised surface mass loss law according to the findings of Section 3.2. Oxidation was suppressed and all mass loss was computed according to the McLain (Ref. 8) law using the sublimation constants of CHAP. The virgin material density was set at 33.5 lb/ft^3 and the char density was 16 lb/ft^3.

Table 13 summarizes the Final Calculation recession and char thickness results. Figure 45 and 46 show the thermocouple results for the two cases with thermocouple data which are not iterative cases already discussed and illustrated in Section 3.2. Figure 47 shows a $p\text{-}q_c$ map of the conditions studied and indicates the percent errors in recession and total pyrolysis penetration predictions.

4.3.2 Discussion

On the whole, the silicone elastomer recession amounts are not well predicted by CHAP I. In Cases 1, 4, 8, 9, and 10, this seems to be due to char swell. All these cases had recession amounts small compared with the char thickness, and a char swell of 25% of the observed char thickness would rationalize the discrepancies quite well. This is a believable amount of char swell for this material.

Cases 5 and 6, however, would require a much larger char swell (about 75% of the observed thickness) to rationalize the overprediction of recession, while Cases 7 and 14 are substantially underpredicted.

TABLE 13

FINAL CALCULATION RESULTS - SILICONE ELASTOMER

Tab. No.	h_e $\left(\frac{BTU}{lb}\right)$	q_c $\left(\frac{BTU}{ft^2 sec}\right)$	p_w (atm)		T_w (°R)	Recession (inches)	Char Thickness (inches)	Pyrolysis Penetration (inches)
1	10,700	63	.0109	Test CHAP	2800 3480	+.052 .021	.205 .172	.153 .193
4	19,700	221	.00847	Test CHAP	3350 4140	.004 .033	.121 .095	.125 .128
5	4,900	273	.284	Test CHAP	4100 4306	.070 .159	.117 .054	.187 .213
6	9,700	481	.293	Test CHAP	4790 4760	.082 .104	.049 .032	.131 .136
7	9,700	539	.293	Test CHAP	---- 	.412 .356	.022 .029	.434 .385
8	5,500	78	.020	Test CHAP	2700 3430	+.025 .042	.217 .184	.192 .226
9	10,200	145	.0199	Test CHAP	3500 3870	.004 .033	.127 .112	.131 .145
10	10,100	66	.0041	Test CHAP	3000 3090	+.036 .002	.109 .105	.073 .107
12	5,200	44	.0070	Test CHAP	2800	+.048 No Option	.200 1 Prediction	.152
14	10,600	417	.139	Test CHAP	4810 4670	.190 .127	.032 .041	.222 .168

Examination of the results in terms of p, q_c, and h_e indicates that the good predictions, that is, those which can be rationalized by assuming 25% char swell, are confined to heat fluxes of less than 250 BTU/ft^{2}sec, and pressures less than .02 atm. The high and low predictions share a common ground at high heat fluxes (roughly 300 to 500 BTU/ft^{2}sec) and high pressures (> 0.1 atm). There are no features evident which distinguish the conditions of the high prediction cases from those of the low prediction cases. That the good predictions are confined to heat fluxes below 250 BTU/ft^{2}sec is somewhat surprising, since the McLain surface recession correlation was developed only for data above this limit.

As was the case for nylon phenolic, inaccuracies in recession prediction are compensated for by opposite inaccuracies in char thickness predictions, so that total pyrolysis penetration predictions are fairly satisfactory. In Cases 4, 5, 6, 8, and 9 this prediction agrees with the data to within about 10%. Similarly, thermocouple predictions are on the whole quite good.

SECTION 5

CONCLUSIONS AND SUMMARY

The CHAP I code has been tested on three materials over a range of environmental conditions. The following subsections summarize the conclusions drawn about best material properties for program input and the range over which the code may be used with confidence in each case.

5.1 NYLON PHENOLIC

5.1.1 Properties

The material considered is defined on p. 2. The properties of Table A-1 of Appendix A were employed for nylon-phenolic, with the following changes:

Densities

The virgin material density was taken as 35 lb/ft^3. The char density was set at 15 lb/ft^3.

Heat of Combustion

This was changed from a constant value of 5000 BTU/lb to the tabular function presented in Table A-4.

Oxidation Kinetic Constants

These were changed from the Table A-1 values to

$A_c = 6.73 \times 10^8$ $lb/ft^2 sec\ atm^{1/2}$

$B_c = 39{,}875°R$

$n = 1/2$

5.1.2 Range of Applicability

Predictions were made in the following approximate ranges:

Enthalpy h_e (BTU/lb)	5000	to	15,000
Cold Wall Heat Flux q_c ($BTU/ft^2 sec$)	40	to	250
Pressure p (atm)	.01	to	.3

In Option 2 (specified heat flux and recession), char thicknesses, total pyrolysis penetration, and thermocouple responses were well predicted. Pyrolysis penetration (measured from the original surface location) was predicted to within ±10 percent and char thickness to within 25 percent. Thermocouple responses met the criteria of Section 3.1.2.

In Option 1 (specified heat flux, pressure, and enthalpy), recession was predicted to within 25 percent in only three cases, all remaining cases but one showing underpredictions of up to 70 percent of the observed recession. The good predictions were observed to be for problems which neared steady state; in strongly transient problems, recession was underpredicted. Pyrolysis penetration predictions for the Option 1 cases were excellent and were within 10 pcercent of the test value except in only two cases. Similarly, thermocouple predictions were good and met the criteria established in almost all instances.

5.1.3 Concluding Remarks

For the cases considered, the CHAP I code did an excellent job in predicting the pyrolysis penetration and thermocouple response in low density nylon phenolic. Recession predictions were good near steady state but poor for transient problems; this may be due to a faulty blowing reduction model during early problem periods when the conventional blowing reduction expressions cause substantial reductions in transfer coefficient due to the large amount of pyrolysis gas.

To obtain good recession agreements in low temperature cases it was necessary to increase surface oxidation kinetics from the nominal value to relatively fast kinetics. However, the values selected are merely literature values often used as reference values. The test data available are certainly not adequate to define the oxidation kinetics with any degree of accuracy.

5.2 AVCOAT 5026-39-HC/G

5.2.1 Properties

The material considered is defined on p. 2. The properties cited in Appendix A were used, with the following changes:

Heat of Combustion

This was changed from the constant value of 5000 BTU/lb cited in Appendix A to the tabular function presented in Table A-4.

Oxidation Kinetic Constants

These were changed from the Table A-3 values to:

$A_c = 6.73 \times 10^8$ lb/ft^{2}sec atm$^{1/2}$

$B_c = 39{,}875°R$

$n = 1/2$

Densities

The virgin density was taken as 31 lb/ft^3.

The char density was taken as 18 lb/ft^3.

Pyrolysis Kinetics

The pyrolysis kinetics pre-exponential constant was changed from the Appendix A value to the faster value

$A = 1.03 \times 10^4$ lb/ft^{2}sec

5.2.2 Range of Applicability

Predictions were made in the following approximate ranges:

Enthalpy h_e (BTU/lb)	3500 to 16,000
Cold Wall Heat Flux q_c (BTU/ft^{2}sec)	90 to 600
Pressure p (atm)	.01 to .5

In Option 2 (specified heat flux and recession), char thicknesses, total pyrolysis penetration, and thermocouple responses were well predicted. Pyrolysis penetration was predicted to within 13 percent and char thickness to within 25 percent. Thermocouple responses met the criterion of Section 3.1.2.

In Option 1 (specified heat flux, pressure, and enthalpy), recession was poorly predicted, with some overpredictions exceeding 100 percent and some underpredictions falling below 50 percent. There was no obvious correlation to the discrepancies with any of the major test parameters: pressure, heat flux, and enthalpy, except that there was a tendency for the predictions to improve as steady state was approached. Total pyrolysis penetration was predicted to within 30 percent except in only 3 of 12 cases. Generally, thermocouple predictions met the criterion of Section 3.1.2.

5.2.3 Concluding Remarks

For the cases considered, the CHAP I code did an excellent job in predicting the pyrolysis penetration and the thermocouple response in Avcoat

5026-39-HC/G. Recession predictions were quite scattered and must be judged unsatisfactory. The scatter may be due to inadequacies in the basic ablation model used; however, it would not be possible to recommend needed changes without a study of considerably more cases than have been studied here.

The CHAP II code should be used in further studies to explore the possible effects of coking in lowering the injected pyrolysis gas fluxes and hence in decreasing the blowing corrections, and to obtain better values of the pyrolysis gas specific heat.

5.3 FILLED SILICONE ELASTOMER

5.3.1 Properties

The material considered is defined on p. 2. The properties of Table A-2 of Appendix A were employed for the calculations with the exception of the densitites and the mass removal law:

Densities

The virgin material density was taken as 33.5 lb/ft^3.

The char density was taken as 16 lb/ft^3.

Heat of Combustion

The heat of combustion was not employed since the oxidation mechanism was suppressed.

Surface Removal

Oxidation was suppressed by setting the oxidation reaction constant A_c equal to zero. The values of B_c and λ are then irrelevant. Surface removal was matched to the McLain model of Ref. 8 by setting the sublimation constants as follows

$$A_s = 33.3 \left(\frac{q_c}{h_e} \right)^{.56} \quad lb/ft^2 sec$$

$$B_c = 29{,}011°R$$

It was necessary to compute A_s for each case considered.

5.3.2 Range of Applicability

Predictions were made in the following approximate ranges:

Enthalpy h_e (BTU/lb)	5000 to 20,000
Cold Wall Heat Flux q_c (BTU/ft^{2}sec)	50 to 500
Pressure p (atm)	.005 to .3

In Option 2 (specified heat flux and recession), char thickness, total pyrolysis penetration, and thermocouple responses were well predicted. Pyrolysis penetration (measured from the original surface location), was predicted to within ±25 percent in three of four cases. Char thickness was predicted to within 20 percent in all cases. Thermocouple predictions were excellent.

In Option 1 (specified heat flux, pressure, and enthalpy), total pyrolysis penetration was predicted to within ±25 percent in all but one of nine cases. Thermocouple predictions were acceptable. Recession predictions were confused by char swell. A reasonable swelling allowance of 25 percent of the char thickness rationalizes five of the nine cases predicted, all at heat fluxes less than 250 BTU/ft^{2}sec. The remaining four were poorly predicted, with no correlation pattern apparent.

Determination of the proper ablation model for the filled silicone elastomer at high heat fluxes will require the study of more cases. Even the low heat flux model apparently successful here should be viewed with suspicion, since the data upon which it is based were obtained at higher heat fluxes.

5.4 OVERALL CONCLUSIONS

Considering all cases examined and all cases studied, the CHAP I code produced excellent predictions of total pyrolysis penetration and of thermocouple responses for all three materials in a heat flux range of 50 BTU/ft^{2}sec to 500 BTU/ft^{2}sec, a pressure range of 0.004 atm to 0.5 atm, and an enthalpy range from 2000 BTU/lb to 18,000 BTU/lb. In addition, recession predictions for nylon phenolic are good as steady state is approached, but strongly transient cases are underpredicted. Recession amounts for Avcoat and the filled silicone elastomer are less well predicted, although again there is some evidence that cases near steady state are better predicted. Further study of these materials, possibly with the CHAP II code to explore the effects of coking, is needed.

REFERENCES

1. Swann, Robert T., and Pittman, Claud M., "Numerical Analysis of the Transient Response of Advanced Thermal Protection Systems for Atmospheric Entry," NASA TN D-1370, July 1962.

2. Swann, Robert T., Pittman, Claud M., and Smith, J. C.: "One-Dimensional Numerical Analysis of the Transient Response of Thermal Protection Systems," NASA TN D-2976, September 1965.

3. Moyer, C. B., Green, K. A., and Wool, M. R., "Demonstration of the Range Over Which the Langley Research Center Digital Computer Charring Ablation Program (CHAP) Can be Used with Confidence, Task I, Collection of Properties Data and Ablation Test Data for Three Charring Materials, and Results of Qualifying Calculations with CHAP," NASA CR-111834, December 1970.

4. Scala, S. M., "The Ablation of Graphite in Dissociated Air, Part I. Theory", Institute of Aerospace Sciences, IAS Paper No. 62-154 (IAS Summer Meeting, Los Angeles, California, June 19-22, 1962).

5. Schaefer, J. W., Flood, D. T., Reese, J. J., Jr., and Clark, K. J., "Experimental and Analytical Evaluation of the Apollo Thermal Protection System Under Simulated Reentry Conditions," Aerotherm Corporation, Mountain View, California, Aerotherm Report No. 67-16, July 15, 1967.

6. Bartlett, E. P., Anderson, L. W., and Curry, D. M., "An Evaluation of Ablation Mechanisms for the Apollo Heat Shield Material," AIAA Paper No. 69-98 (AIAA 7th Aerospace Sciences Meeting, New York, N.Y., January 20-22, 1969), 1969.

7. Bartlett, E. P. and Anderson, L. W., "An Evaluation of Ablation Mechanisms for the Apollo Heat Shield Material," Aerotherm Corporation, Mountain View, California, Aerotherm Report No. 68-38, Part II, October 15, 1968.

8. McLain, A. G., "Investigation of Char Formation and Surface Recession of a Composite Ablation Material with a Silicone Resin Base," NASA TN D-6004, October, 1970.

9. Zoby, E. V., "Empirical Stagnation-Point Heat Transfer Relation in Several Gas Mixtures at High Enthalpy Levels," NASA TN D-4799, October 1968.

10. Hiester, N. K., and Clark, C. F., "Comparative Evaluation of Ablating Materials in Arc Plasma Jets," NASA CR-1207, December 1968.

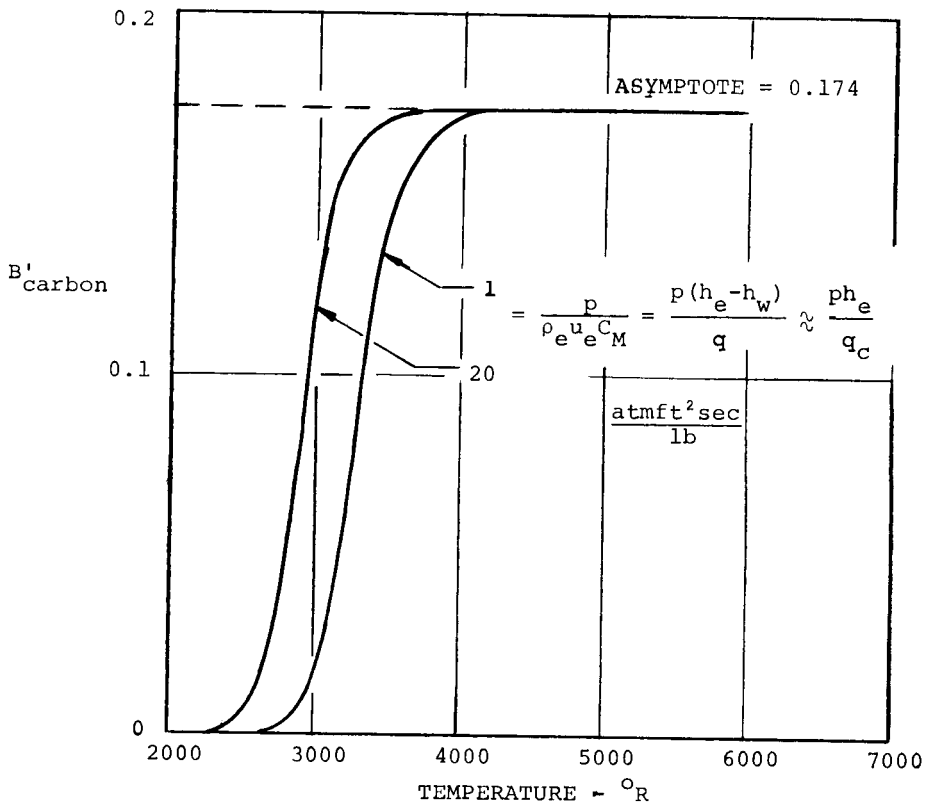

FIGURE 1 RATE OF FIRST ORDER CARBON OXIDATION ACCORDING TO EQUATION 14, $A = 1 \times 10^{10}$ LB/FT^{2}SEC ATM
$B = 76{,}500^oR$
$\lambda = 0.75$

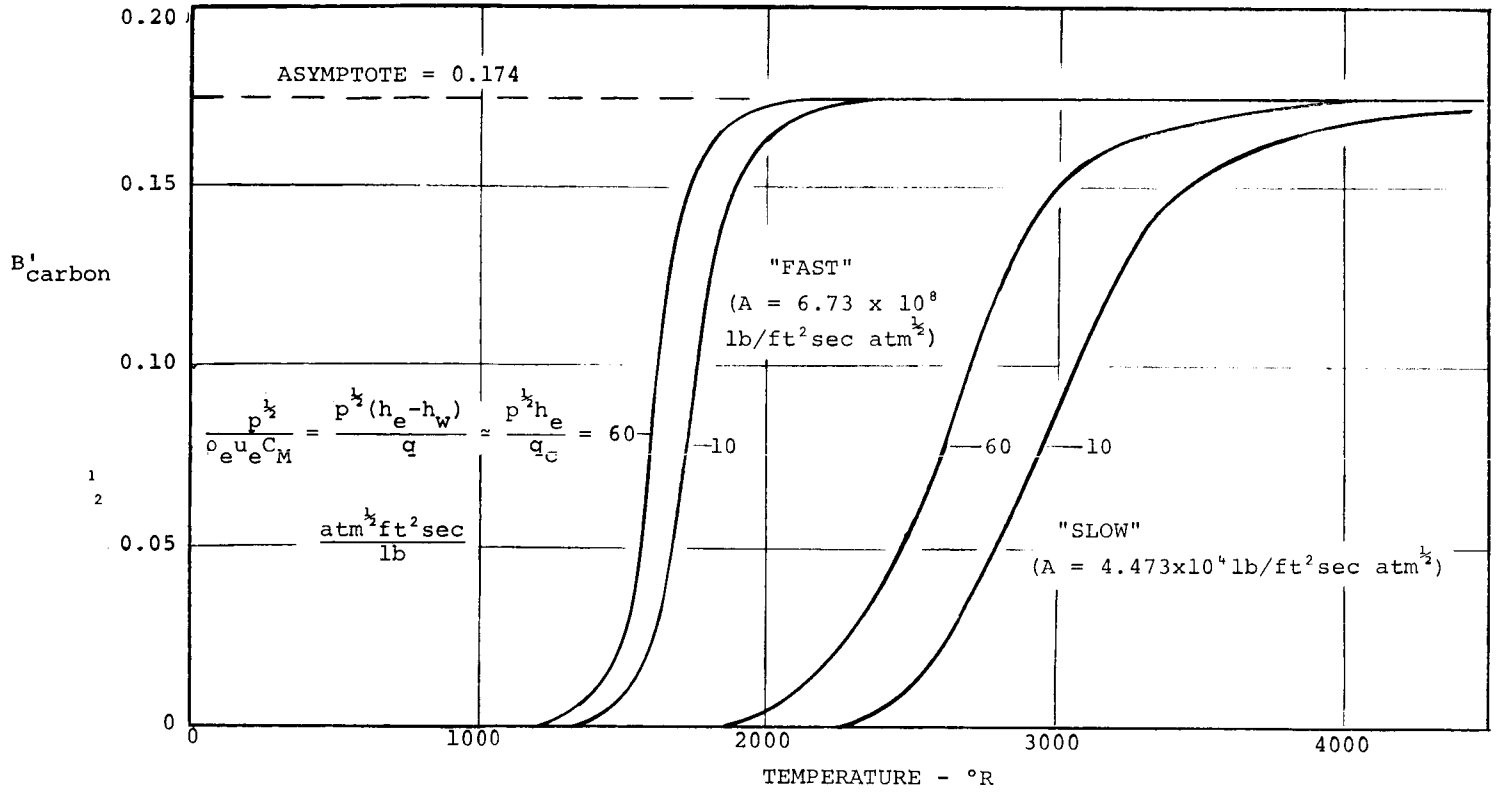

FIGURE 2 RATE OF HALF-ORDER CARBON OXIDATION ACCORDING TO EQUATION (6), REF. 1
B = 39.875°R, λ = 0.75

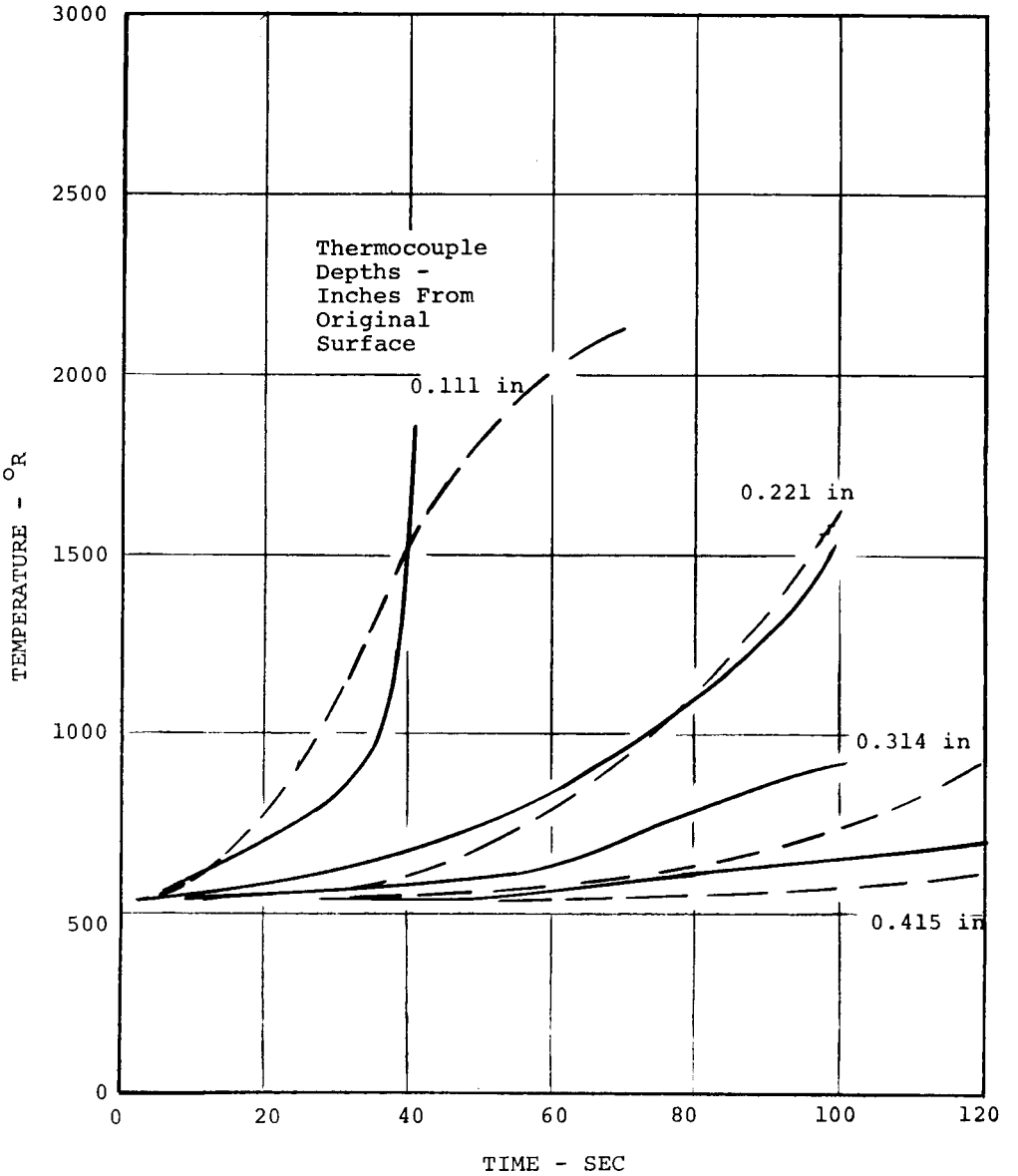

	TEST RESULTS	CHAP RESULTS
CHAP input (in)		Appendix A
Total recession (in)	.107	same
Final char δ(in)	.178	.179
Total penetration (in)	.285	.286
Final surf. temp (°R)	3350	2548
Code	———	----

FIGURE 3 ITERATIVE CASE, NYLON PHENOLIC TAB NO. 21, OPT. 2
q_c = 43.2 BTU/ft^{2}H^{2}sec, p = .0070 atm, h_e = 5140 BTU/lb

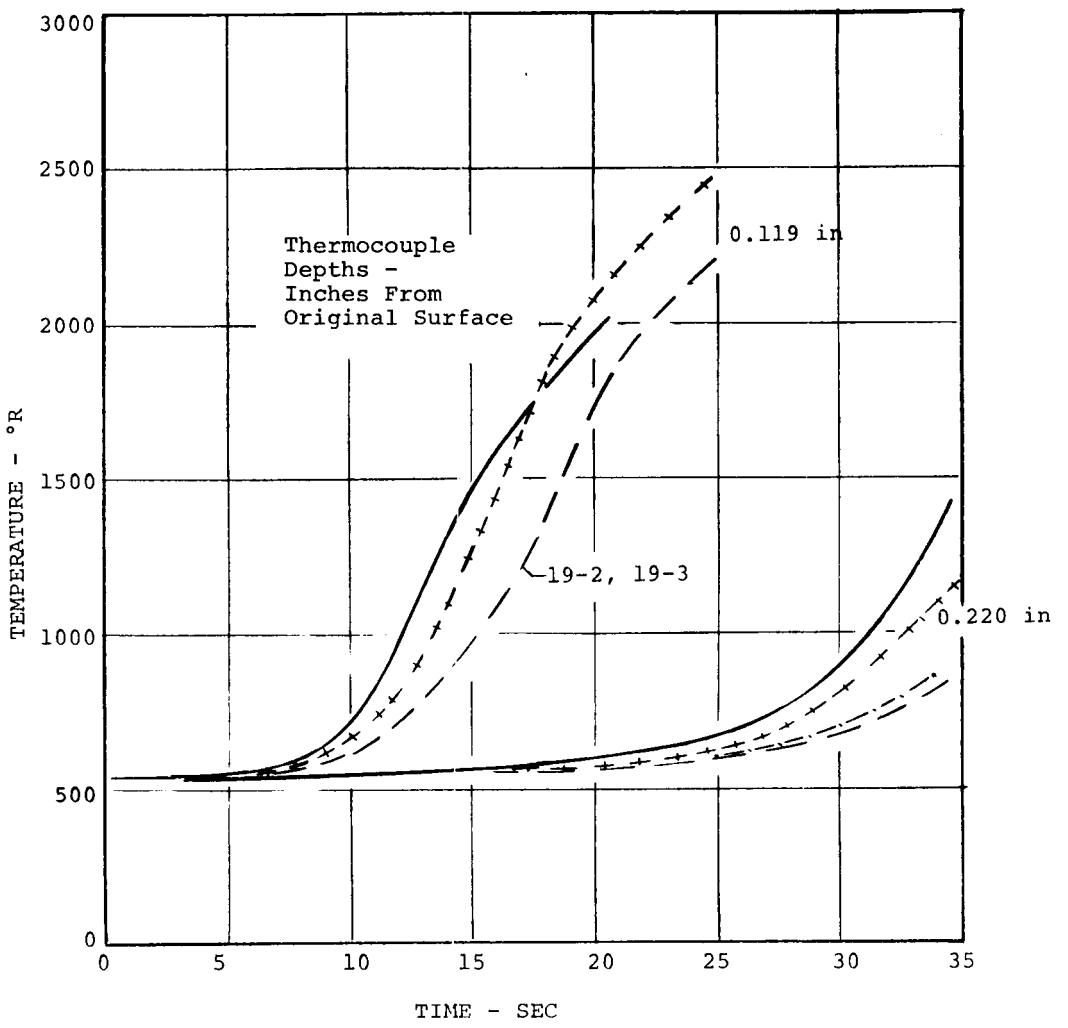

	TEST RESULTS	CHAP RESULTS		
		19-2	19-3	19-5
CHAP input		Appendix A	High k_{virg} above 900°R	q_c + 20%
Total recession (in)	.073	same	same	same
Final char δ (in)	.159	.125	.125	.144
Total penetration (in)	.232	.198	.198	.217
Final surf. temp (°R)	4350	3203	3202	3480
Code	———	— —	—·—·—	+ + +

FIGURE 4 ITERATIVE CASE, NYLON PHENOLIC, TAB NO. 19, OPT. 2
q_c = 145 BTU/ft^{2}sec, p = .0199 atm, h_e = 10,200 BTU/lb

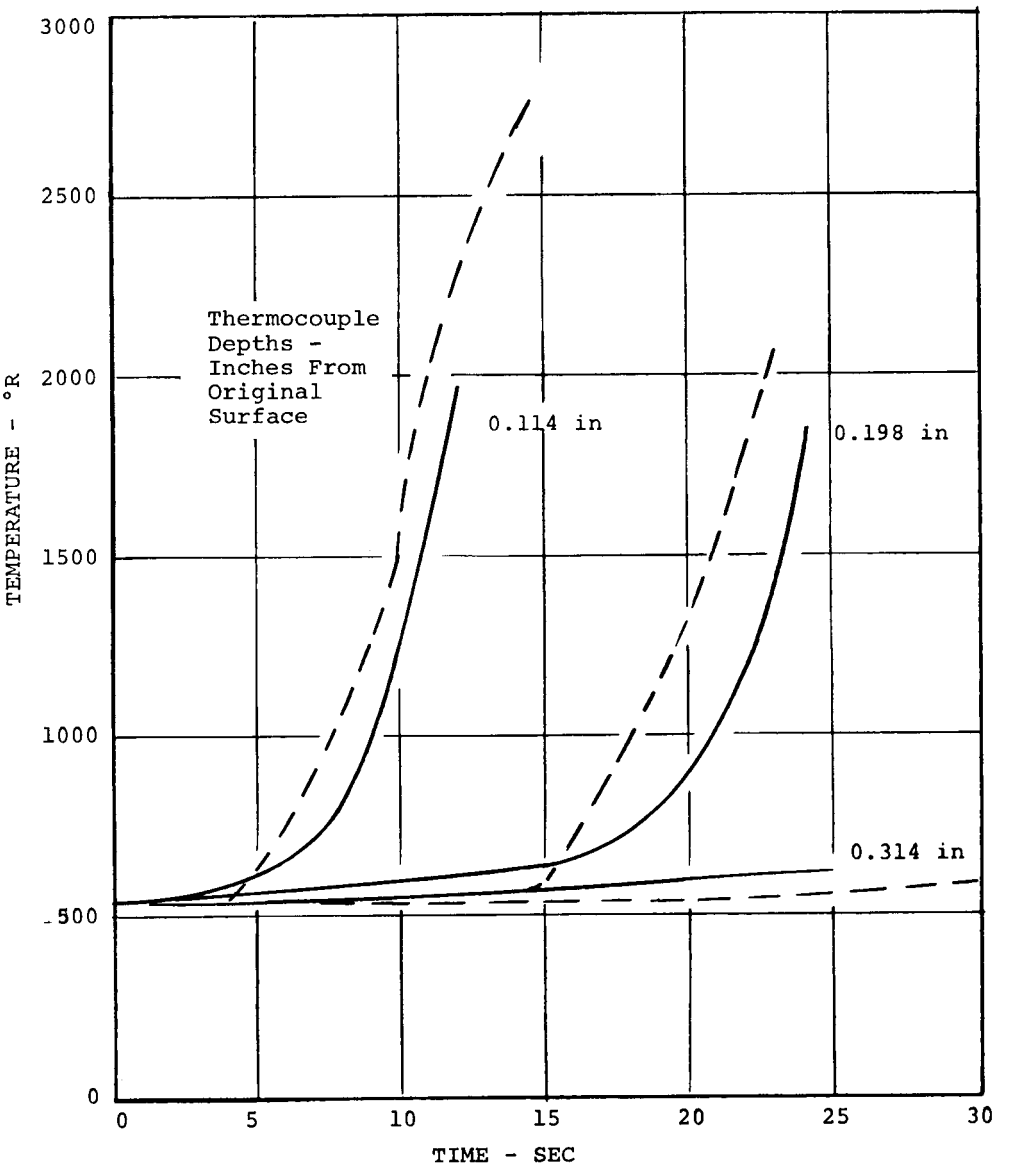

	TEST RESULTS	CHAP RESULTS
CHAP input		Appendix A
Total recession (in)	.137	same
Final char δ(in)	.099	.130
Total penetration (in)	.236	.267
Final surf. temp (°R)	4650	3890
Code	———	– – –

FIGURE 5 ITERATIVE CASE, NYLON PHENOLIC TAB NO. 16, OPT. 2
q_c = 256 BTU/ft²sec, p = .264 atm, h_e = 4900 BTU/lb

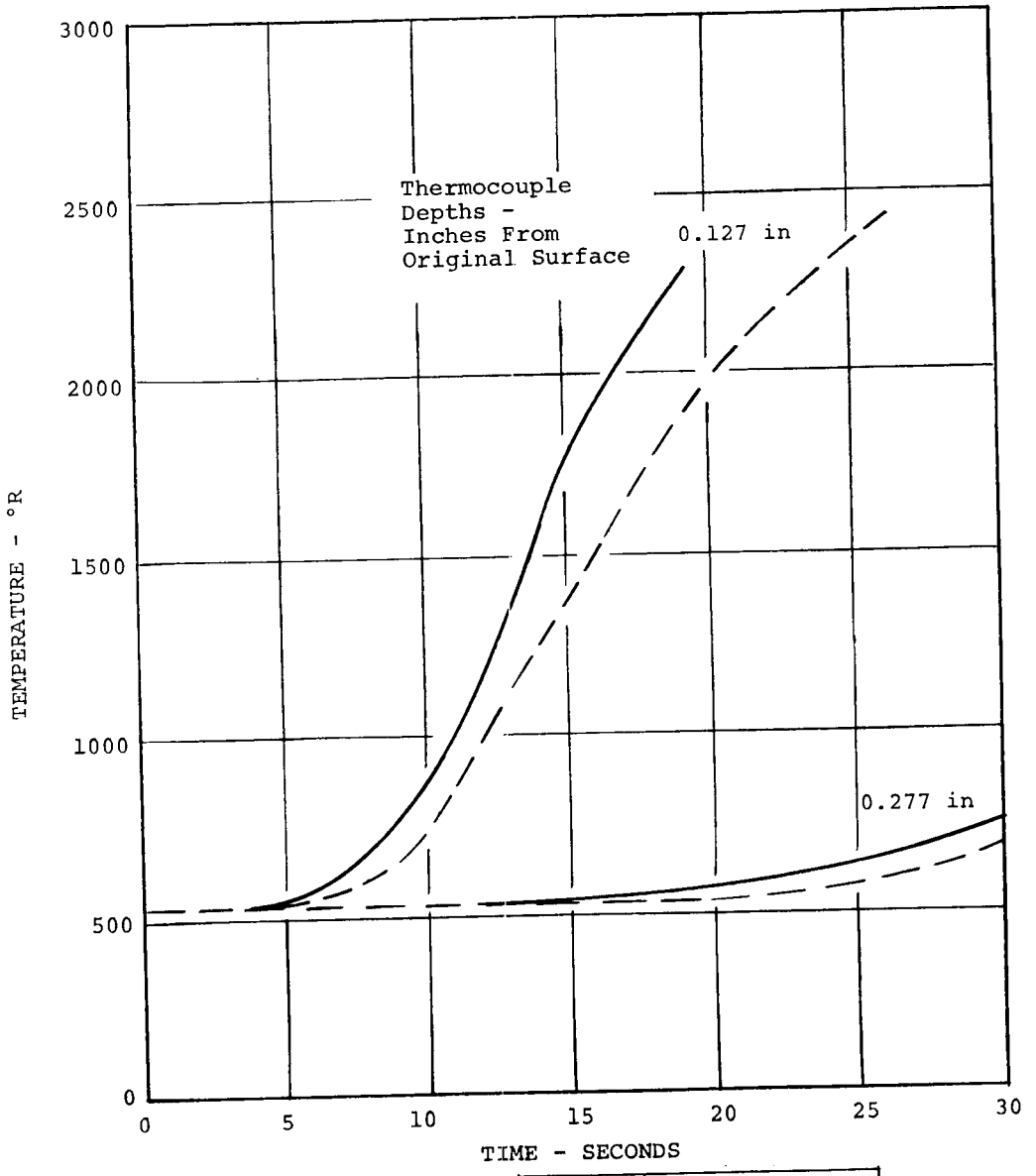

	TEST RESULTS	CHAP RESULTS 66-1
CHAP input		Appendix A
Total recession (in)	.096	same
Final char δ(in)	.10	.14
Pyrolysis zone δ(in)	.04	---
Total penetration (in)	.236	.236
Final surf. temp. (°R)	4100	3030
Code		- - -

FIGURE 6 ITERATIVE CASE, AVCOAT 5026-39HC/G TAB NO. 66, OPT. 2
q_c = 119 BTU/ft^{2}sec, p = .0279 atm, h_e = 10,976 BTU/lb

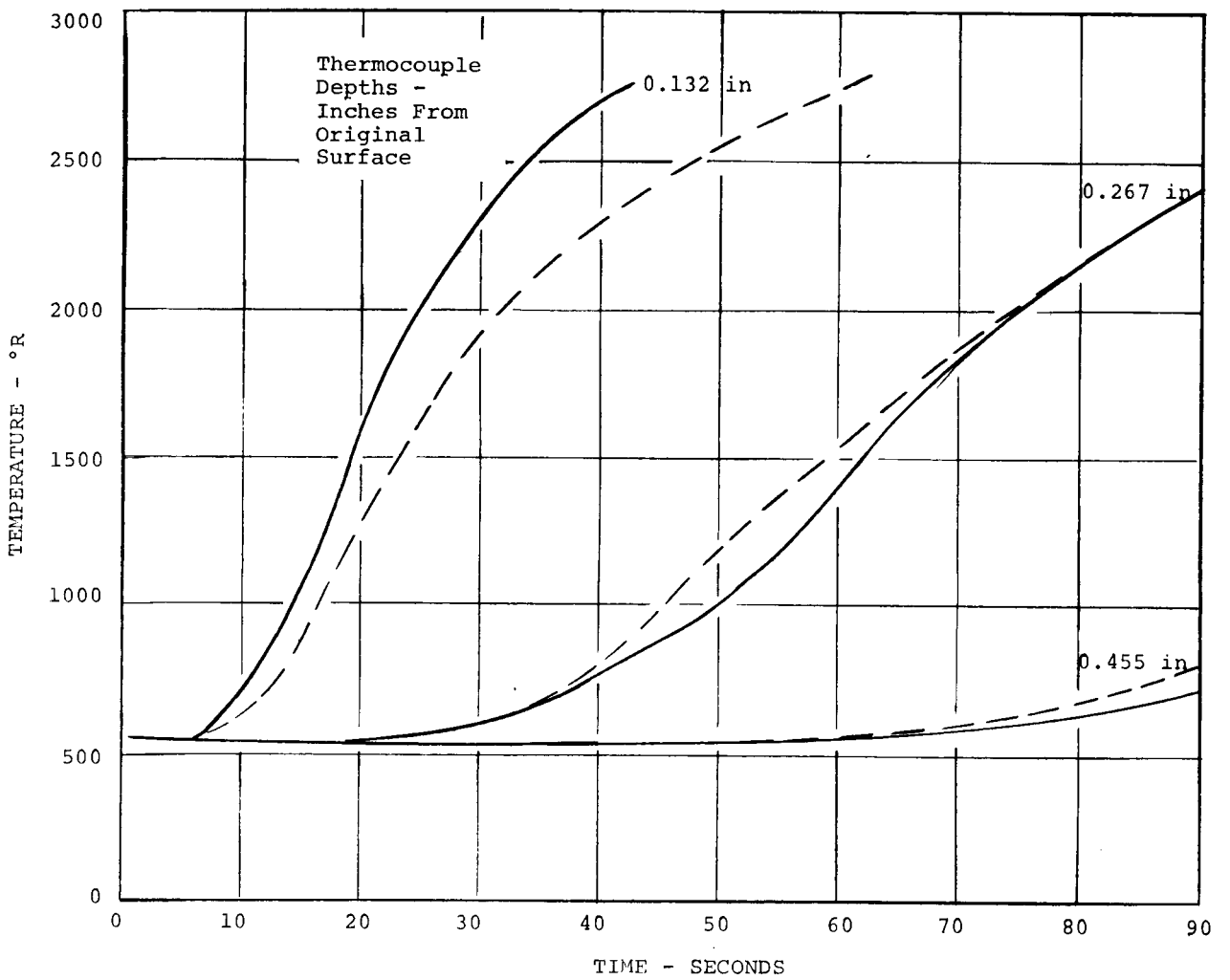

	TEST RESULTS	CHAP RESULTS 62-1
CHAP input		Appendix A
Total recession (in)	.137	Same
Final char δ (in)	.13	.273
Pyrolysis zone δ (in)	.060	----
Total penetration (in)	.327	.410
Final surface temp (°R)	3280	3145
Code	——	----

FIGURE 7 ITERATIVE CASE, AVCOAT 5026-39HC/G TAB NO. 62 OPT. 2
q_c = 91 BTU/ft^{2}sec, p = .0081 atm, h_e = 13,500 BTU/lb

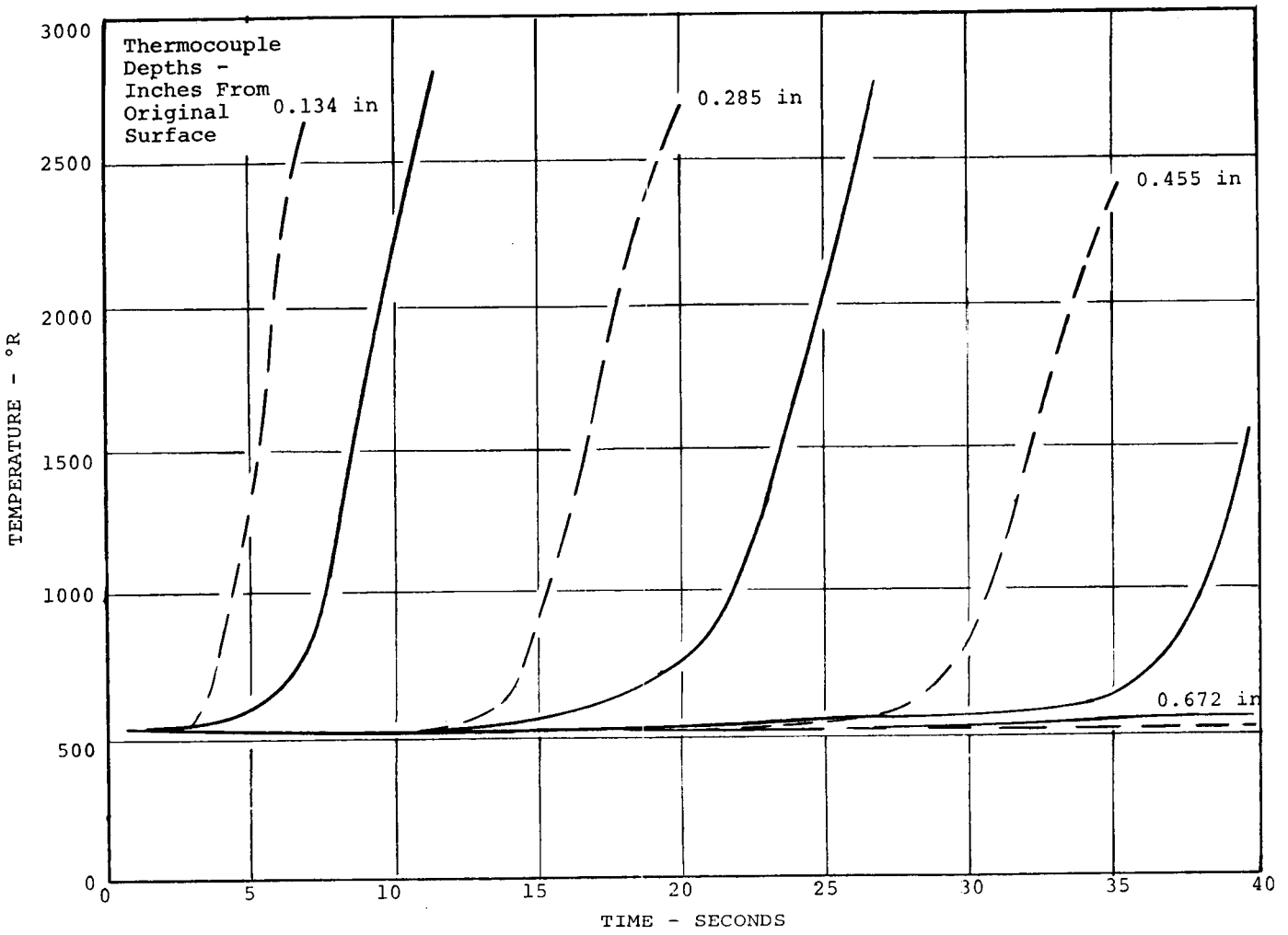

	TEST RESULTS	CHAP RESULTS 92-1
CHAP input		Appendix A
Total recession	.388	same
Final char δ(in)	.08	.151
Pyrolysis zone δ(in)	.02	--
Total penetration (in)	.488	.539
Final surf. temp (°R)	4820	5210
Code	———	- - -

FIGURE 8 ITERATIVE CASE, AVCOAT 5026-39HC/G TAB NO. 92, OPT. 2
q_c = 560 BTU/ft^{2}sec, p = .0817 atm, h_e = 10,586 BTU/lb

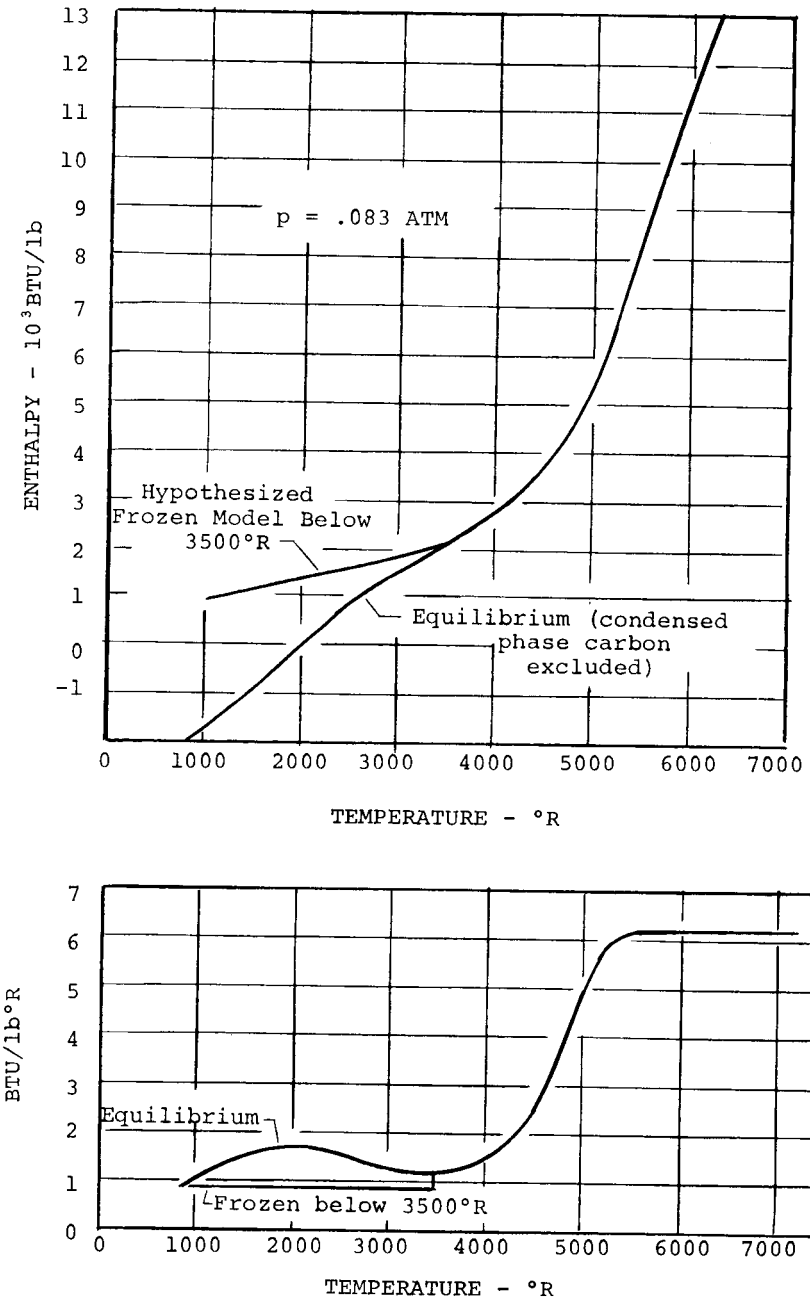

FIGURE 9 ENTHALPY AND SPECIFIC HEAT OF AVCOAT PYROLYSIS GAS (REFERENCE 5)

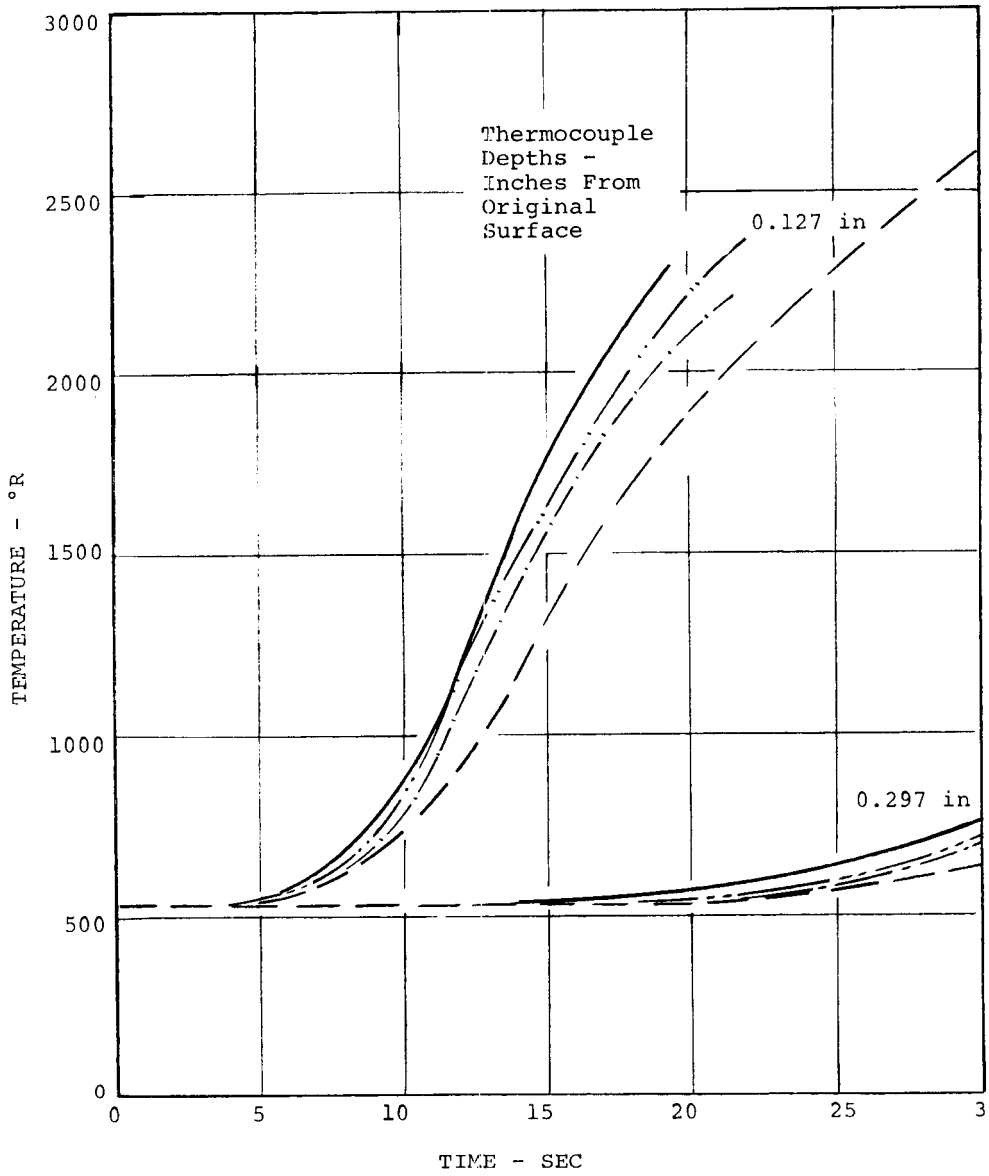

	TEST RESULTS	CHAP RESULTS 66-3	66-4	66-4A
CHAP input		- - Slow Pyrolysis Kinetics - - Equil. $\bar{C}_p$	Froz/Equil. $\bar{C}_p$	Equil. $\bar{C}_p$, q_c + 20%
Total recession (in)	.096	same	same	same
Final char δ(in)	.10	.117	.134	.136
Pyrolysis zone δ(in)	.04	----	----	----
Total penetration (in)	.236	.213	.230	.232
Final surf. temp (°R)	4100	3034	3078	3350
Code	———	- - -	—·—·—	—··—··—·—

FIGURE 10 ITERATIVE CASE, AVCOAT 5026-39HC/G TAB NO. 66, OPT. 2
q_c = 119 BTU/ft^{2}sec, p = .0279 atm, h_e = 10,976 BTU/lb

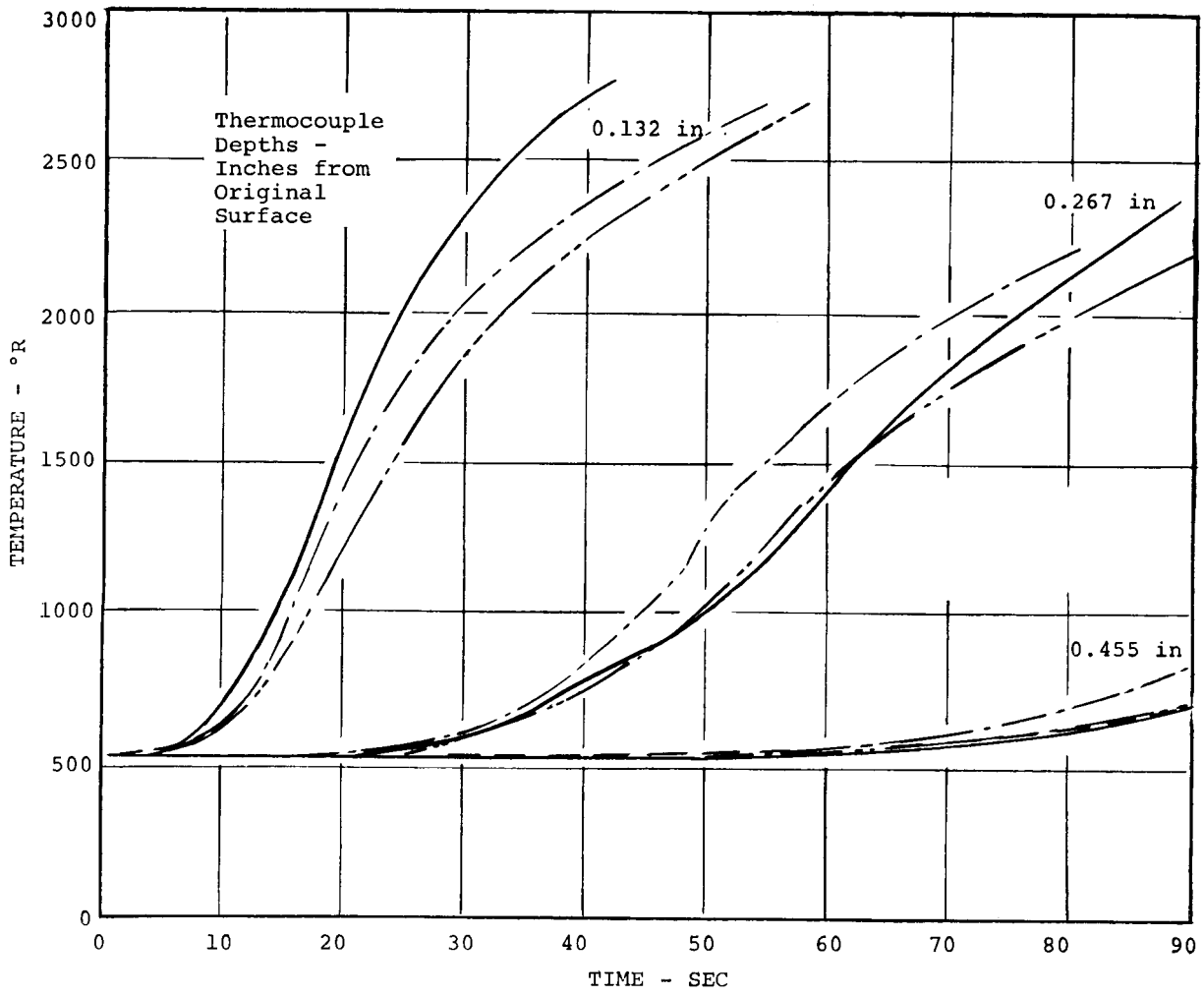

	TEST RESULTS	CHAP RESULTS	
		62-4	62-4A
		- Slow Pyrolysis Kinetics -	
CHAP input		Equil. $\bar{C}_p$	Froz/Equil. $\bar{C}_p$
Total recession (in)	.137	same	same
Final char δ(in)	.13	.233	.254
Pyrolysis zone δ(in)	.060	----	----
Total penetration (in)	.327	.370	.391
Final surf. temp. (°R)	3280	3150	3150
	-·-·-	-"-"-	-·-·-

FIGURE 11 ITERATIVE CASE, AVCOAT 5026-39HC/G TAB NO. 62, OPT. 2
q_c = 91 BTU/ft^{2}sec, p = .0081 atm, h = 13,500 BTU/lb

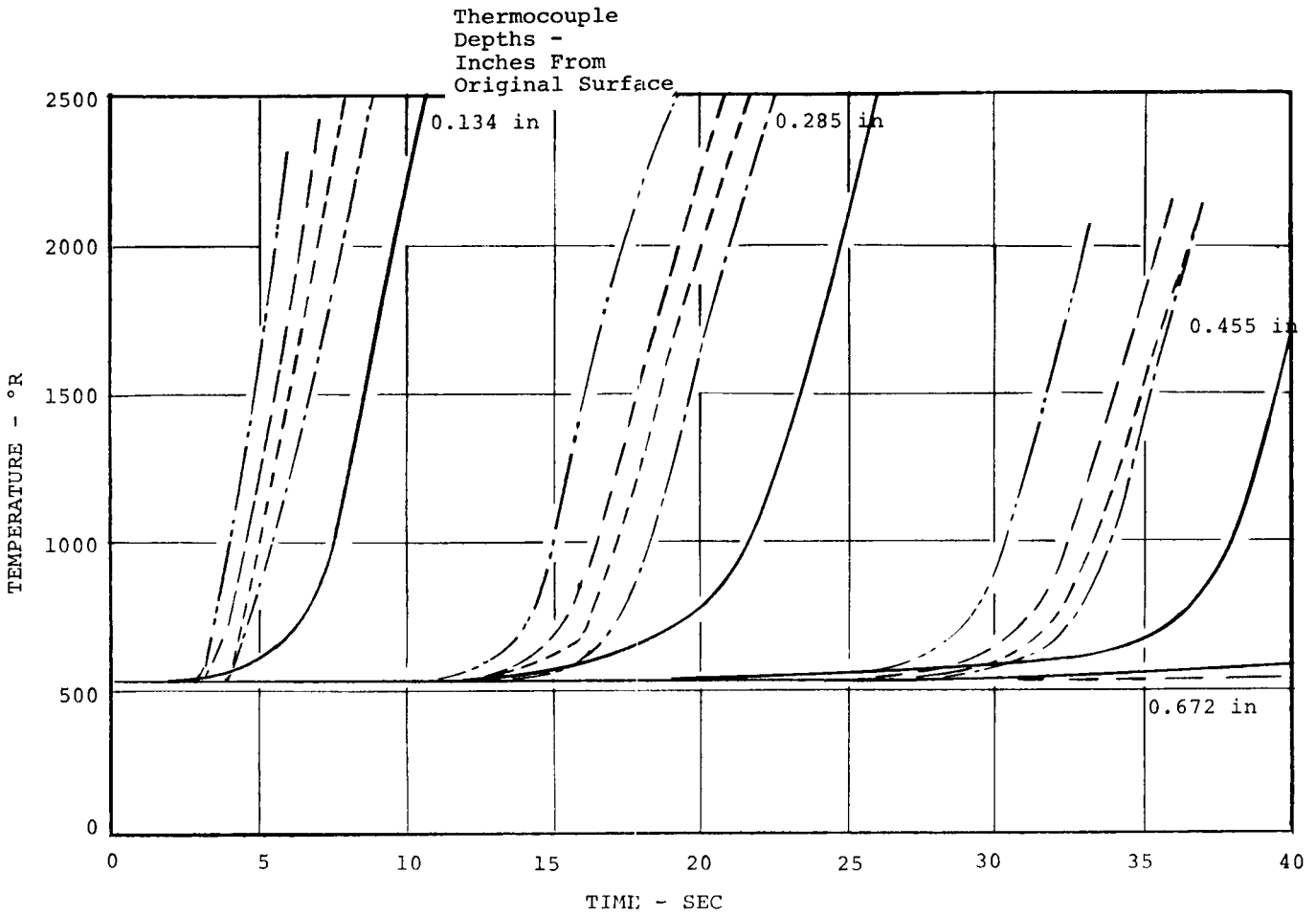

	TEST RESULTS	CHAP RESULTS 92-3	92-4	92-5	92-5A
CHAP input		- - - - Slow Pyrolysis Kinetics - - - -			
		- - - - - Equil. $\bar{C}_p$ - - - - -			Equil/ Froz. $\bar{C}_p$
		3 sec recess. delay		q_c - 20%	
Total recession (in)	.388	same	same	same	same
Final char δ(in)	.08	.125	.116	.115	.150
Pyrolysis zone δ(in)	.02	--	--	--	--
Total penetration (in)	.488	.513	.504	.503	.538
Final surface temp (°R)	4820	5076	5012	4677	5145
Code	———	——	- - -	-·-·-	-··-··

FIGURE 12 ITERATIVE CASE, AVCOAT 5026-39HC/G TAB NO. 92, OPT. 2
q_c = 560 BTU/ft^{2}sec, p = .0817 atm, h_e = 10,586 BTU/lb

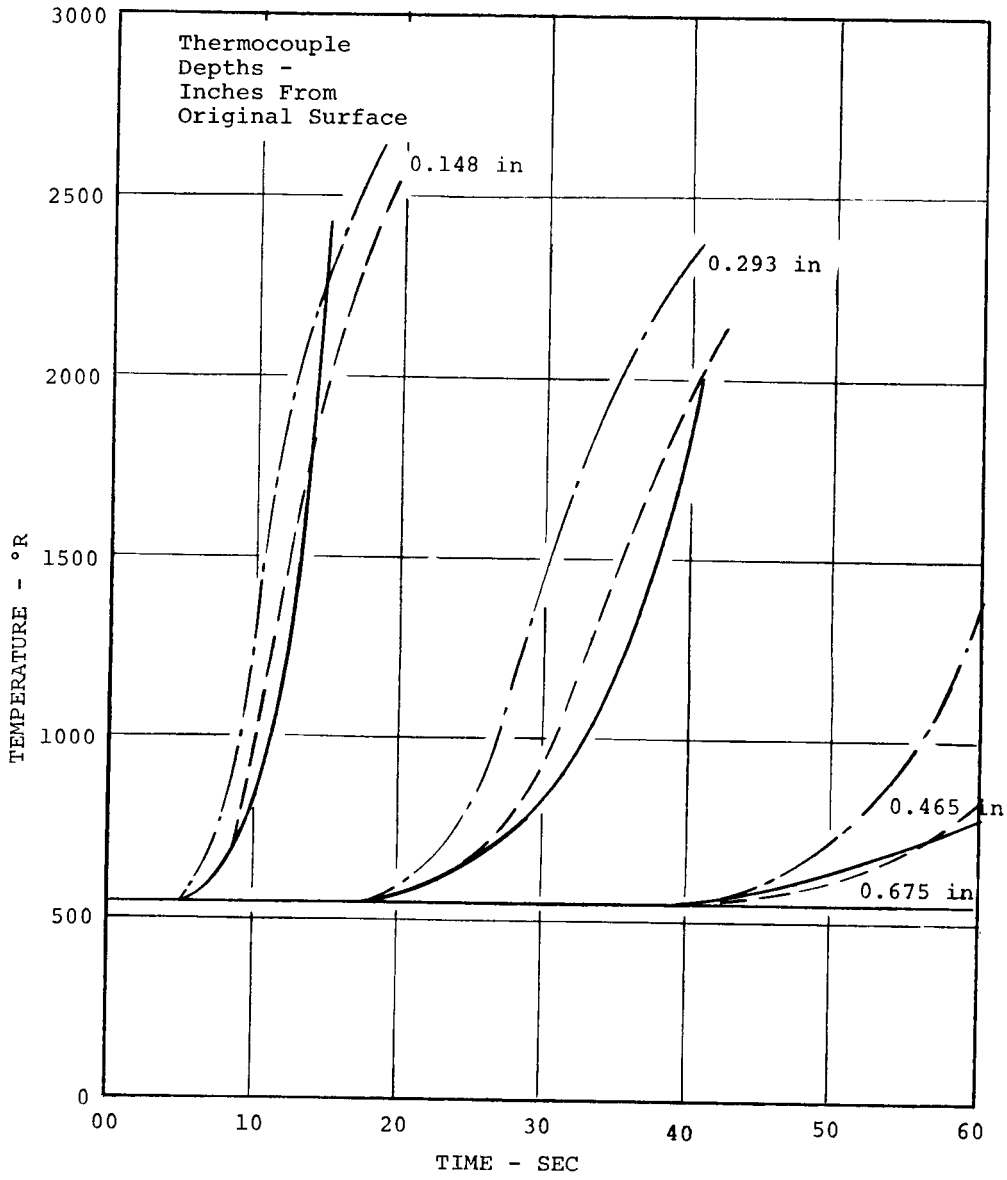

	TEST RESULTS	CHAP RESULTS 52-1	CHAP RESULTS 52-1A
		-- Slow Pyrolysis Kinetics - -	
CHAP input		Equil $\bar{C}_p$	Froz./equil. $\bar{C}_p$
Total recession (in)	.215	same	same
Final char δ(in)	.160	.211	.251
Pyrolysis zone δ(in)	.040	--	--
Total penetration (in)	.415	.426	.466
Final surf. temp (°R)	4370	4130	4150
Code	———	- - -	-·-·-·-

FIGURE 13 ITERATIVE CASE, AVCOAT 5026-39HC/G TAB NO. 52, OPT. 2
q_c = 215 BTU/ft^{2}sec, p = .029 atm, h_e = 10,445 BTU/lb, C_e = .07

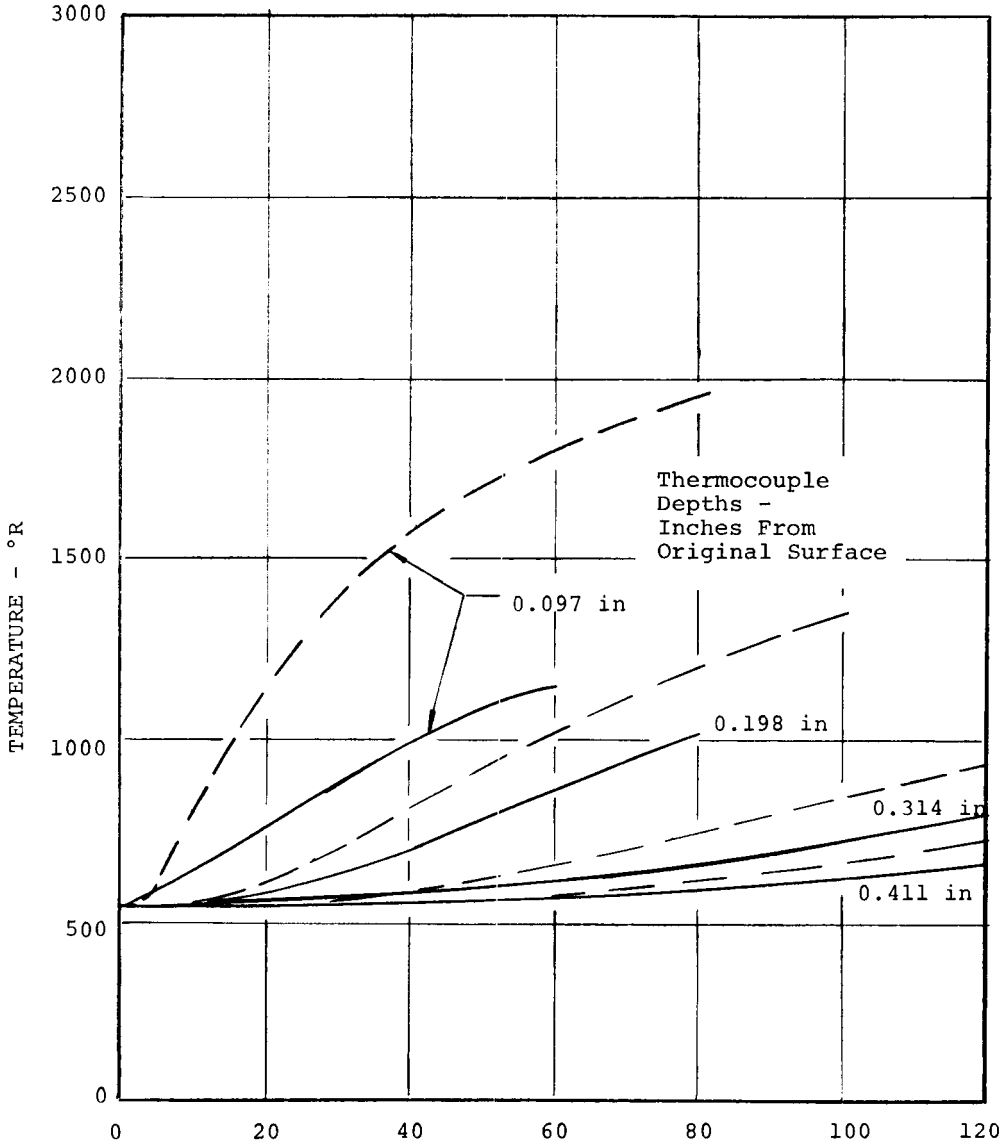

	TEST RESULTS	CHAP RESULTS 12-1
CHAP input		Appendix A
Total recession (in)	+.048	0
Final char δ(in)	.200	.212
Total penetration (in)	.152	.212
Final surf. temp (°R)	3020	2975
Code	———	- - - -

FIGURE 14 ITERATIVE CASE, SILICONE ELASTOMER TAB NO. 12, OPT. 2
q_c = 44.2 BTU/ft^{2}sec, p = .0070 atm, h_e = 10,647 BTU/lb

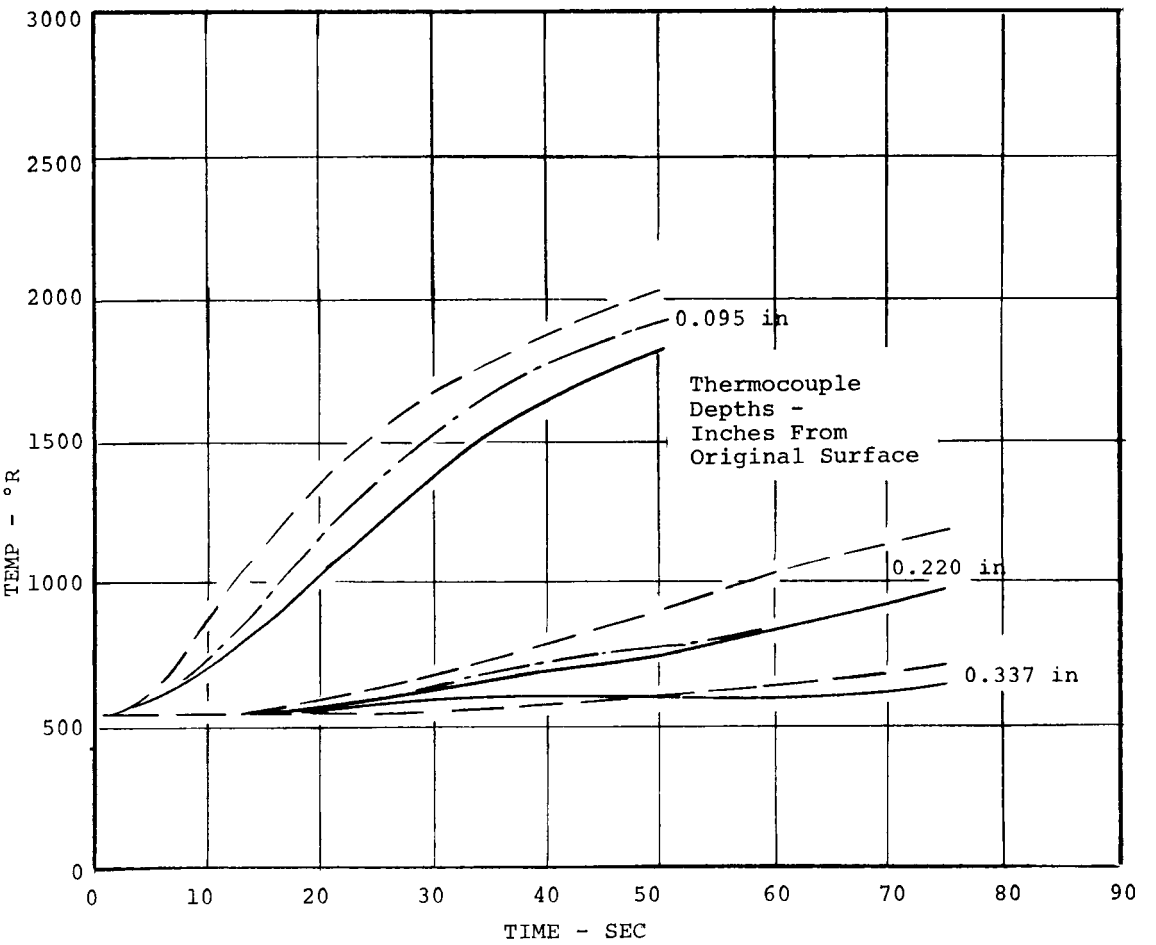

	TEST RESULTS	CHAP RESULTS 1-1	CHAP RESULTS 1-1A
CHAP input		- - Appendix A - - -	Corrected for char swell
Total recession (in)	+.052	0	0
Fina char δ (in)	.205	.188	.188
Total penetration (in)	.153	.188	.188
Final surf. temp (°R)	3000	3540	3540
Code	———	- - -	-·-·-

FIGURE 15 ITERATIVE CASE, SILICONE ELASTOMER TAB NO. 1, OPT. 2
q_c = 87 BTU/ft^{2}sec, p = .0109 atm, h_e = 10,670 BTU/lb

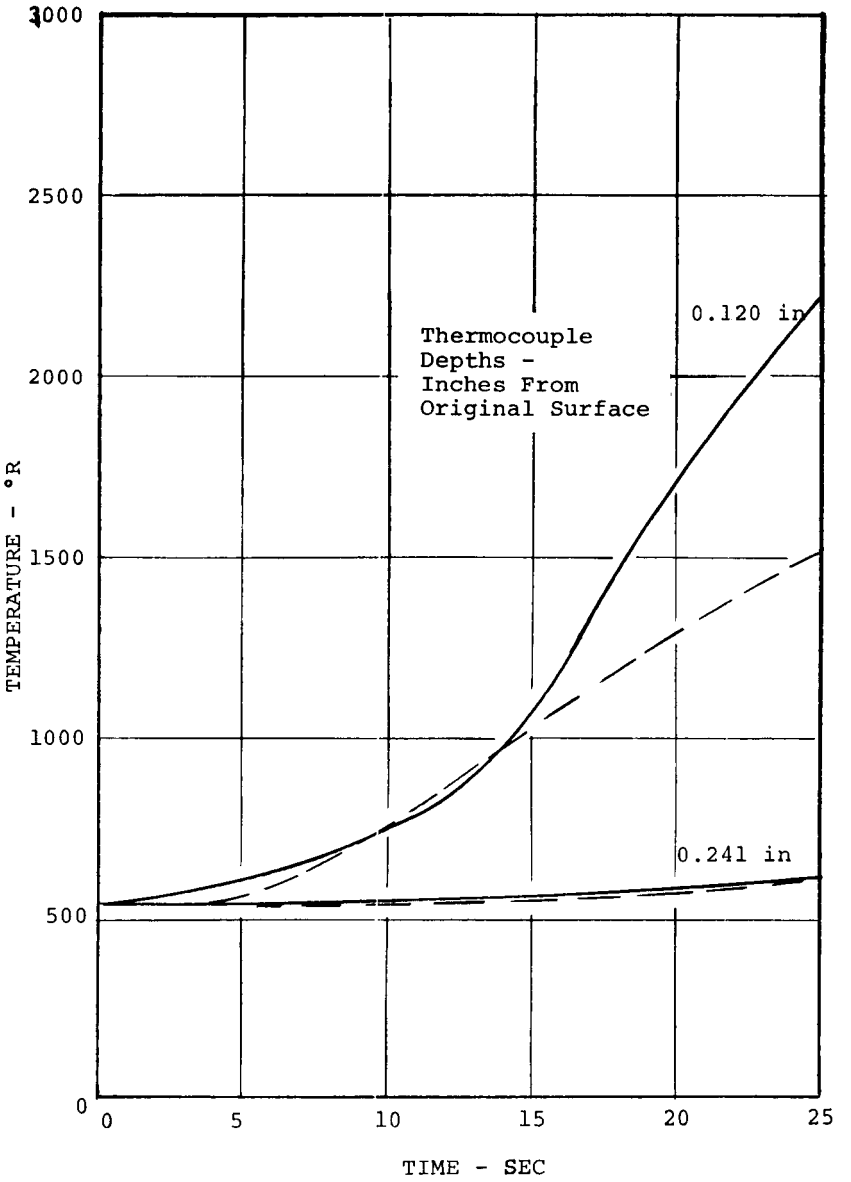

	TEST	CHAP RESULTS 4-1
CHAP input		Appendix A
Total recession (in)	.004	same
Final char δ (in)	.121	..118
Total penetration (in)	.125	.122
Final surf. temp (°R)	3550	4397
Code	——	– – –

FIGURE 16 ITERATIVE CASE, SILICONE ELASTOMER TAB NO. 4, OPT. 2
q_c = 221 BTU/ft^{2}sec, p = .00847 atm, h_e = 19,721 BTU/lb

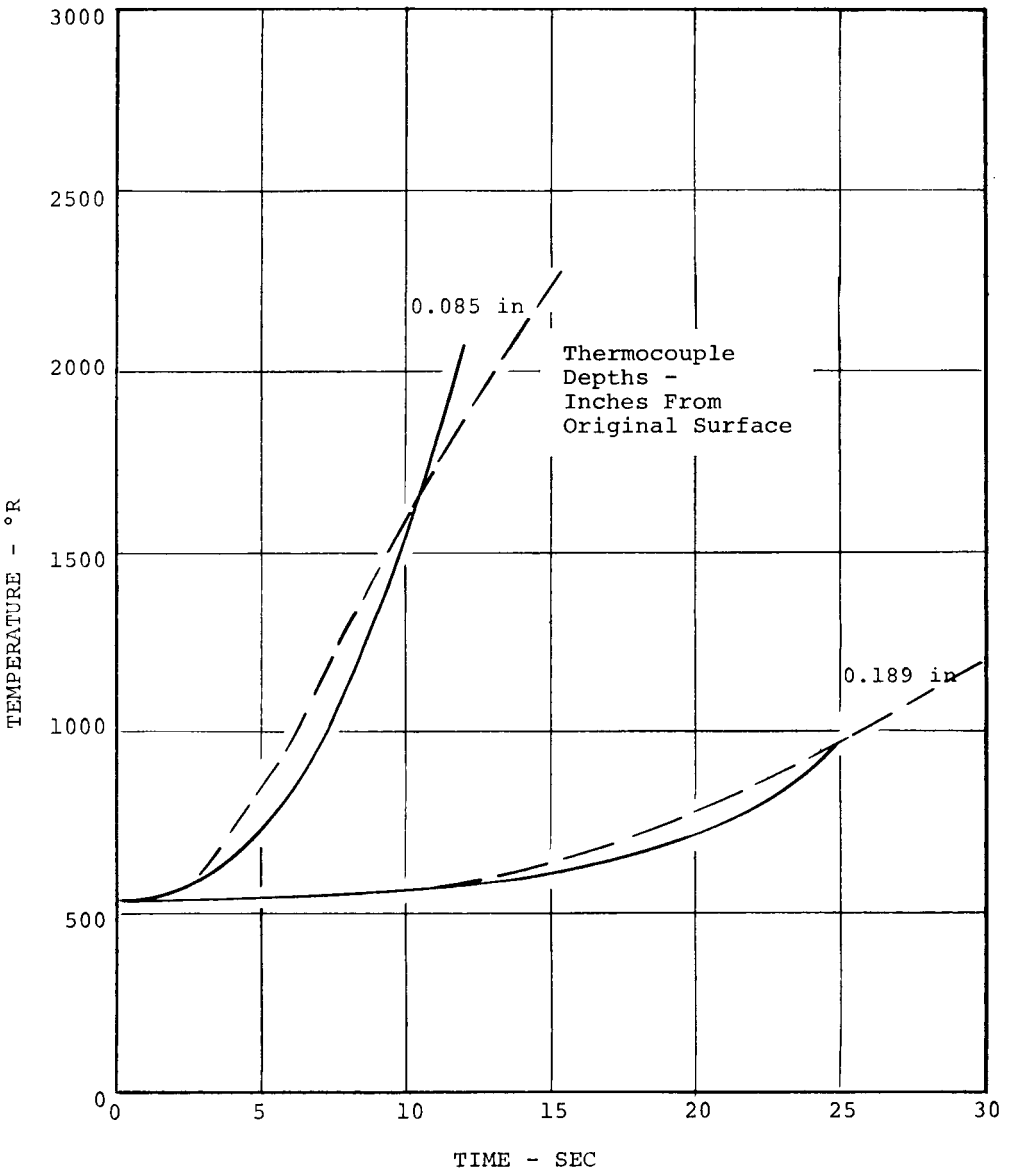

	TEST RESULTS	CHAP RESULTS 5-1
CHAP input		Appendix A
Total recession (in)	.070	same
Final char δ(in)	.117	.097
Total penetration (in)	.187	.167
Final surf. temp. (°R)	4300	4534
Code	———	– – –

FIGURE 17 ITERATIVE CASE, SILICONE ELASTOMER TAB NO. 5, OPT. 2
q_c = 273 BTU/ft^{2}sec, p = .284 atm, h_e = 49,000 BTU/lb

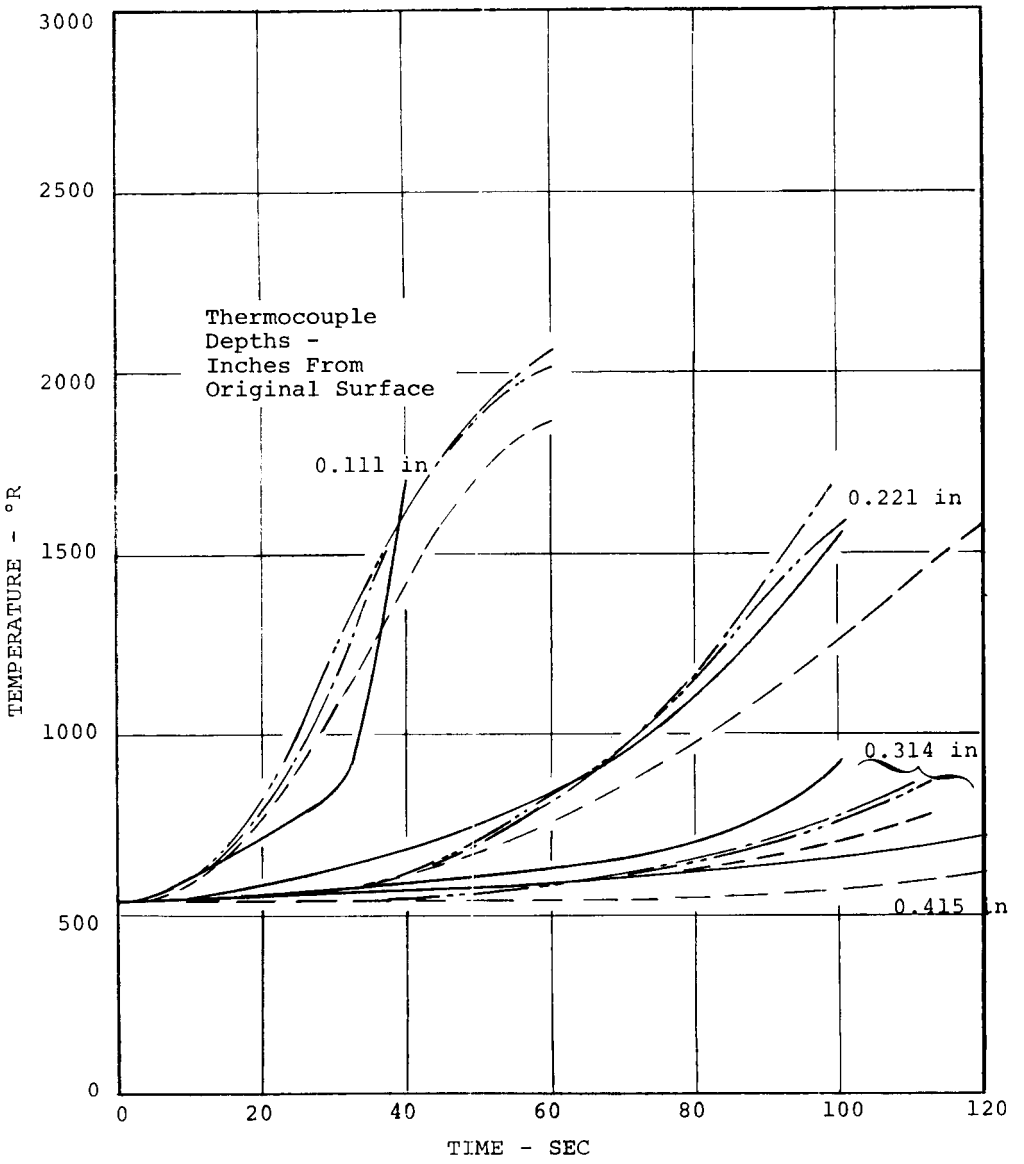

	TEST RESULTS	CHAP RESULTS 21-3	21-4	21-5
CHAP input		Appendix A	"Scala fast" kinetics	App. A kinetics q + 20%
Total recession (in)	.107	.000	.092	.024
Final char δ(in)	.178	.258	.199	.263
Total penetration (in)	.285	.258	.291	.287
Final surf. temp (°R)	3350	2719	2660	2850
Code	———	– – –	–·–·–	–··–··–

FIGURE 18 ITERATIVE CASE, NYLON PHENOLIC TAB NO. 21
q_c = 43.2 BTU/ft^{2}sec, p = .007 atm, h_e = 5140 BTU/lb

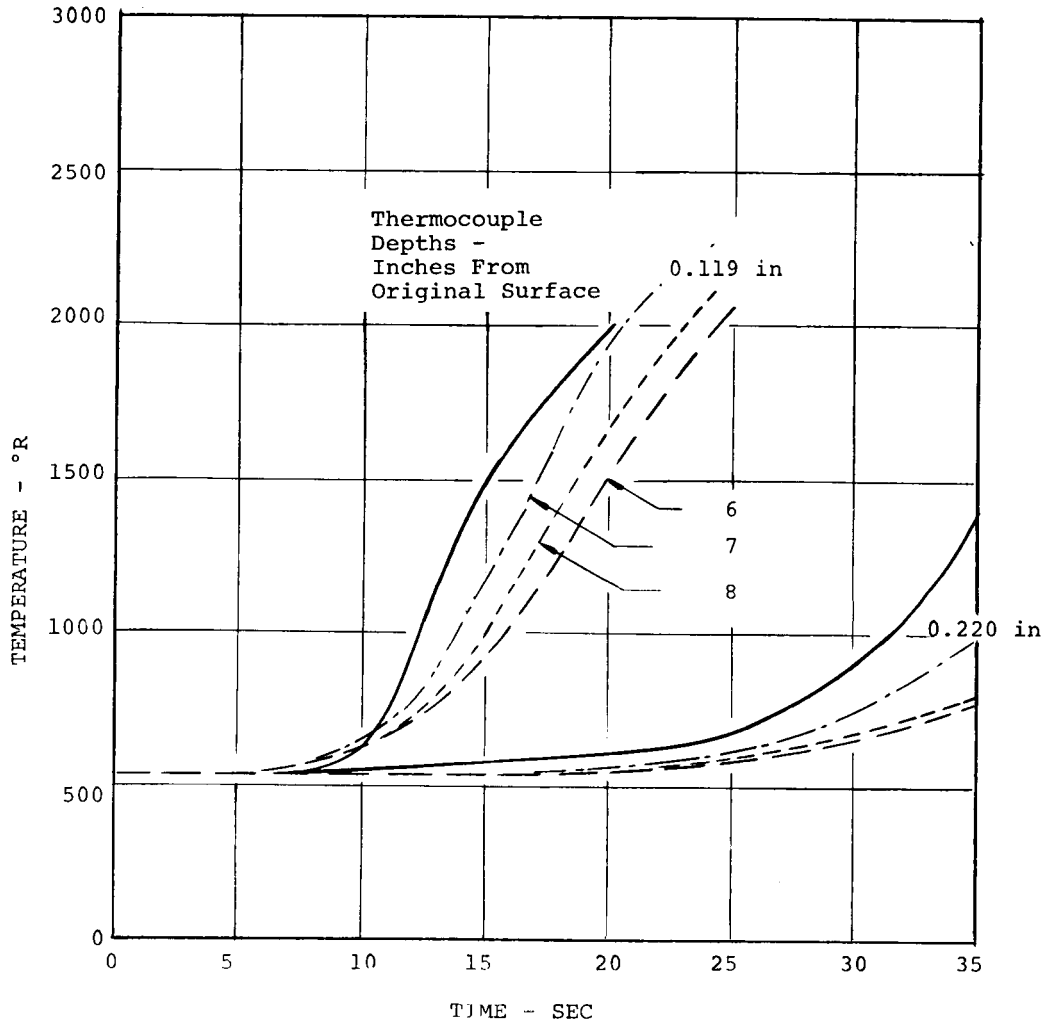

	TEST RESULTS	CHAP RESULTS 19-6	19-7	19-8
CHAP input		- Appendix A -	q_c + 20%	"Scala fast" kinetics
Total recession (in)	.073	.022	.035	.040
Final char δ (in)	.159	.166	.172	.156
Total penetration (in)	.232	.188	.207	.196
Final surf. temp (°R)	4350	3470	3682	3420
Code	———	— —	– – –	– – – –

FIGURE 19 ITERATIVE CASE, NYLON PHENOLIC TAB NO. 19
q_c = 145 BTU/ft^{2}sec, p = .0199 atm, h_e = 10,200 BTU/lb

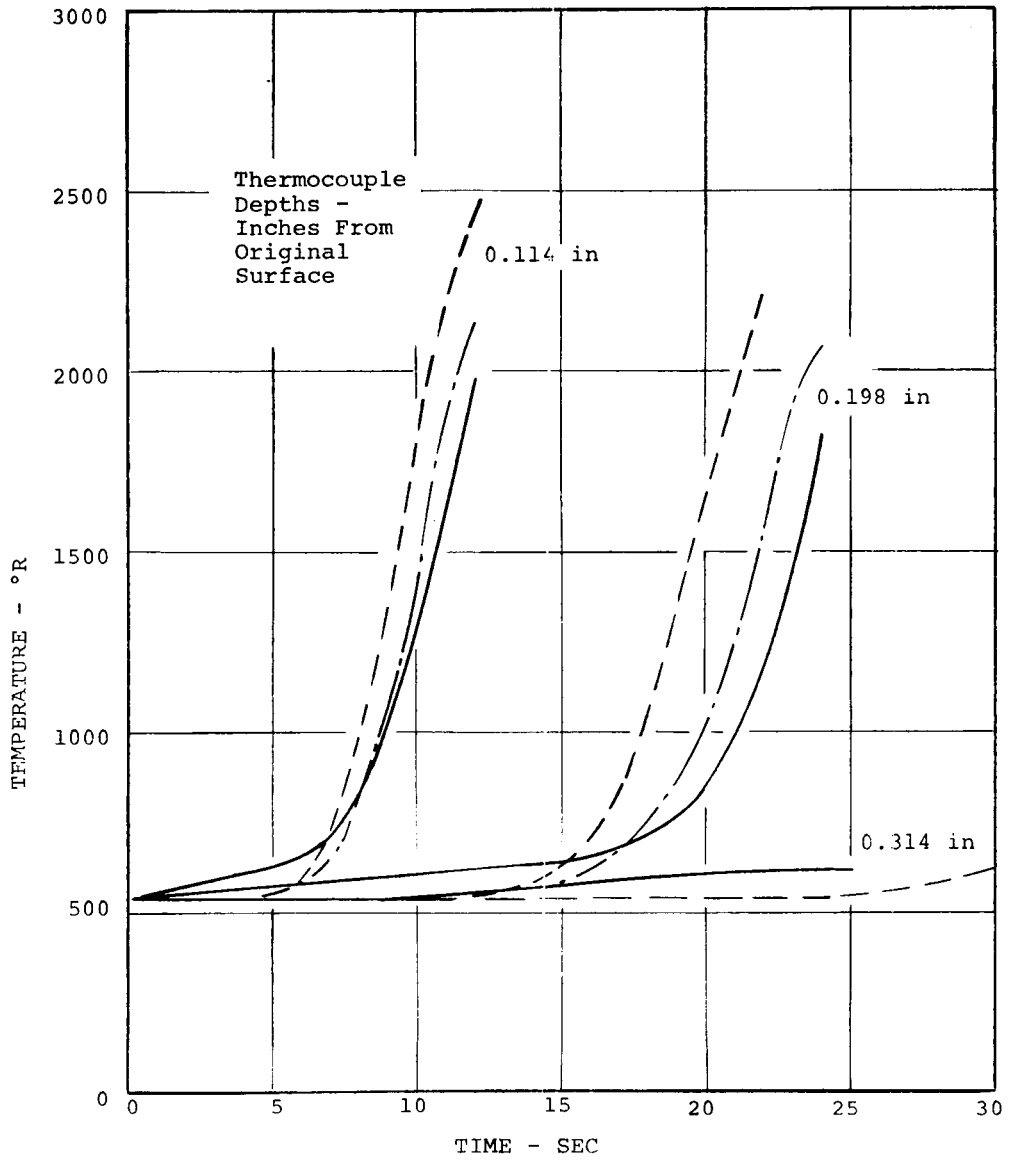

	TEST RESULTS	CHAP RESULTS 16-4	CHAP RESULTS 16-5
CHAP input		Appendix A	"Scala fast" kinetics q_c - 20%
Total recession (in)	.137	.154	.127
Final char δ(in)	.099	.126	.128
Total penetration (in)	.236	.280	.255
Fina surf. temp (°R)	4650	4022	3804
Code	———	– – –	—·—·—·—

FIGURE 20 ITERATIVE CASE, NYLON PHENOLIC TAB NO. 16
q_c = 256 BTU/ft^{2}sec, p = .284 atm, h_e = 4900 BTU/lb

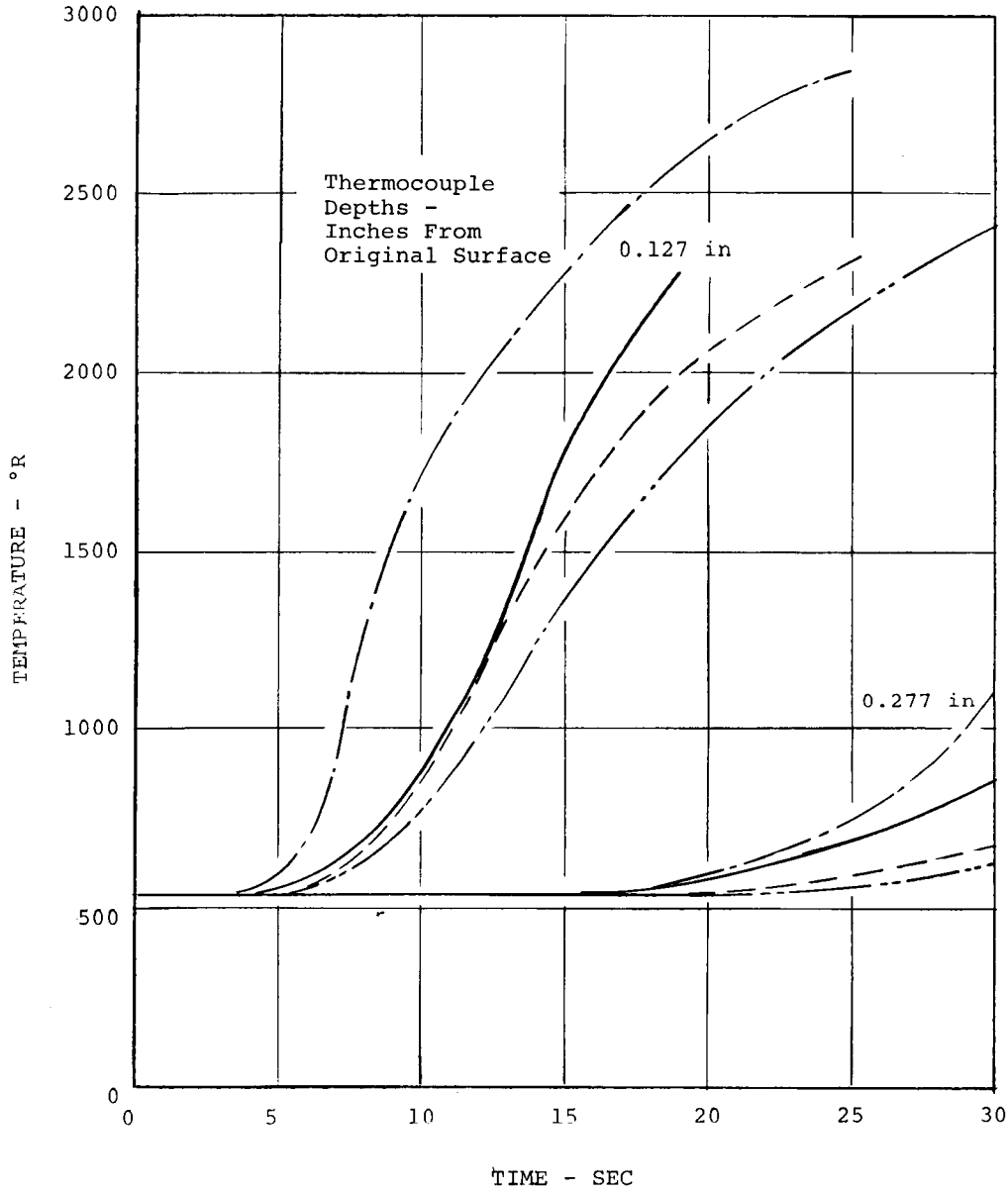

	TEST RESULTS	CHAP RESULTS		
		66-6	66-8	66-9
CHAP input		Froz/equil. $\bar{C}_p$	- - Equil. $\bar{C}_p$ - -	
			$\alpha_p = 0$	"Scala fast" kinetics
Total recession (in)	.096	.025	.056	.041
Final char δ(in)	.10	.196	.213	.167
Pyrolysis zone δ(in)	.04	--	--	--
Total penetration (in)	.236	.221	.269	.211
Final surf. temp (°R)	4100	3450	3760	3410
Code	———	- - -	—·—·—	—··—··—

FIGURE 21 ITERATIVE CASE, AVCOAT 5026-39HC/G TAB No. 66
q_c = 117 BTU/ft^{2}sec, p = .0279 atm, h_e = 10,976 BTU/lb

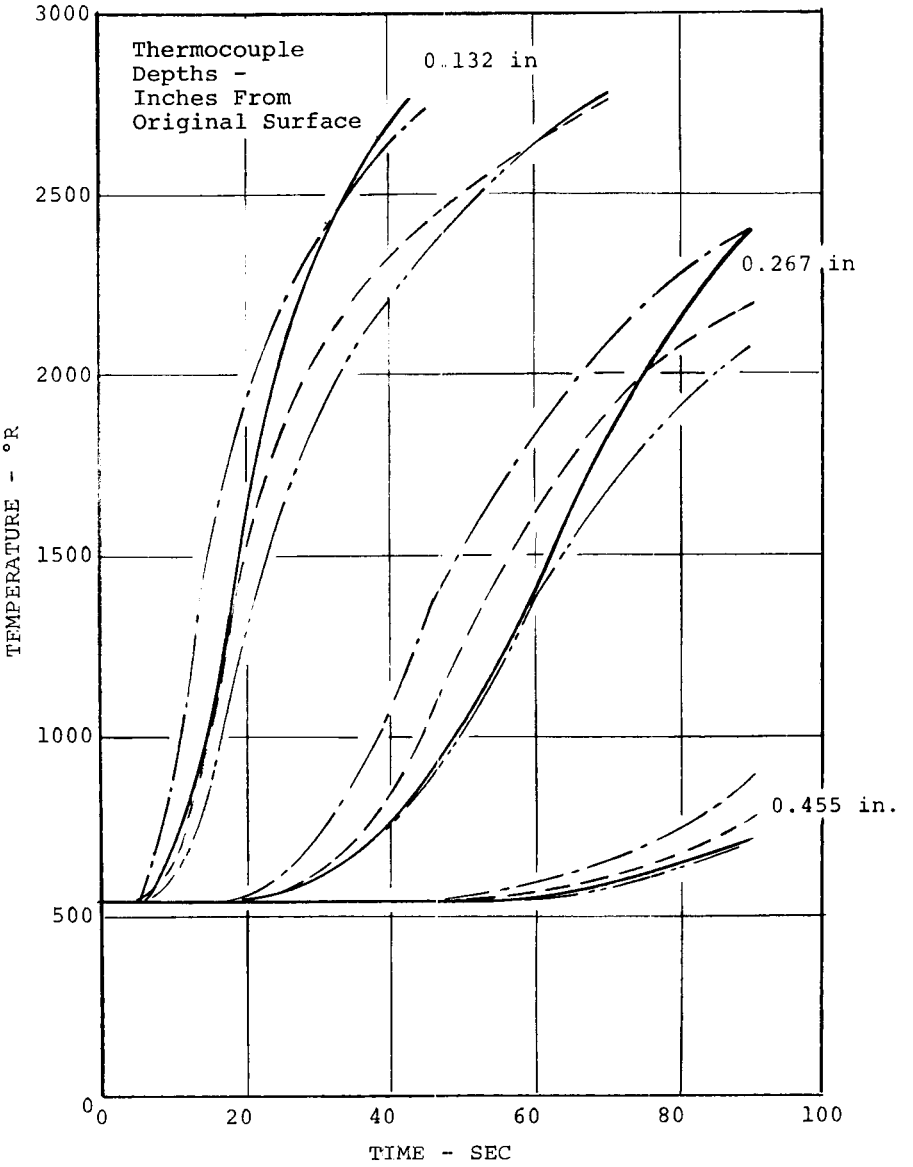

	TEST RESULTS	CHAP RESULTS 62-5	62-6	62-7
CHAP input		Froz/equil. $\bar{C}_p$	—— Equil. $\bar{C}_p$ —— "Scala fast" kinetics	$\alpha_p = 0$
Total recession (in)	.137	.035	.079	.087
Final char δ(in)	.13	.347	.281	.320
Pyrolysis zone δ(in)	.06	--	--	--
Total penetration (in)	.327	.382	.360	.407
Final surf. temp (°R)	3280	3402	3340	3600
Code	——	- - -	-·-·-·-	-·-·-·-

FIGURE 22 ITERATIVE CASE, AVCOAT 5026-39HC/G TAB NO. 62
q_c = 91 BTU/ft^{2}sec, p = .0081 atm, h_e = 13,500 BTU/lb

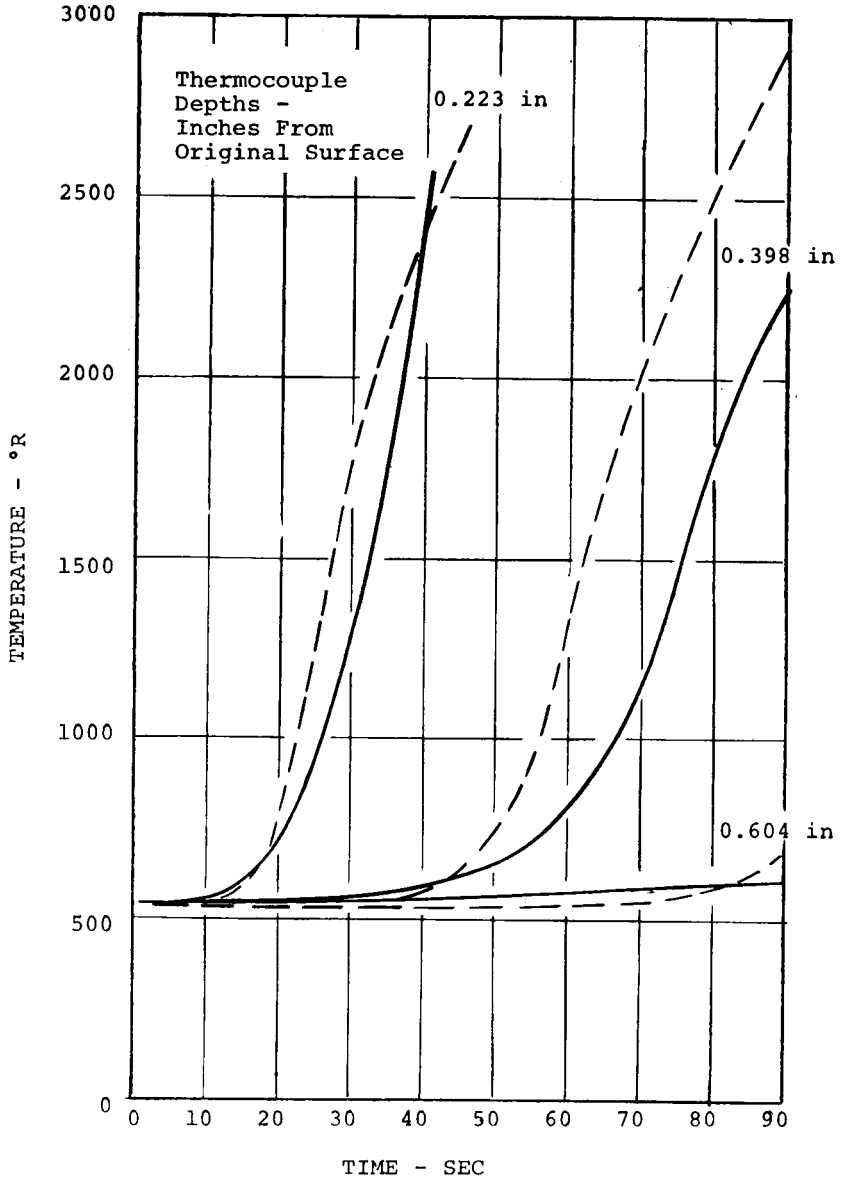

	TEST RESULTS	CHAP RESULTS 83-1
CHAP input		Frozen/equil. $\bar{C}_p$
Total recession (in)	.241	.329
Final char δ (in)	.125	.208
Pyrolysis zone δ (in)	.050	--
Total penetration (in)	.416	.537
Final surf. temp (°R)	3500	3540
Code	———	– – –

FIGURE 23 ITERATIVE CASE AVCOAT 5026-39HC/G TAB NO. 83
q_c = 115 BTU/ft^{2}sec, p = .0289 atm, h_e = 3,692 BTU/lb

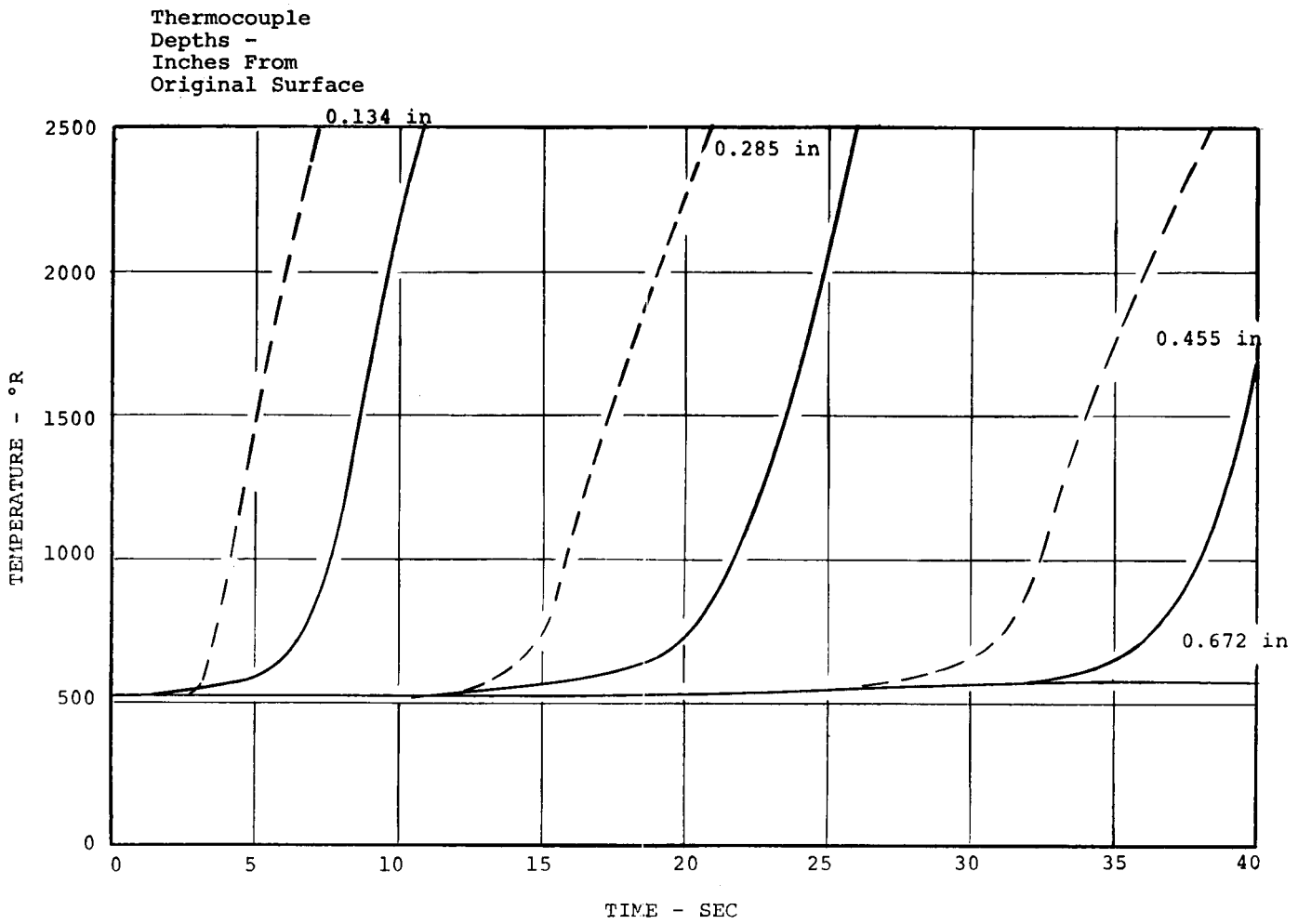

	TEST RESULTS	CHAP RESULTS 92-6
CHAP input		Frozen/equil. $\bar{C}_p$
Total recession (in)	.388	.345
Final char δ (in)	.08	.166
Pyrolysis zone δ (in)	.02	--
Total penetration (in)	.488	.511
Final surf. temp (°R)	4820	5260
Code	———	- - -

FIGURE 24 ITERATIVE CASE, AVCOAT 5026-39HC/G TAB NO. 92
q_c = 560 BTU/ft^{2}sec, p = .0817 atm, h_e = 10,588 BTU/lb

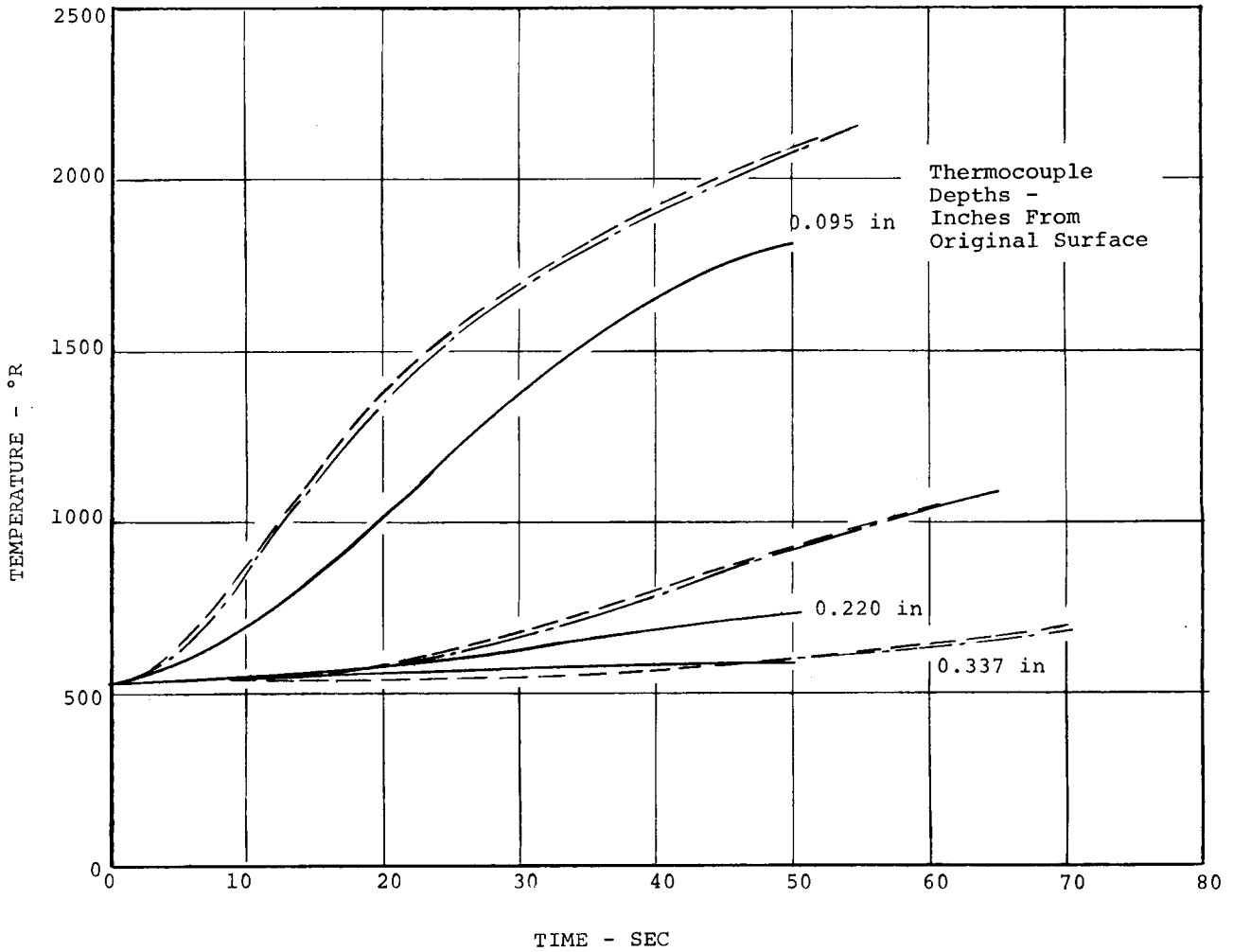

	TEST RESULTS	CHAP RESULTS 1-2	1-3
CHAP input	----	Melting at 3800°R	Ref. 8 recess. model
Total recession (in)	+.052	.008	.021
Final char δ (in)	.205	.185	.172
Total penetration (in)	.153	.193	.193
Final surf. temp (°R)	3000	3590	3480
Code	———	— — —	—·—·—

FIGURE 25 ITERATIVE CASE, SILICONE ELASTOMER TAB NO. 1
q_c = 87 BTU/ft^{2}sec, p = .0109 atm, h_e = 10,670 BTU/lb

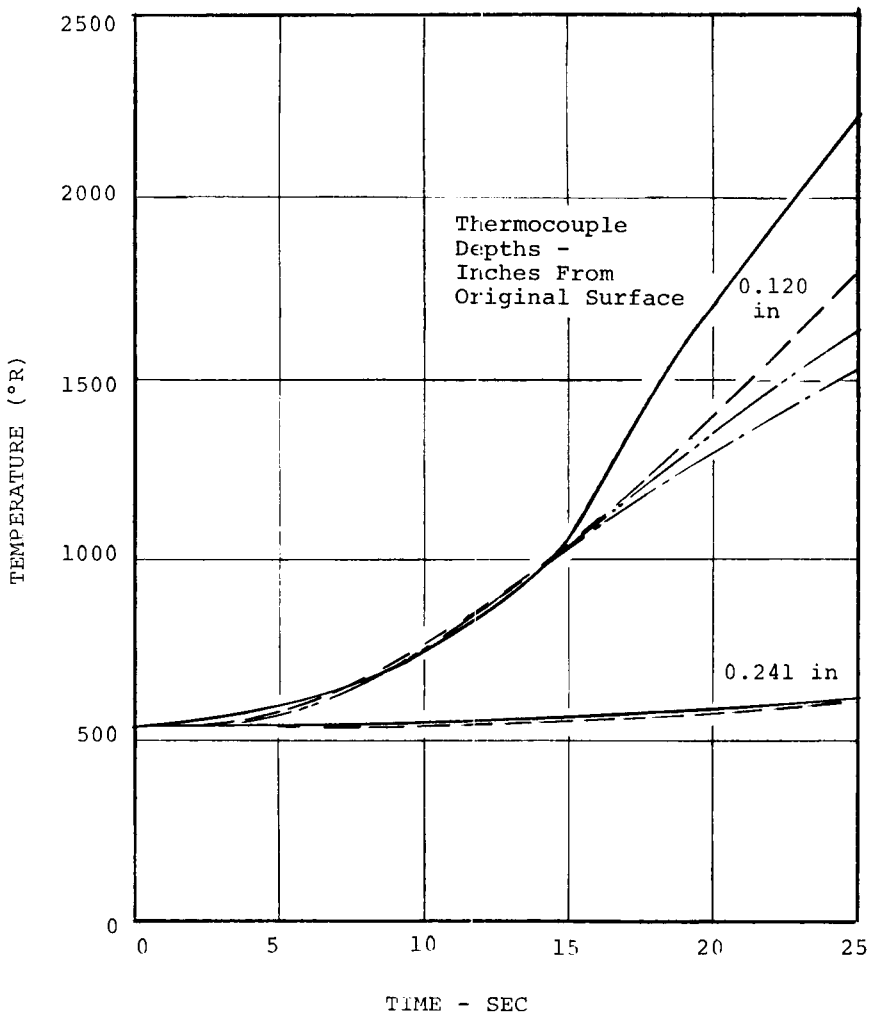

	TEST RESULTS	CHAP RESULTS 4-2	4-3	4-4
CHAP input		Melting at 3800°R	Melting suppressed	Ref. 8 recess. model
Total recession (in)	.004	.060	.003	.033
Final char δ(in)	.121	.072	.119	.095
Total penetration (in)	.125	.132	.122	.128
Final surf. temp (°R)	3550	3840	4450	4140
Code	———	— — —	—·—·—·—	—··—··—

FIGURE 26 ITERATIVE CASE, SILICONE ELASTOMER TAB. NO 4
q_c = 221 BTU/ft^{2}sec, p = .0085 atm, h_e = 19,721 BTU/lb

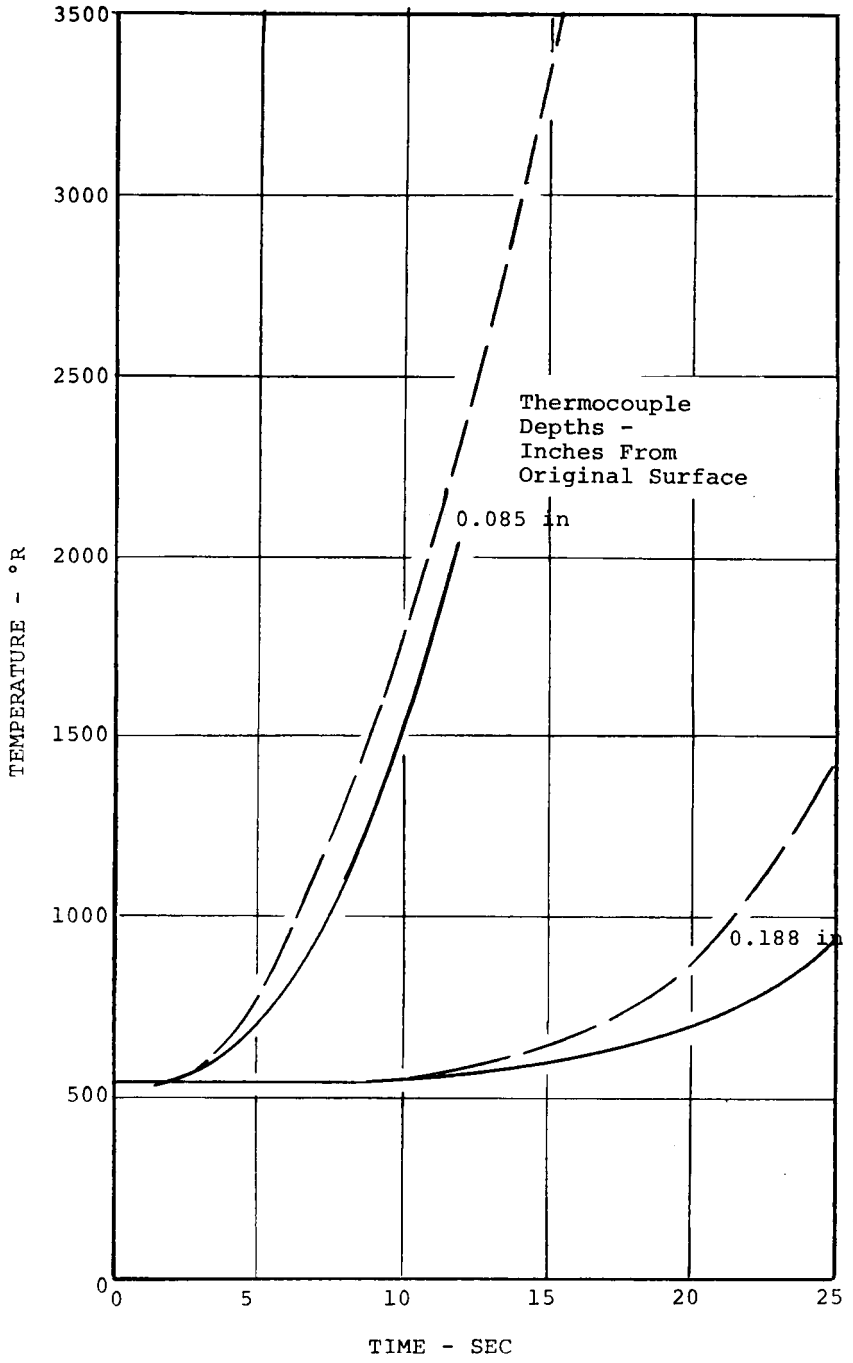

	TEST RESULTS	CHAP RESULTS
CHAP input	----	Ref. 8 recess. model
Total recession (in)	.070	.159
Final char δ(in)	.117	.054
Total penetration (in)	.187	.213
Final surf. temp. (°R)	4300	4306
Code	———	– – –

FIGURE 27 ITERATIVE CASE, SILICONE ELASTOMER TAB NO. 5
q_c = 273 BTU/ft^{2}sec, p = .284 atm, h_e = 4900 BTU/lb

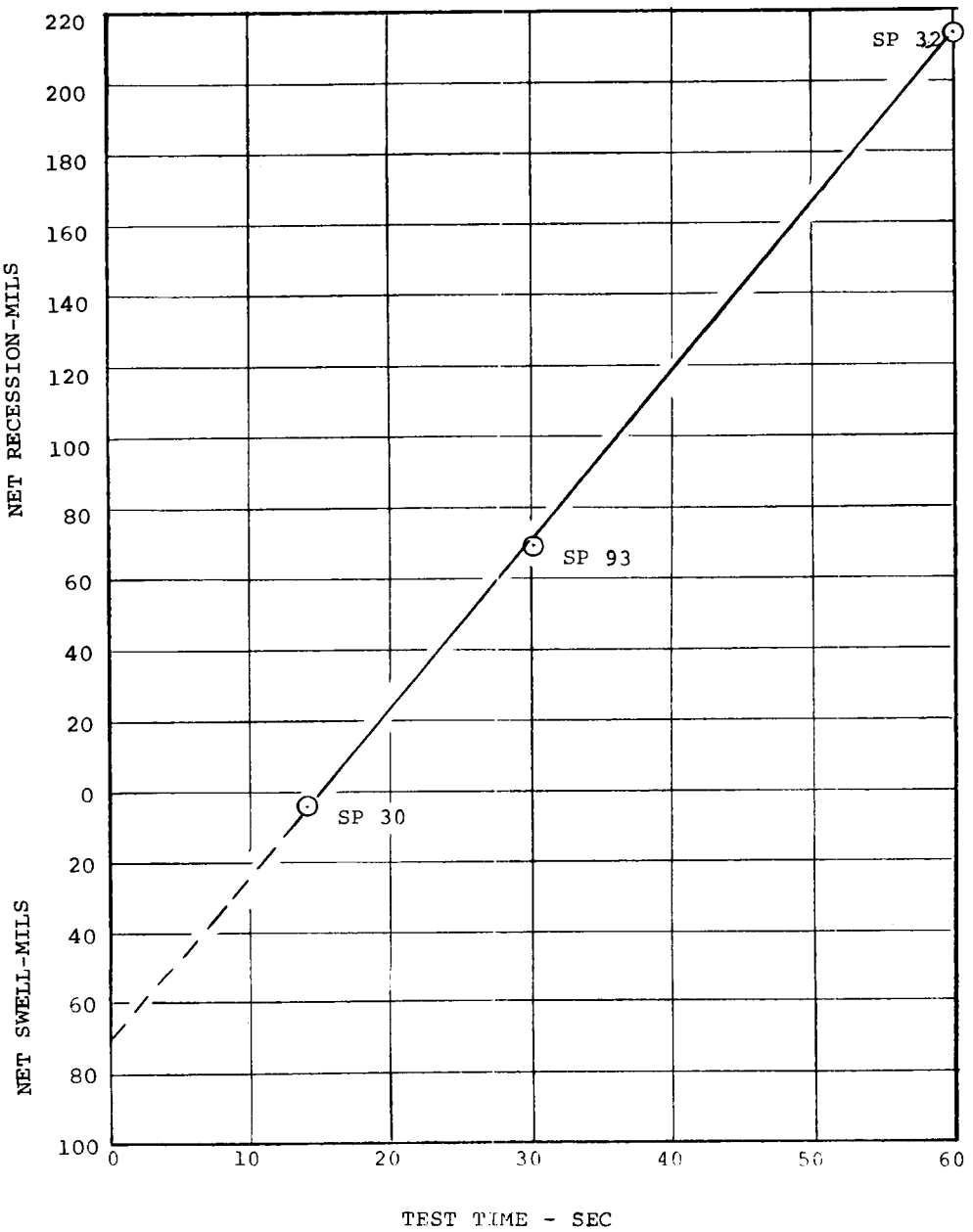

FIGURE 28 NET OBSERVED RECESSION, TESTS SP30, SP93, SP32 OF REF 10

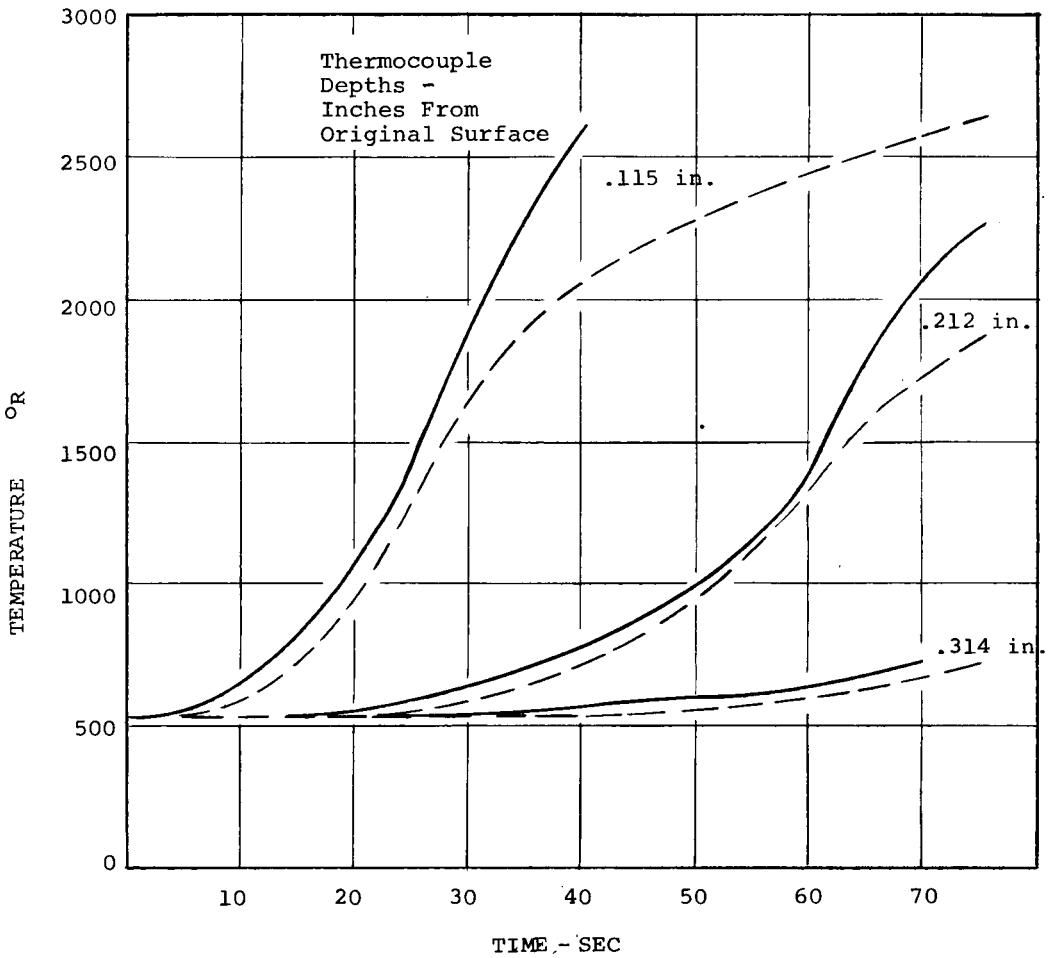

	TEST RESULTS	CHAP RESULTS
Total recession (in)	.115	.049
Final char δ (in)	.132	.206
Total penetration (in)	.247	.255
Final surf. temp. (°R)	3500	3060
Code	———	– – –

FIGURE 29 FINAL CASE, NYLON PHENOLIC TAB NO. 7
q_c = 85 BTU/ft^{2}sec, p = .0111 atm, h_e = 10,322 BTU/lb

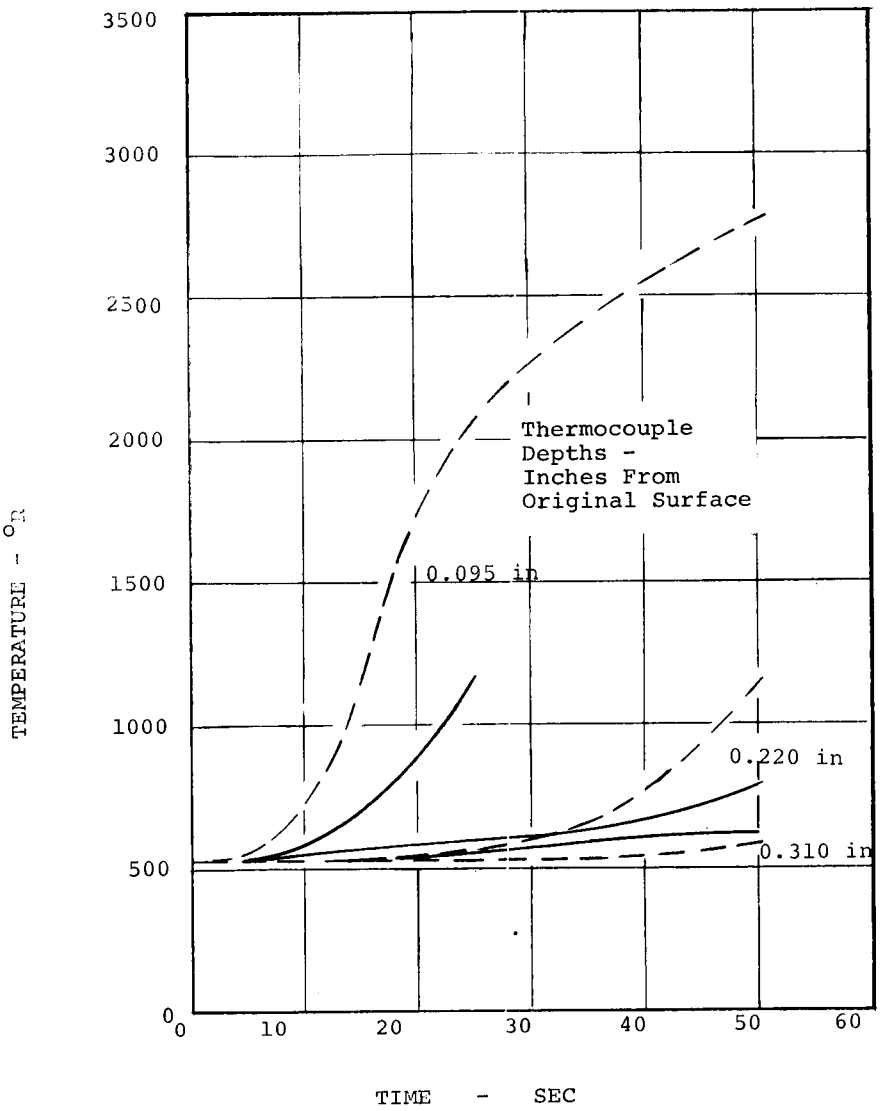

	TEST RESULTS	CHAP RESULTS
Total recession (in)	.064	.035
Final char δ (in)	.117	.183
Total penetration (in)	.181	.218
Final surf. temp (°R)	--	3250
Code	———	– – –

FIGURE 30 FINAL CASE, NYLON PHENOLIC TAB NO. 12
q_c = 117 BTU/ft^{2}sec, p = .00572 atm, h_e = 12,664 BTU/lb

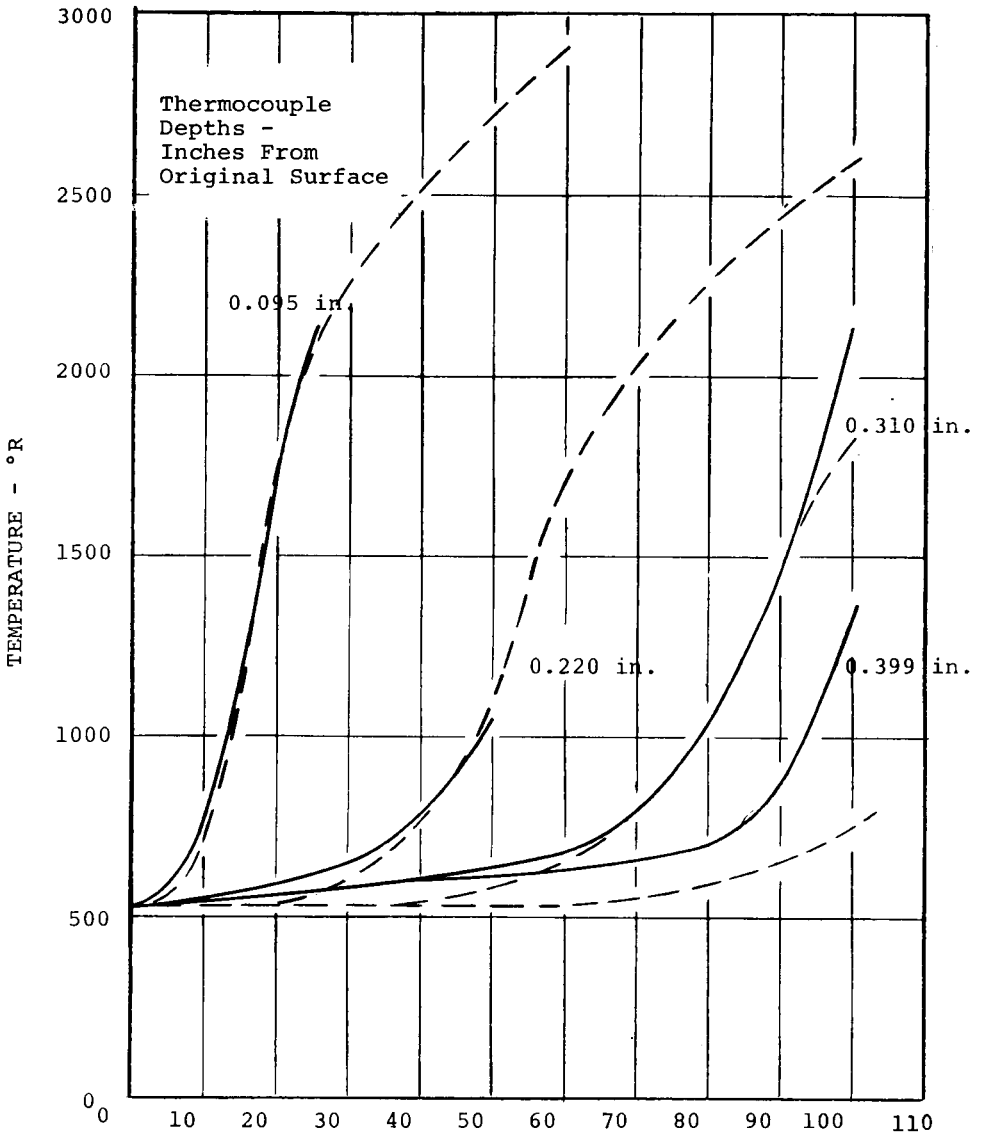

	TEST RESULTS	CHAP RESULTS
Total recession (in)	.189	.140
Final char δ(in)	.156	.208
Total penetration (in)	.345	.348
Final surf. temp (°R)	3600	3130
Code	——	- - -

FIGURE 31 FINAL CASE, NYLON PHENOLIC TAB NO. 18
q_c = 80 BTU/ft^{2}sec, p = .0204 atm, h_e = 5,583 BTU/lb

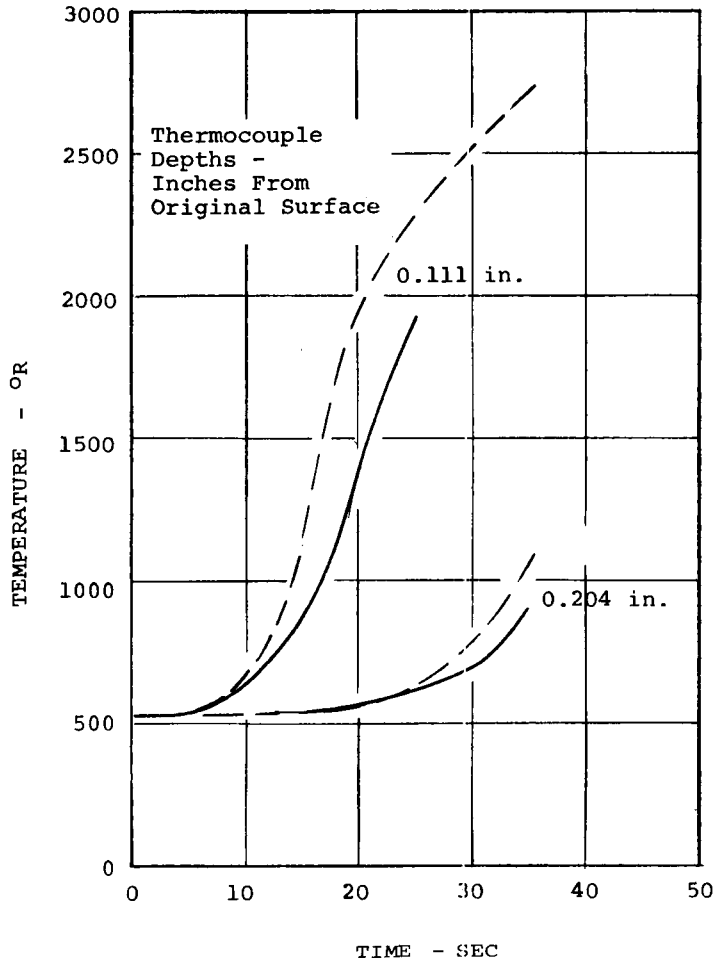

	TEST RESULTS	CHAP RESULTS
Total recession (in)	.025	.040
Final char δ (in)	.135	.156
Total penetration (in)	.160	.196
Final surf. temp (°R)	3800	3540
Code	———	– – –

FIGURE 32 FINAL CASE, NYLON PHENOLIC TAB NO. 20
q_c = 144 BTU/ft^{2}sec, p = .0199 atm, h_e = 10,200 BTU/lb

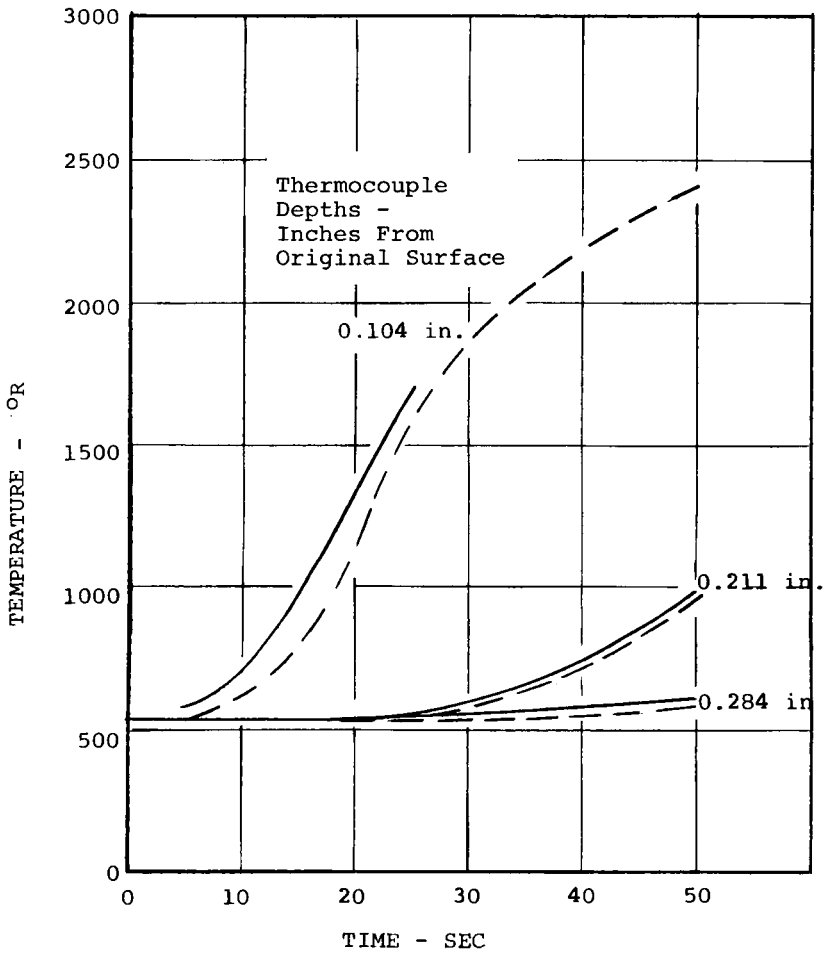

	TEST RESULTS	CHAP RESULTS
Total recession (in)	.054	.022
Final char δ (in)	.124	.171
Total penetration (in)	.178	.193
Final surf. temp (°R)	3500	3040
Code	———	– – –

FIGURE 33 FINAL CASE, NYLON PHENOLIC TAB NO. 23
q_c = 103 BTU/ft^{2}sec, p = .00511 atm, h_e = 14,855 BTU/lb

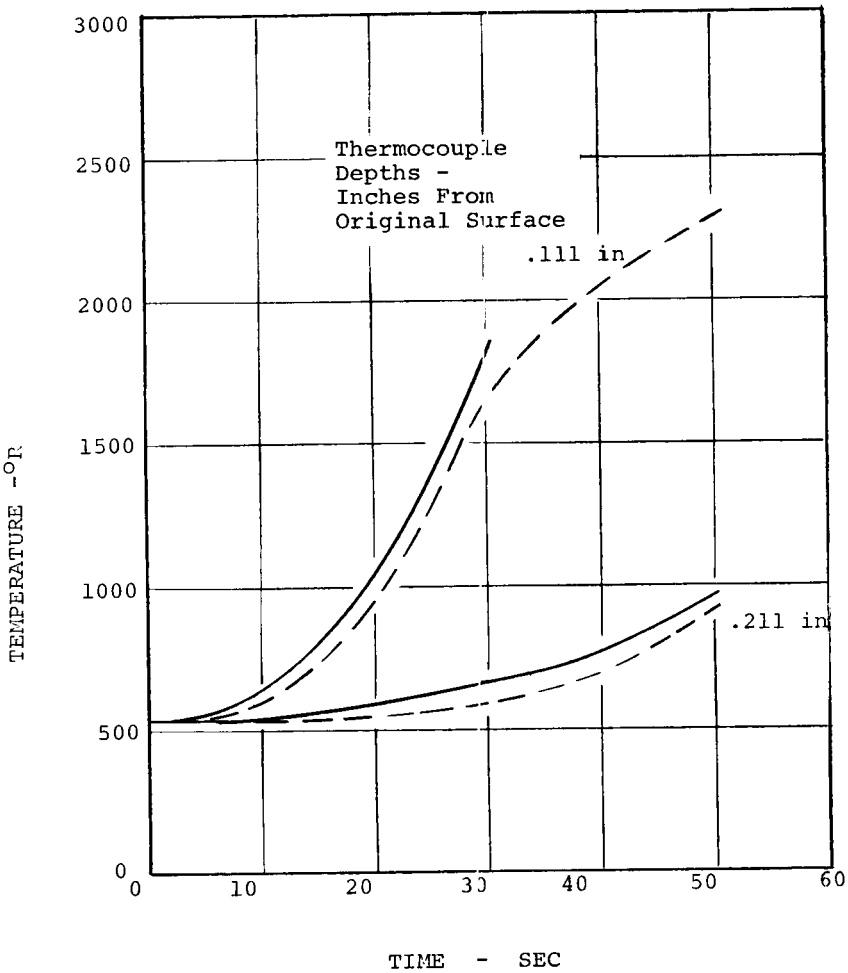

	TEST RESULTS	CHAP RESULTS
Total recession (in)	.049	.021
Final char δ (in)	.122	.167
Total penetration (in)	.171	.188
Final surf. temp (°R)	3400	2980
Code	———	— — —

FIGURE 34 FINAL CASE, NYLON PHENOLIC TAB NO. 24
q_c = 98 BTU/ft^{2}sec, p = .00511 atm, h_e = 14,855 BTU/lb

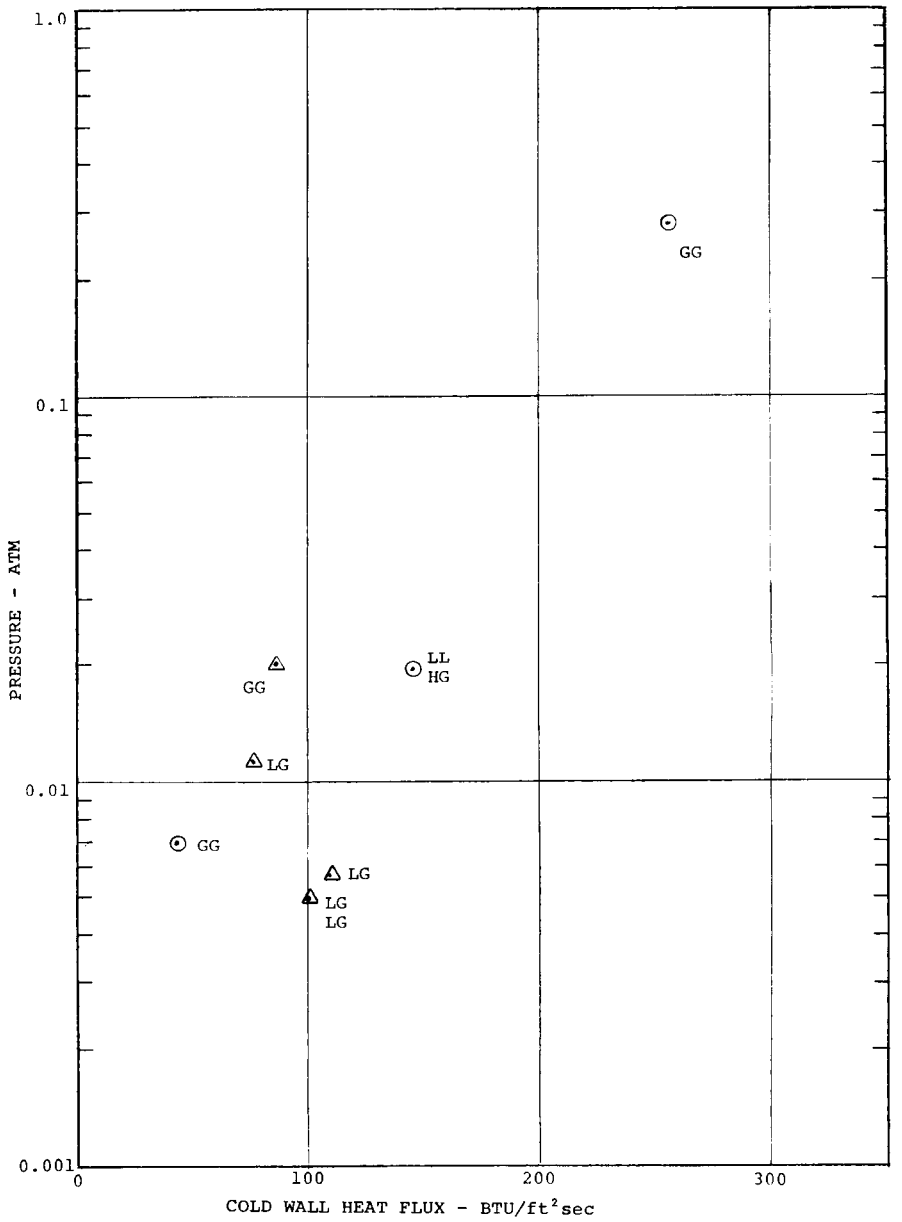

FIGURE 35

ABLATION CASE MAP, LOW DENSITY NYLON PHENOLIC

⊙ Iterative Case

△ Final Case

Recession and Pyrolysis Plane Penetration
Prediction Results Indicated by:

Recession	Pyrolysis Penetration
L < 75%	L < 90%
75% < G < 125%	90% < G < 125%
H > 125%	H > 125%

Example: LG denotes low recession prediction, satisfactory pyrolysis prediction

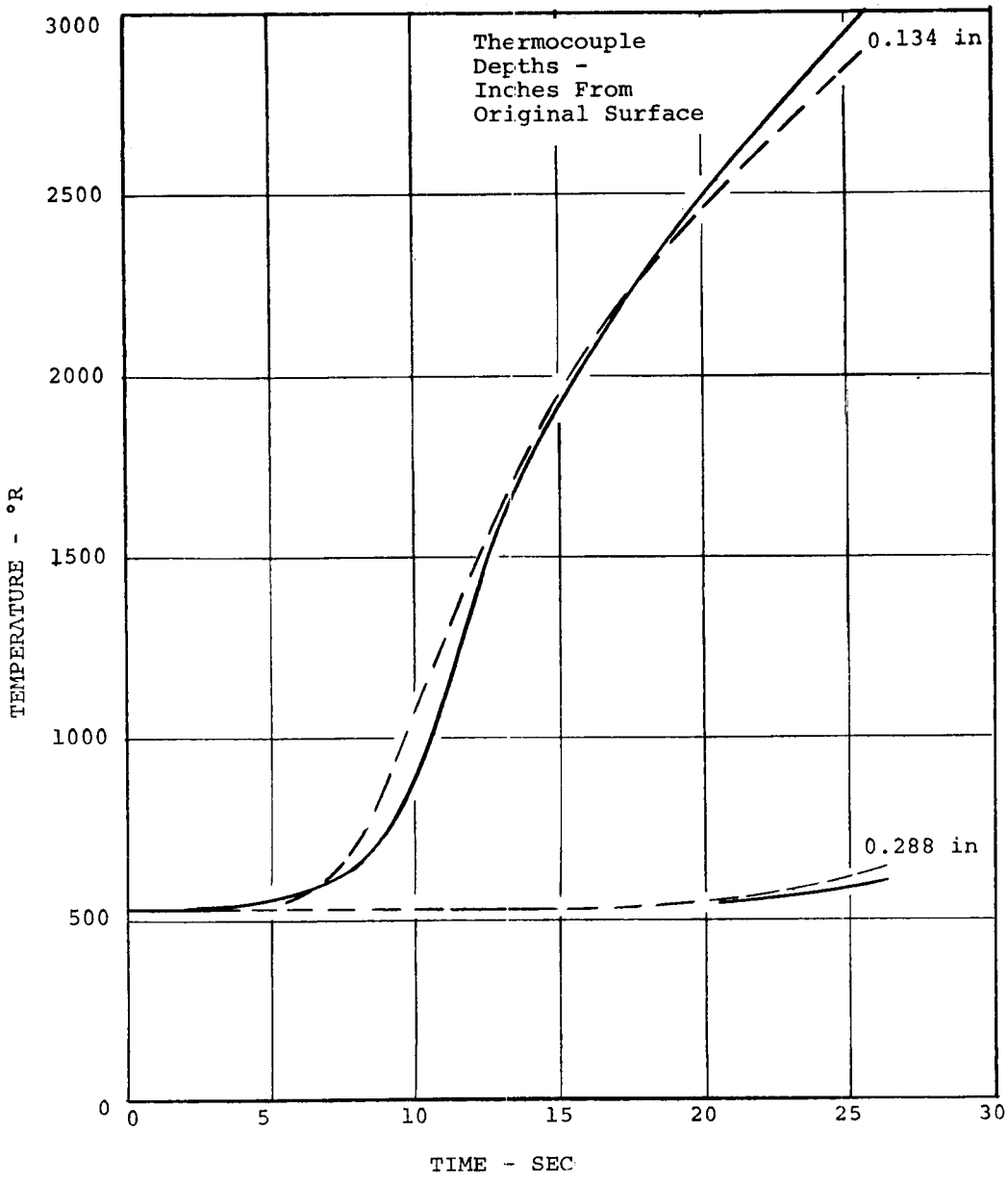

	TEST RESULTS	CHAP RESULTS
Total recession (in)	.081	.075
Final Char δ(in)	.090	.159
Pyrolysis Zone δ(in)	.02	--
Total penetration (in)	.191	.234
Final surf. temp (°R)	4100	3870
Code	———	– – –

FIGURE 36 FINAL CASE, AVCOAT 5026-39HC/G TAB NO. 27
q_c = 102 BTU/ft^{2}sec, q_R = 66 BTU/ft^{2}sec, p = .071 atm,
h_e = 5100 BTU/lb

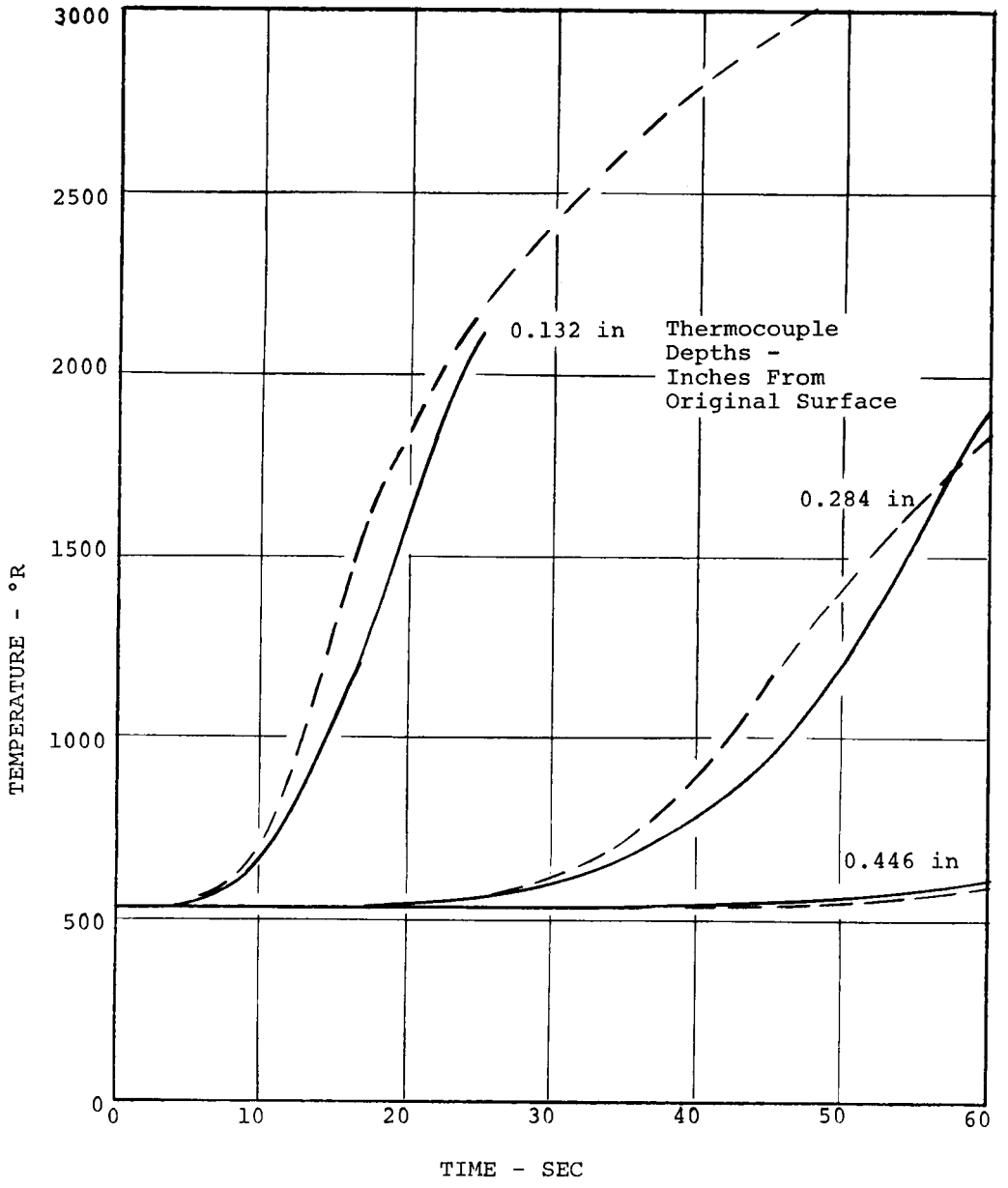

	TEST RESULTS	CHAP RESULTS
Total recession (in)	.147	.075
Final char δ (in)	.10	.262
Pyrolysis zone δ (in)	.07	--
Total penetration (in)	.317	.337
Final surface temp (°R)	3600	3840
Code	———	- - -

FIGURE 37 FINAL CASE, AVCOAT 5026-39HC/G TAB NO. 41
q_c = 155 BTU/ft^{2}sec, p = .008 atm, h_e = 16,300 BTU/lb

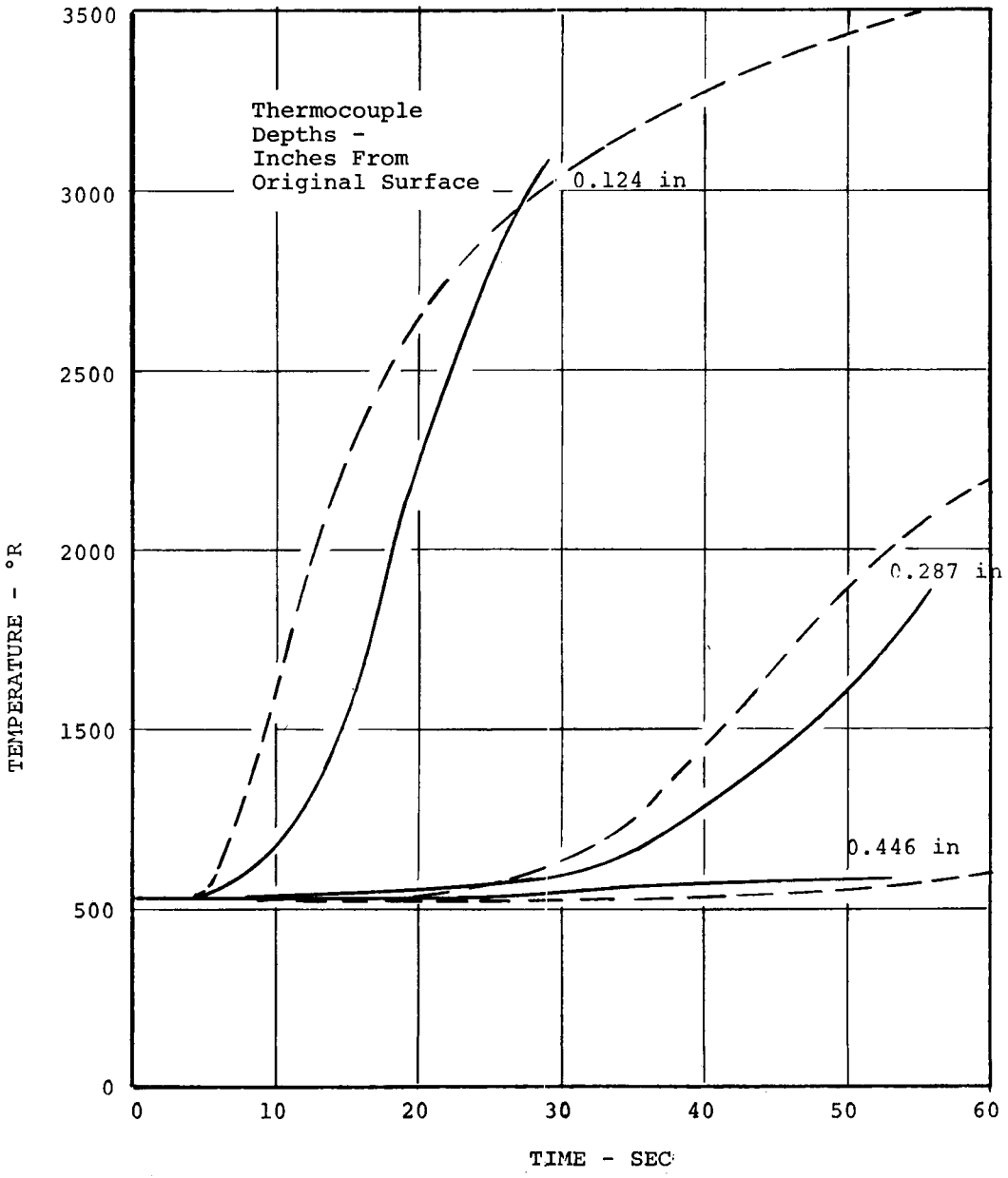

	TEST RESULTS	CHAP RESULTS
Total recession (in)	.050	.000
Final char δ(in)	.210	.334
Pyrolysis zone δ(in)	.06	--
Total penetration (in)	.320	.334
Final surf. temp (°R)	3800	4040
Code	———	— — —

FIGURE 38 FINAL CASE, AVCOAT 5026-39HC/G TAB NO. 46
q_c = 151 BTU/ft^{2}sec, p = .0278 atm, h_e = 5800 BTU/lb, f_o = 0

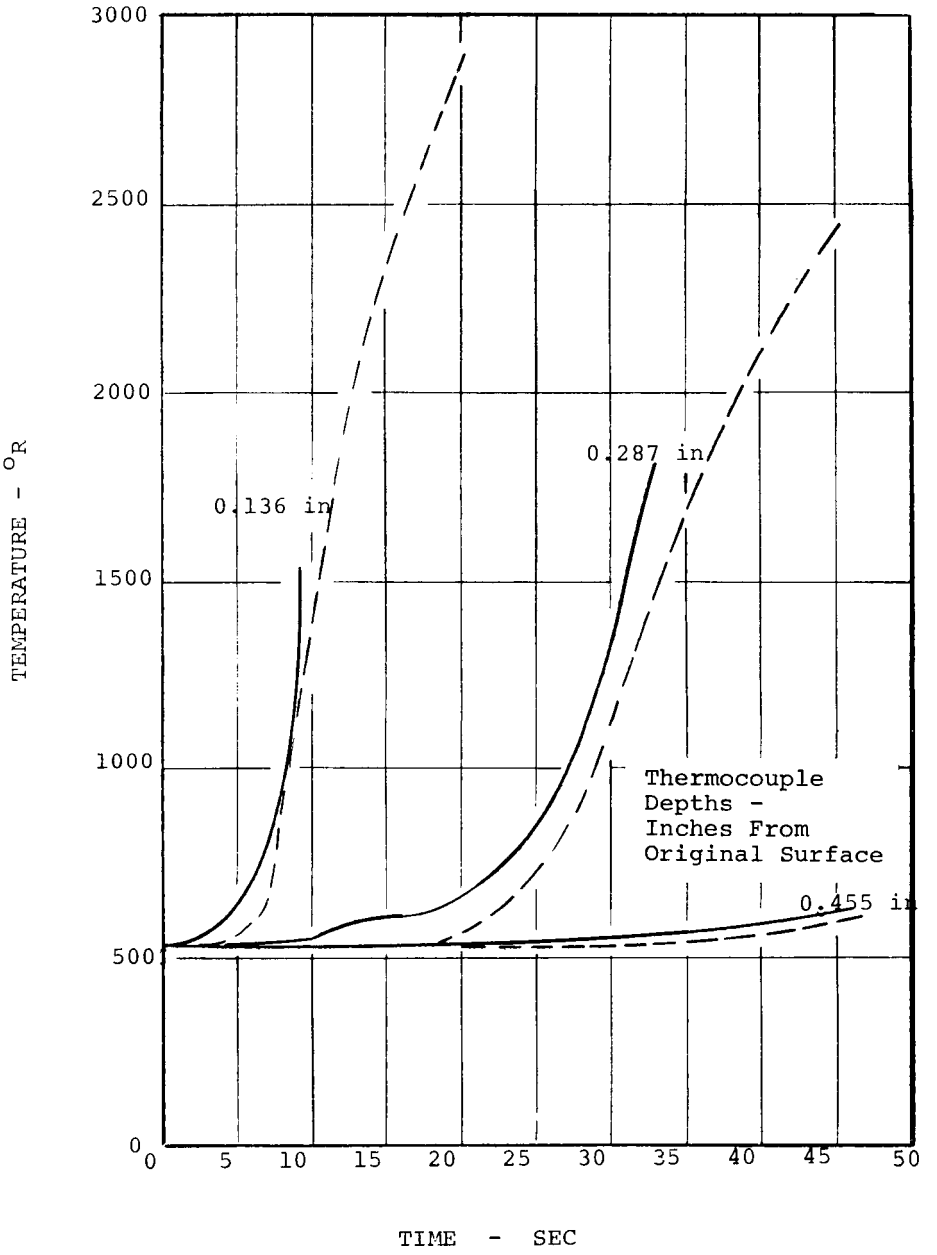

	TEST RESULTS	CHAP RESULTS
Total recession (in)	.215	.127
Final char δ(in)	.08	.230
Pyrolysis zone δ(in)	.04	--
Total penetration (in)	.335	.357
Final surf. temp (°R)	4600	4780
Code	———	— — —

FIGURE 39 FINAL CASE, AVCOAT 5026-39 HC/G TAB NO. 55
q_c = 313 BTU/ft^{2}sec, p = .0287 atm, h_e = 17,400 BTU/lb

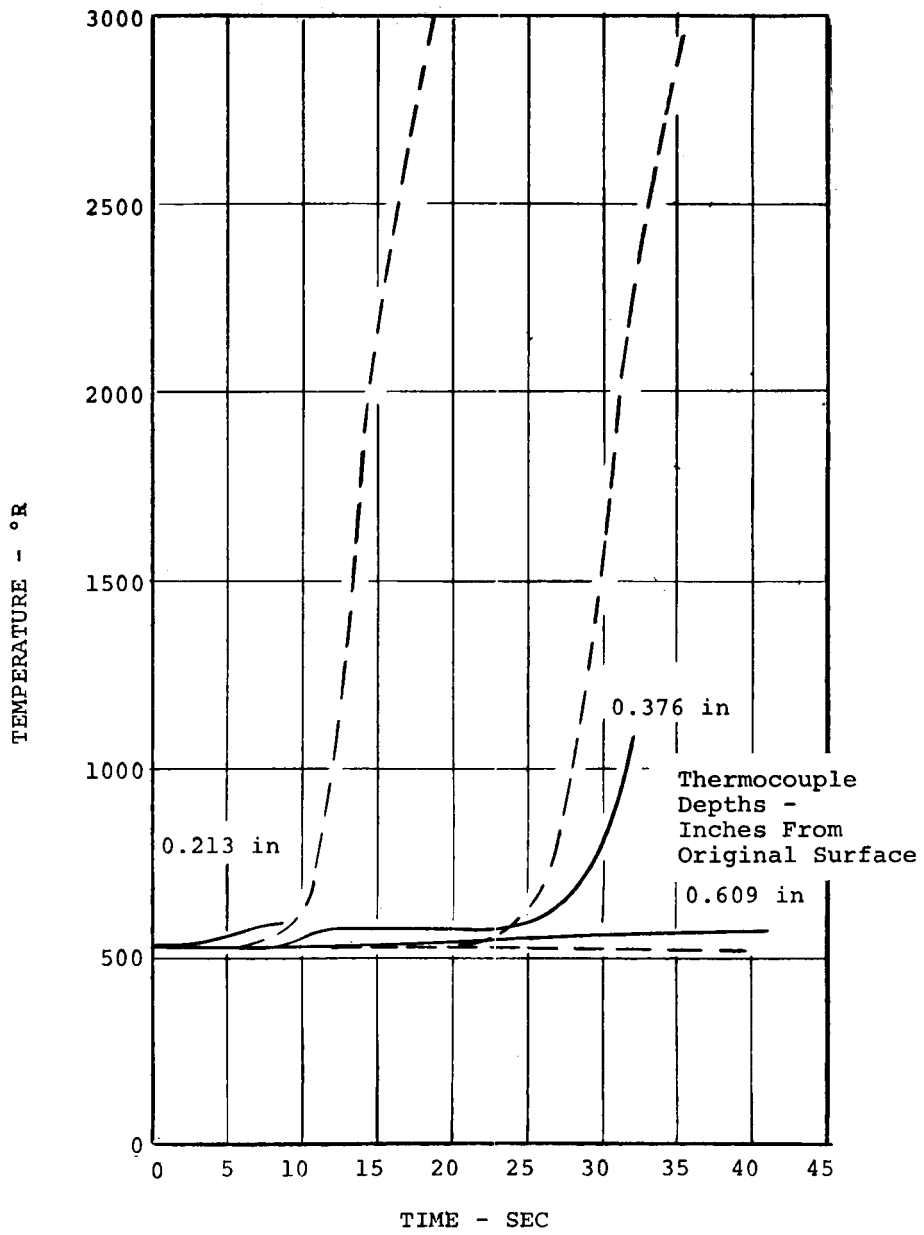

	TEST RESULTS	CHAP RESULTS
Total recession (in)	.338	.350
Fina char δ(in)	.045	.32
Pyrolysis zone δ(in)	.03	--
Total penetration (in)	.413	.670
Final surf. temp (°R)	4640	5260
Code	———	- - -

FIGURE 40 FINAL CASE, AVCOAT 5026-39HC/G TAB NO. 94
q_c = 505 BTU/ft^{2}sec, p = .0842 atm, h_c = 10,400 BTU/lb

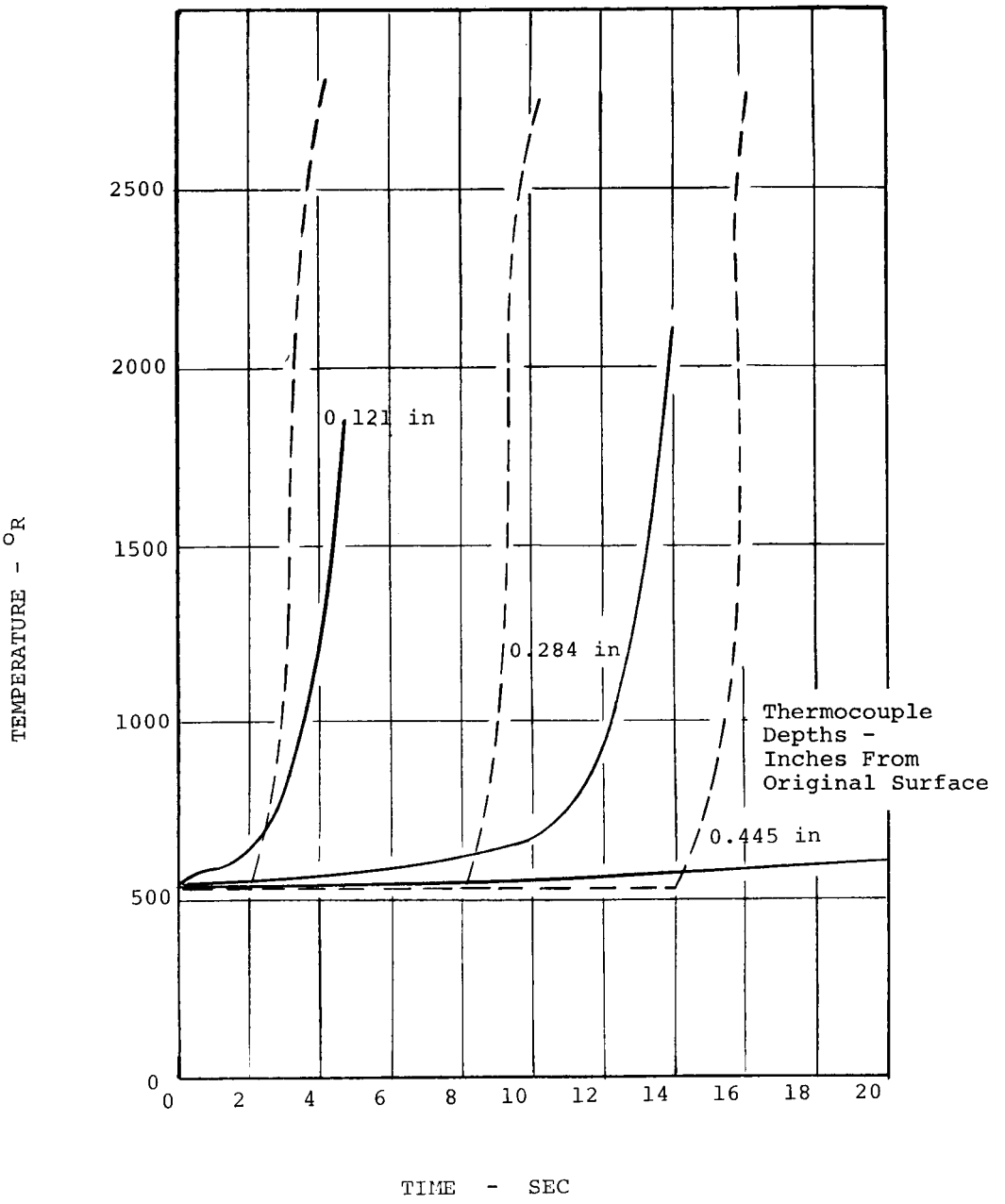

	TEST RESULTS	CHAP RESULTS
Total recession (in)	.325	.538
Final char δ(in)	.040	.034
Pyrolysis zone δ(in)	.01	--
Total penetration (in)	.375	.572
Final surf. temp (°R)	4800	4480
Code	———	– – –

FIGURE 41 FINAL CASE, AVCOAT 5026-39HC/G TAB NO. 95
q_c = 510 BTU/ft^{2}sec, p = .373 atm, h_e = 3515 BTU/lb

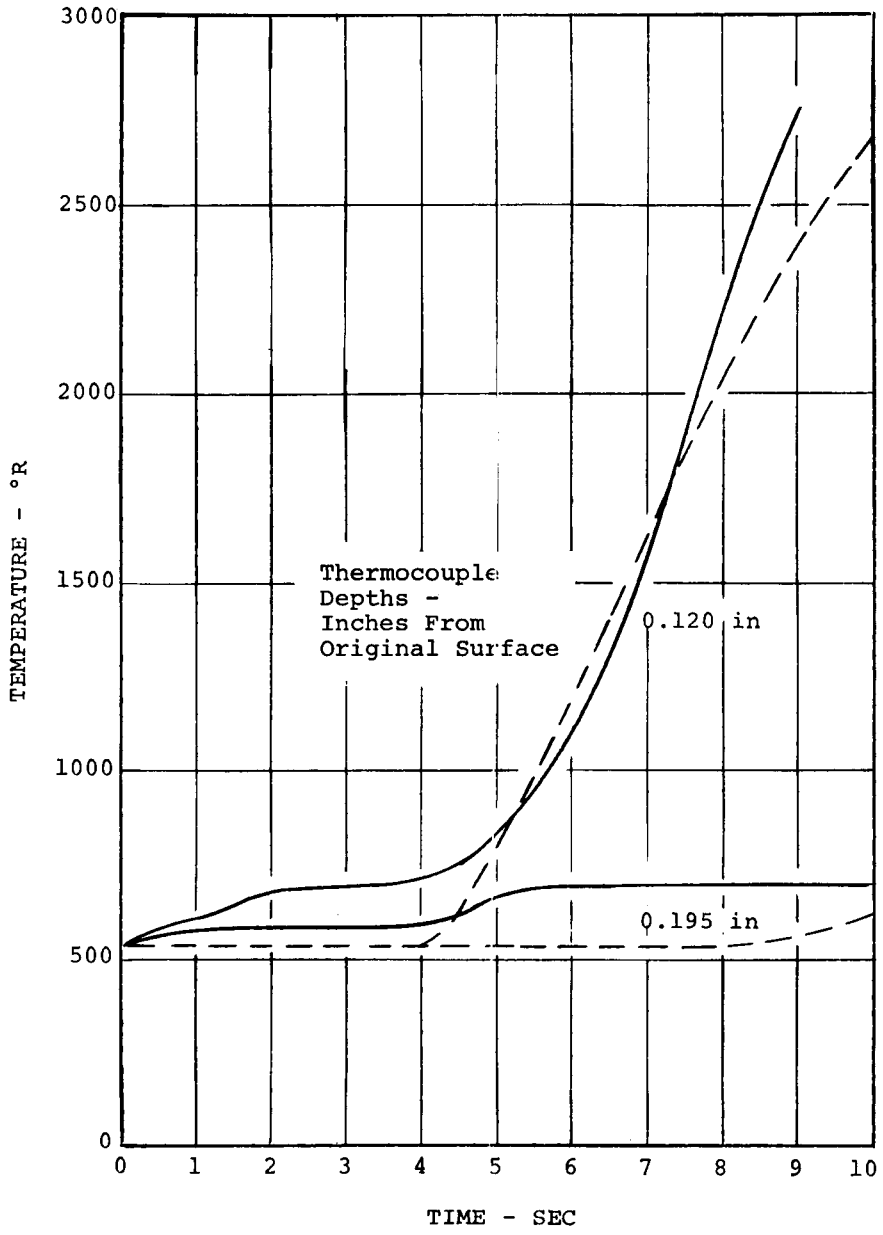

	TEST RESULTS	CHAP RESULTS
Total recession (in)	.059	.077
Final char δ (in)	.067	.082
Total penetration (in)	.126	.159
Final surf. temp (°R)	3600	4130
Code	———	- - - -

FIGURE 42 FINAL CASE, AVCOAT 5026-39HC/G TAB NO. 109
q_c = 250 BTU/ft^{2}sec, p = .50 atm, h_e = 5,420 BTU/lb

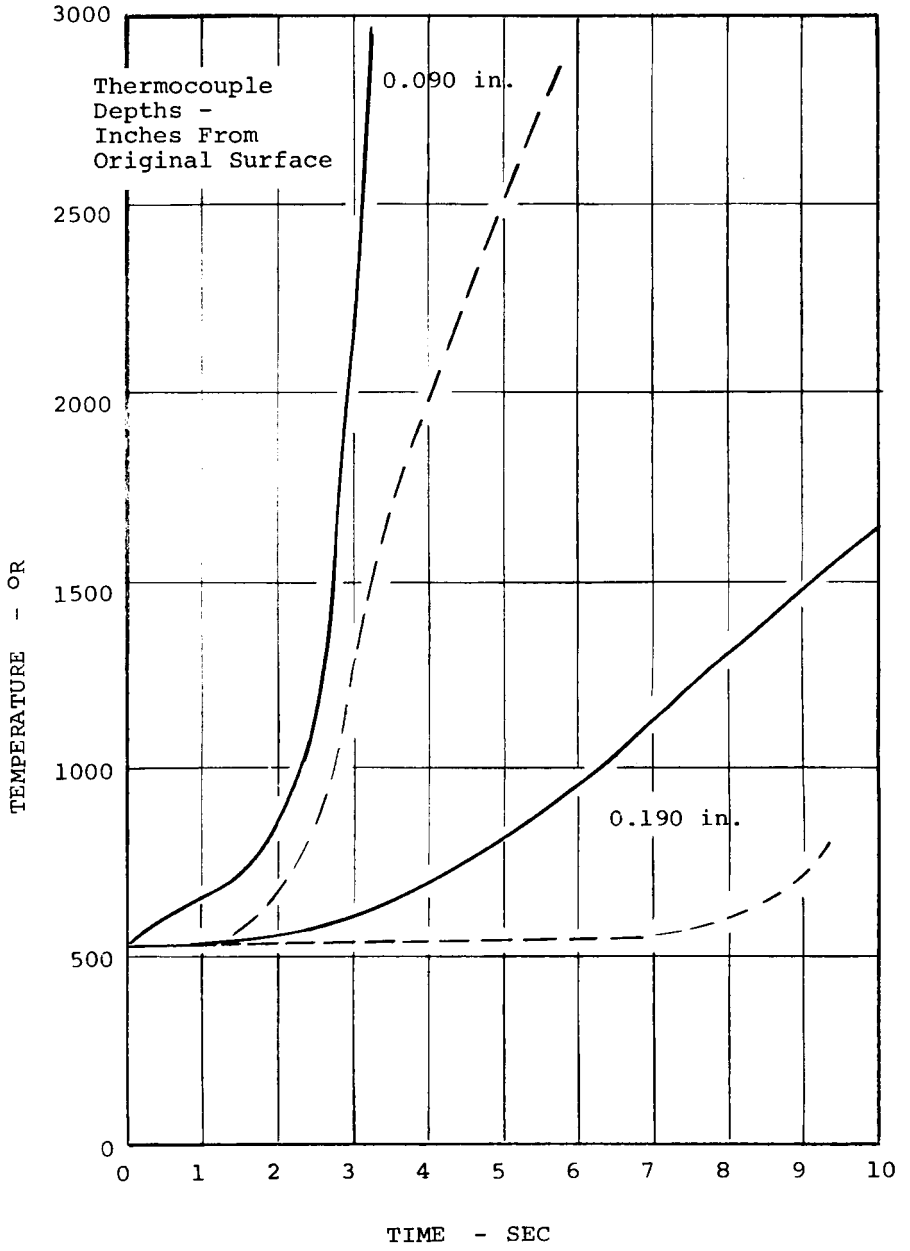

	TEST RESULTS	CHAP RESULTS
Total recession (in)	.028	.064
Final char δ(in)	.022	.104
Total penetration (in)	.050	.168
Final surf. temp (°R)	4300	5310
Code	———	----

FIGURE 43 FINAL CASE, AVCOAT 5026-39HC/G TAB NO. 112
q_c = 595 BTU/ft^{2}sec, p = .50 atm, h_e = 13,400 BTU/lb

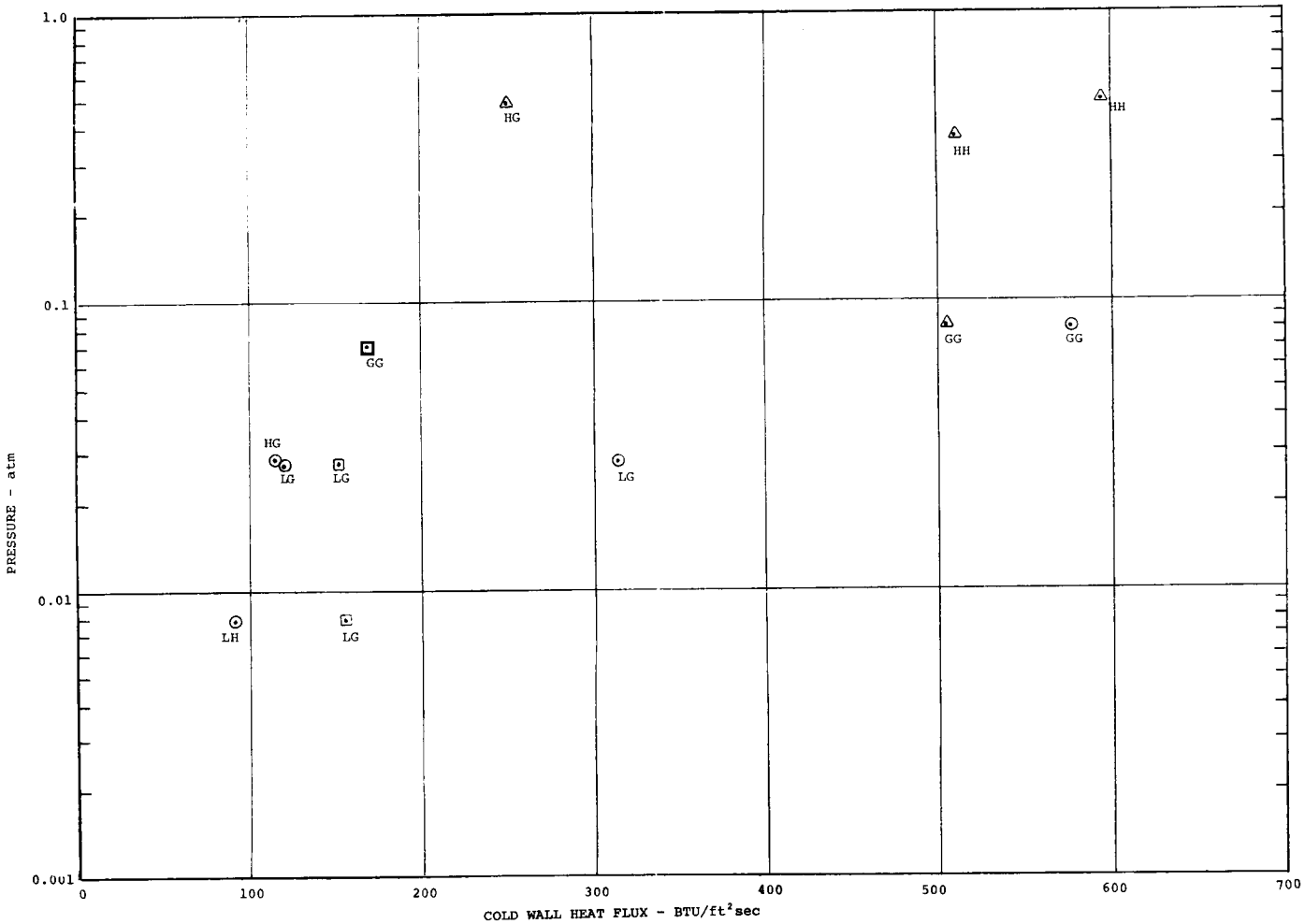

FIGURE 44

ABLATION CASE MAP, AVCOAT 5026-39HC/G

⊙ Iterative Case

△ Final Case

⊡ Supplemental Final Case

Recession and Pyrolysis Plane Penetration Prediction Results Indicated by:

Recession	Pyrolysis Penetration
L < 75%	L < 90%
75% < G < 125%	90% < G < 125%
H > 125%	H > 125%

Example: LG denotes low recession prediction, satisfactory pyrolysis prediction

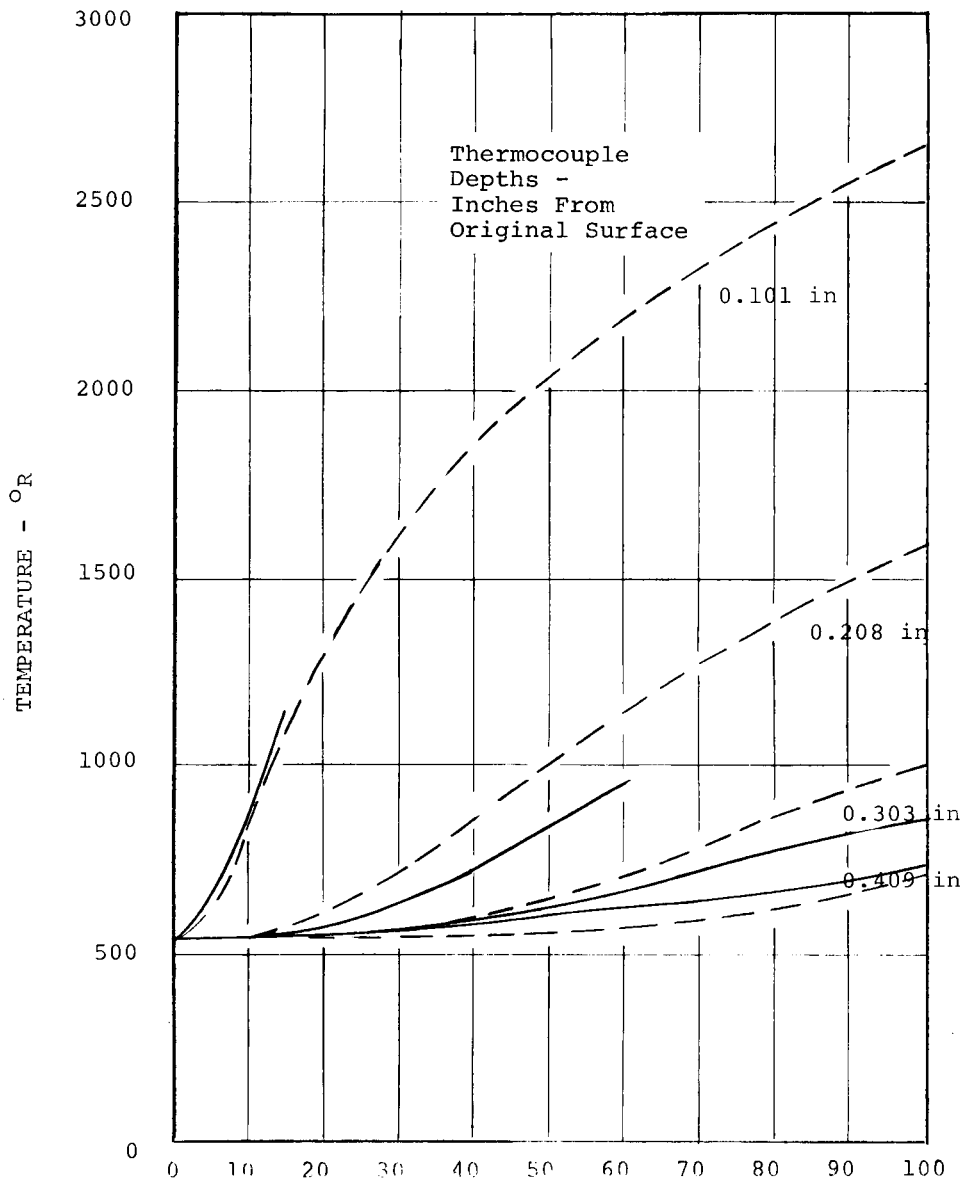

	TEST RESULTS	CHAP RESULTS
Total recession (in)	+.025	.042
Final char δ(in)	.217	.184
Total penetration (in)	.192	.226
Final surf. temp (°R)	2700	3430
Code	———	– – –

FIGURE 45 FINAL CASE, SILICONE ELASTOMER TAB NO. 8
q_c = 77.7 BTU/ft^{2}sec, p = .020 atm, h_e = 5500 BTU/lb

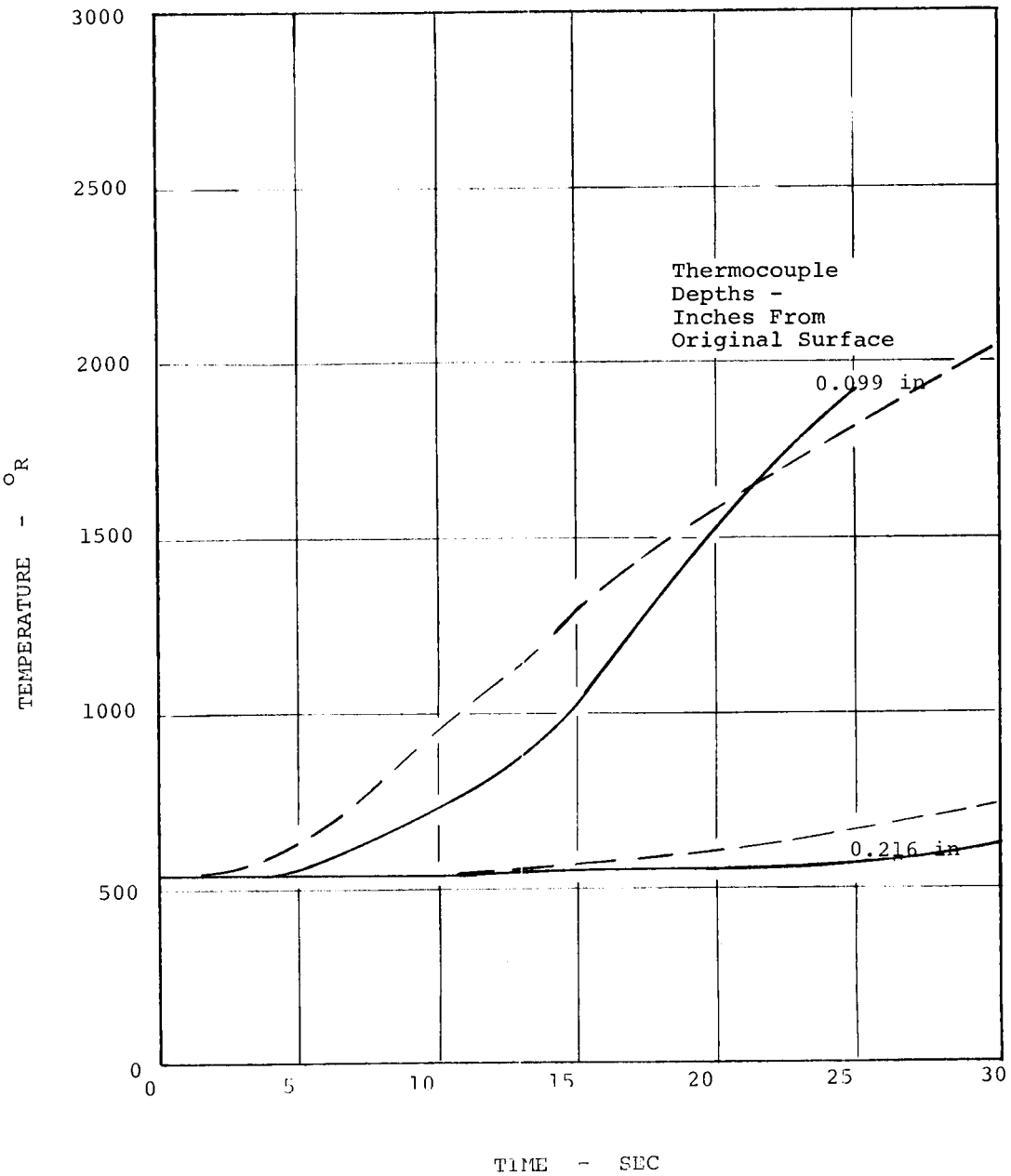

	TEST RESULTS	CHAP RESULTS
Total recession (in)	.004	.033
Final char δ(in)	.127	.112
Total penetration (in)	.131	.145
Final surf. temp (°R)	3460	3870
Code	———	– – –

FIGURE 46 FINAL CASE, SILICONE ELASTOMER TAB NO. 9
$\dot{q}_c$ = 145 BTU/ft^{2}sec, p = .0199 atm, h_e = 10,200 BTU/lb

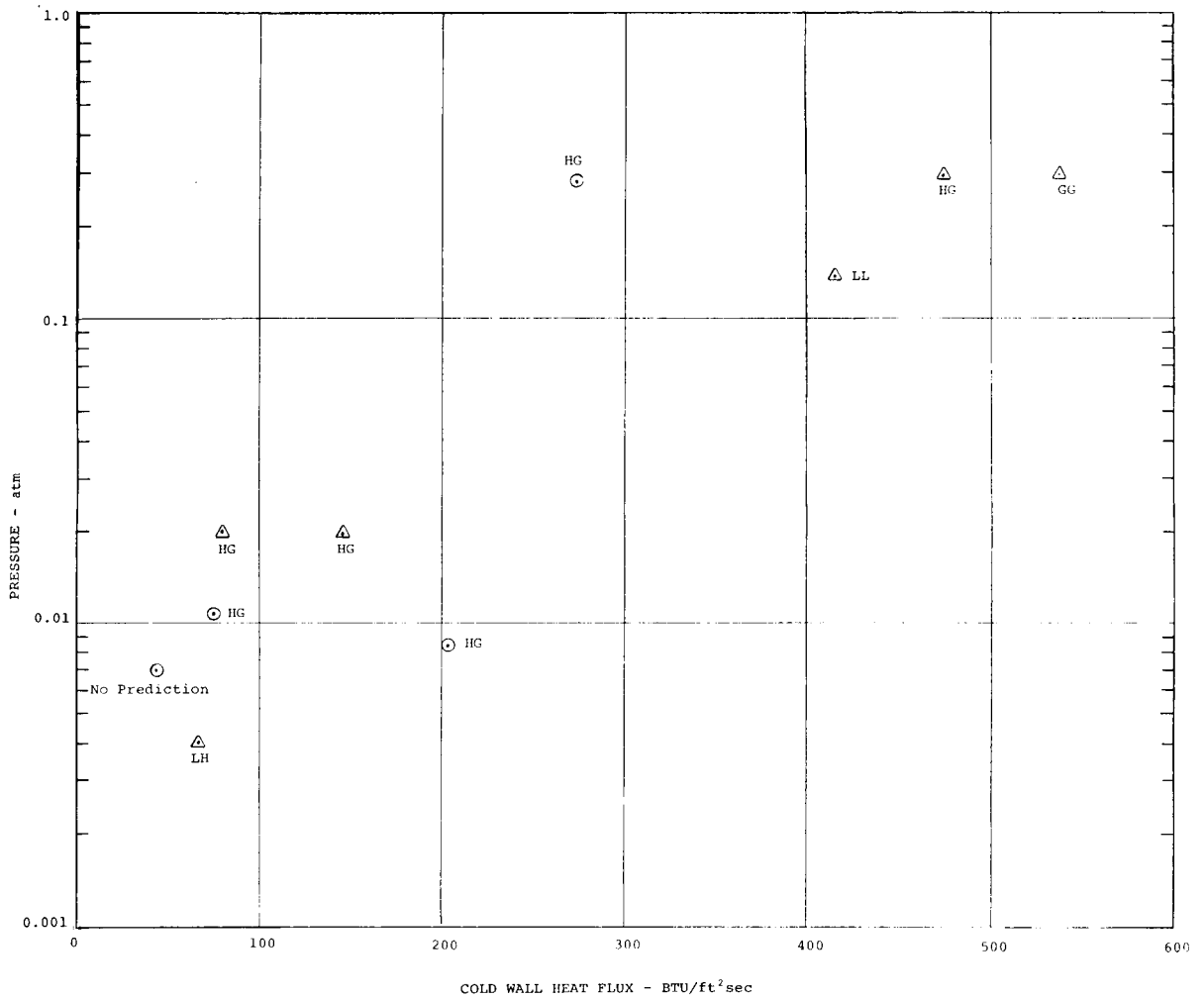

FIGURE 47

ABLATION CASE MAP, FILLED SILICONE ELASTOMER

(Iterative CAse

/ Final Case

Recession and Pyrolysis Plane Penetration Prediction Results Indicated by:

Recession	Pyrolysis Penetration
L < 75%	L < 90%
75% < G < 125%	90% < G < 125%
H > 125%	H > 125%

Example: LG denotes low recession prediction, satisfactory pyrolysis prediction

APPENDIX A

PROPERTY VALUES USED IN QUALIFYING CALCULATIONS

APPENDIX A

PROPERTY VALUES USED IN QUALIFYING CALCULATIONS

TABLE A-1

NOMINAL THERMOCHEMICAL PROPERTIES FOR LOW DENSITY PHENOLIC NYLON

VIRGIN MATERIAL PROPERTIES

Density ρ_v	36 lb/ft^3

Specific Heat - BTU/lb°R

Temperature °R	c_{p_v}
560	.36
660	.43
760	.495
860	.535
950	.545
1060	.545

Thermal Conductivity - BTU/ft-sec°R

Temperature °R	k_v
540	1.28×10^{-5}
700	1.28×10^{-5}
900	1.41×10^{-5}
1100	1.48×10^{-5}
1280	1.51×10^{-5}

PYROLYSIS CONSTANTS

Reaction-rate constant A	1.586×10^6 lb/ft^{2}sec
Activation Temperature B	23,200 °R
Effective Heat of Pyrolysis	550 BTU/lb

TABLE A-1 (Continued)

Effective Specific Heat of Pyrolysis Gases

BTU/lb°R

Temperature °R	$\bar{C}_p$
500	.87
1000	.87
1500	.87
1800	1.15
2000	1.97
2100	2.80
2500	3.25
2800	2.80
3000	1.80
3300	1.24
3500	1.05
4000	1.2
5000	2.2
6000	4.78

CHARRED MATERIAL PROPERTIES

Density ρ_v	12 lb/ft^3

Specific Heat - BTU/lb°R

Temperature °R	c_{p_v}
All	.54

Thermal Conductivity - BTU/ft-sec°R

Temperature °R	k_v
500	2.5×10^{-5}
1500	2.5×10^{-5}
2000	8×10^{-5}
2500	20×10^{-5}
300	30×10^{-5}
3500	42.5×10^{-5}
4000	60×10^{-5}
4500	76.2×10^{-5}
5000	100×10^{-5}
5500	123×10^{-5}

TABLE A-1 (Concluded)

SURFACE CONSTANTS

Activation Temperature, B_c, °R	12
Reaction Rate Constant, A_c, $lb/ft^2 sec\text{-}atm$	76,500
Reaction order, n	1
Mass of Char Removed Per Unit Mass of Oxygen, λ, lb/lb	.75
Heat of Combustion, Δh_c, BTU/lb	5,000
Surface Emittance	.8

TABLE A-2

NOMINAL THERMOCHEMICAL PROPERTIES FOR FILLED SILICONE RESIN IN HONEYCOMB

VIRGIN MATERIAL PROPERTIES

Density ρ_v	40 lb/ft^3

Specific Heat - BTU/lb°R

Temperature °R	c_{p_v}
510	.354
560	.365
660	.382
760	.396
860	.410
960	.419
1060	.427

Thermal Conductivity - BTU/ft-sec°R

Temperature °R	k_v
All	1.98×10^{-5}

PYROLYSIS CONSTANTS

Reaction Rate Constant A	2700 lb/ft^{2}sec
Activation Temperature B	20,000°R
Effective Heat of Pyrolysis Δh_p	250 BTU/lb

Effective Specific Heat of Pyrolysis Gases - BTU/lb°R

Temperature °R	$\overline{c}_p$
All	1.0

TABLE A-2 (Concluded)

CHARRED MATERIAL PROPERTIES

Density ρ_c	20 lb/ft^3

Specific Heat - BTU/lb°R

Temperature °R	Cp_c
All	.43

Thermal Conductivity - BTU/ft-sec°R

Temperature °R	k_c
500	1.9×10^{-5}
1000	2.4×10^{-5}
1500	2.9×10^{-5}
2000	3.3×10^{-5}
2500	3.7×10^{-5}
3000	4.0×10^{-5}
2500	4.2×10^{-5}
4000	4.4×10^{-5}

SURFACE CONSTANTS

Activation Temperature, B_c, °R	39,872
Reaction Rate Constant, A_c, $lb/ft^2 sec\text{-}atm^{\frac{1}{2}}$	6.73 x 10
Reaction order, n	.5
Mass of char removed per unit mass of oxygen, λ, lb/lb	5,000 0.1
Heat of Combustion, Δh_e, BTU/lb	5,000
Melt Temperature, °R	3,800
Heat of Fusion, BTU/lb	60

TABLE A-3

NOMINAL THERMOCHEMICAL PROPERTIES FOR AVCOAT 5026-39-He/G

VIRGIN MATERIAL PROPERTIES

Density ρ_v	32 lb/ft^3

Specific Heat - BTU/lb°R

Temperature °R	c_{p_v}
560	.329
660	.364
760	.397
860	.406
960	.418
1060	.424
1160	.425

Thermal Conductivity - BTU/ft-sec°R

Temperature °R	c_{p_v}
500	1.4×10^{-5}
600	1.4×10^{-5}
723	1.46×10^{-5}
973	1.68×10^{-5}
1070	1.71×10^{-5}
1135	1.59×10^{-5}
1244	1.42×10^{-5}
1250	1.31×10^{-5}
1400	1.31×10^{-5}

TABLE A-3 (Continued)

PYROLYSIS CONSTANTS

Reaction Rate Constant A	128,000 lb/ft^{2}sec
Activation Temperature B	19,600°R
Effective Heat of Pyrolysis Δh_p	200-250 BTU/lb

Effective Specific Heat of Pyrolysis Gases - BTU/lb°R

Temperature °R	$\bar{C}_p$
All	1.0

CHARRED MATERIAL PROPERTIES

Density, ρ_c	20 lb/ft^3

Specific Heat - BTU/lb°R

Temperature °R	c_{p_e}
720	.25
1080	.3
1440	.348
1800	.397
2160	.445
2520	.494
2574	.5
5000	.5

TABLE A-3 (Concluded)

Thermal Conductivity - BTU/ft-sec°R

Temperature °R	k_c
540	3.88×10^{-5}
1660	3.88×10^{-5}
1860	6.10×10^{-5}
2060	8.33×10^{-5}
2460	11.7×10^{-5}
3060	16.7×10^{-5}
3460	19.5×10^{-5}
5460	20.0×10^{-5}

SURFACE CONSTANTS

Activation Temperatures, B_c, °R	76,500
Reaction Rate Constant, A_c, $lb/ft^2 sec\text{-}atm$	1×10^{10}
Reaction order, n	1.0
Mass of Char Removed per Unit Mass of Oxygen, λ, lb/lb	1.5
Heat of Combustion, Δh_c, BTU/lb	5,000

TABLE A-4

HEAT OF COMBUSTION (BTU/lb) FOR CARBON

Temperature (°R)	Pressure (atm)			
	0.1	1.0	10.0	100.0
1800	4110	4110	4110	4110
2700	4266	4226	4226	4266
3600	4454	4447	4446	4445
4500	4871	4697	4656	4643
5400	6265	5295	4983	4884
6300	10220	6995	5679	5245
7200	13540	13050	7134	5869

NASA-Langley, 1972 —— 33 CR-1980